We are IntechOpen,
the world's leading publisher of Open Access books
Built by scientists, for scientists

6,900
Open access books available

186,000
International authors and editors

200M
Downloads

154
Countries delivered to

Our authors are among the

TOP 1%
most cited scientists

12.2%
Contributors from top 500 universities

CLARIVATE ANALYTICS
BOOK CITATION INDEX
INDEXED

WEB OF SCIENCE™

Selection of our books indexed in the Book Citation Index
in Web of Science™ Core Collection (BKCI)

Interested in publishing with us?
Contact book.department@intechopen.com

Numbers displayed above are based on latest data collected.
For more information visit www.intechopen.com

Chapter

Semiconductor Nanocomposites for Visible Light Photocatalysis of Water Pollutants

Fatima Imtiaz, Jamshaid Rashid and Ming Xu

Abstract

Semiconductor photocatalysis gained reputation in the early 1970s when Fujishima and Honda revealed the potential of TiO_2 to split water in to hydrogen and oxygen in a photoelectrochemical cell. Their work provided the base for the development of semiconductor photocatalysis for the environmental remediation and energy applications. Photoactivity of some semiconductors was found to be low due to larger band gap energy and higher electron-hole pair recombination rate. To avoid these problems, the development of visible light responsive photocatalytic materials by different approaches, such as metal and/or non-metal doping, co-doping, coupling of semiconductors, composites and heterojunctions materials synthesis has been widely investigated and explored in systematic manner. This chapter emphasizes on the different type of tailored photocatalyst materials having the enhanced visible light absorption properties, lower band gap energy and recombination rate of electron-hole pairs and production of reactive radical species. Visible light active semiconductors for the environmental remediation purposes, particularly for water treatment and disinfection are also discussed in detail. Studies on the photocatalytic degradation of emerging organic compounds like cyanotoxins, VOCs, phenols, pharmaceuticals, etc., by employing variety of modified semiconductors, are summarized, and a mechanistic aspects of the photocatalysis has been discussed.

Keywords: visible light photocatalysis, semiconductor composites, organic pollutants, mechanism, wastewater treatment

1. Introduction to photocatalysis

Catalysis refers to a phenomenon in which a substance (the catalyst) speed up a kinetically slow reaction and the catalyst is fully restored at the end of each catalytic cycle and the "Photocatalysis" is defined as a specific process for the acceleration of the "photoreaction" in the presence of a catalyst [1]. Photocatalysis can also be regarded as the catalysis of photochemical reaction on a solid substrate, mostly a semiconductor [2]. The term "Photocatalysis" is still an arguable subject due to controversies, according to some researchers the "light" acts as a catalyst, while it always acts as a "reactant" where it is spent in the chemical process [3].

The word "photoreaction" is sometimes explained as a "Photoinduced" or "Photoactivated," process, whereas in the field of photocatalysis, "catalytic

activity" is the ability of a catalyst to show performance under light depending upon the reaction sites/active sites at the catalyst. The performance of a catalyst can be determined by its "turnover frequency" which is "number of turnovers per unit time of reaction, it is used to show how many times one active site produces a reaction product(s) within unit time." In case of photocatalysis, the reaction rate depends on the frequency of irradiated light which acts as the initiator of photoreaction. The term photocatalysis indicates the relation of light and some substance; (say a catalyst) so in the absence of light, the process of photocatalytic activities on active sites is not possible [1, 4].

1.1 Brief history of semiconductor photocatalysis

In 1839, the production of voltage and an electric current were reported when silver chloride electrode, immersed in electrolyte solution (connected to counter electrode) exhibited illumination under sunlight, which lately was known as "Becquerel effect" led to the beginning of existing era of photo electrochemistry [3]. In 1921, the Renz published first article on the degradation of carbon compounds by using titanium dioxide. In 1924 the photocatalytic deposition of silver on zinc oxide was observed for the production of metallic silver [2]. In 1929, the "chalking" (fading of paints) effect of titanium white (TiO_2), under the strong sunlight was observed, which in 1938 became the basis for self-cleaning property and modification in the concept of photo-induced reduction [5].

During 1950s, the insights of photocatalysis were shifted to ZnO. In 1953, two studies for the production of H_2O_2 on ZnO under the UV irradiation started a series of follow-up studies in the upcoming years which explained that an organic compound is oxidized when atmospheric oxygen is reduced. Till 1955, the photocatalytic behaviour of ZnO, Sb_2O_3 and TiO_2 including photoconductivity and fluorescence were well known. In 1958, the adsorption of reduced O_2 on the TiO_2 surface, as a result of photoexcitation, having the ability to degrade a dye was studied. During 1960s and 1970s, the processes and concepts of photo-oxidation of CN^- and photo-deposition of Pt, Cu, Pd, and other metals on TiO_2, WO_3, Al_2O_3, and SnO_2 to be used as co-catalysts, had been evolved. In 1972 the field of photo-electrochemical got more attention when Fujishima and Honda reported the ability of an illuminated TiO_2 and Pt electrode to generate the H_2 gas by a publication in *Nature*, which opened the doors for the close associations between photo electrochemistry and photocatalysis. By the end of that decade and by the mid of 1980s many other semiconductors, the ideas for nano-sized TiO_2 particles and coupled semiconductors had been evolved. The decades of 1980–2000 were important for the field of photoelectrochemistry as major breakthroughs during this era led to the discovery of large number of applications varying from self-cleaning surfaces to disinfection of water [2, 6, 7].

1.2 Semiconductor photocatalysis

The phenomenon gained importance during late 1970s and mid 1980s after the evolution of H_2 by illuminated TiO_2 (pristine semiconductor) in the presence of noble metal electrode, after that great concern was shown in water splitting followed by emergence of new era of photo electrochemistry at a single semiconductor crystal. The processes of semiconductor photocatalysis for environmental concerns have gained fame during the last 3 decades [8, 9].

Semiconductor photocatalysis can be of two types (i) homogenous photocatalysis, (ii) heterogeneous photocatalysis, depending on the phase differences of reactants and catalysts, triggered the concept of advanced oxidation

processes (AOPs) at the end of twentieth century. TiO_2 is the semiconductor which can act as both the hetero and homogenous photocatalyst photoreactions [10] (**Figure 1**).

Heterogeneous photocatalysis is a process which includes a large variety of reactions: reductions oxidations, dehydrogenation, transfer of charge carriers, bacterial inactivation, organic pollutant degradation, water detoxification, etc. under both UV and visible light irradiation [1, 11]. Having TiO_2 as a semiconductor, the general mechanism is illustrated in **Figure 2**.

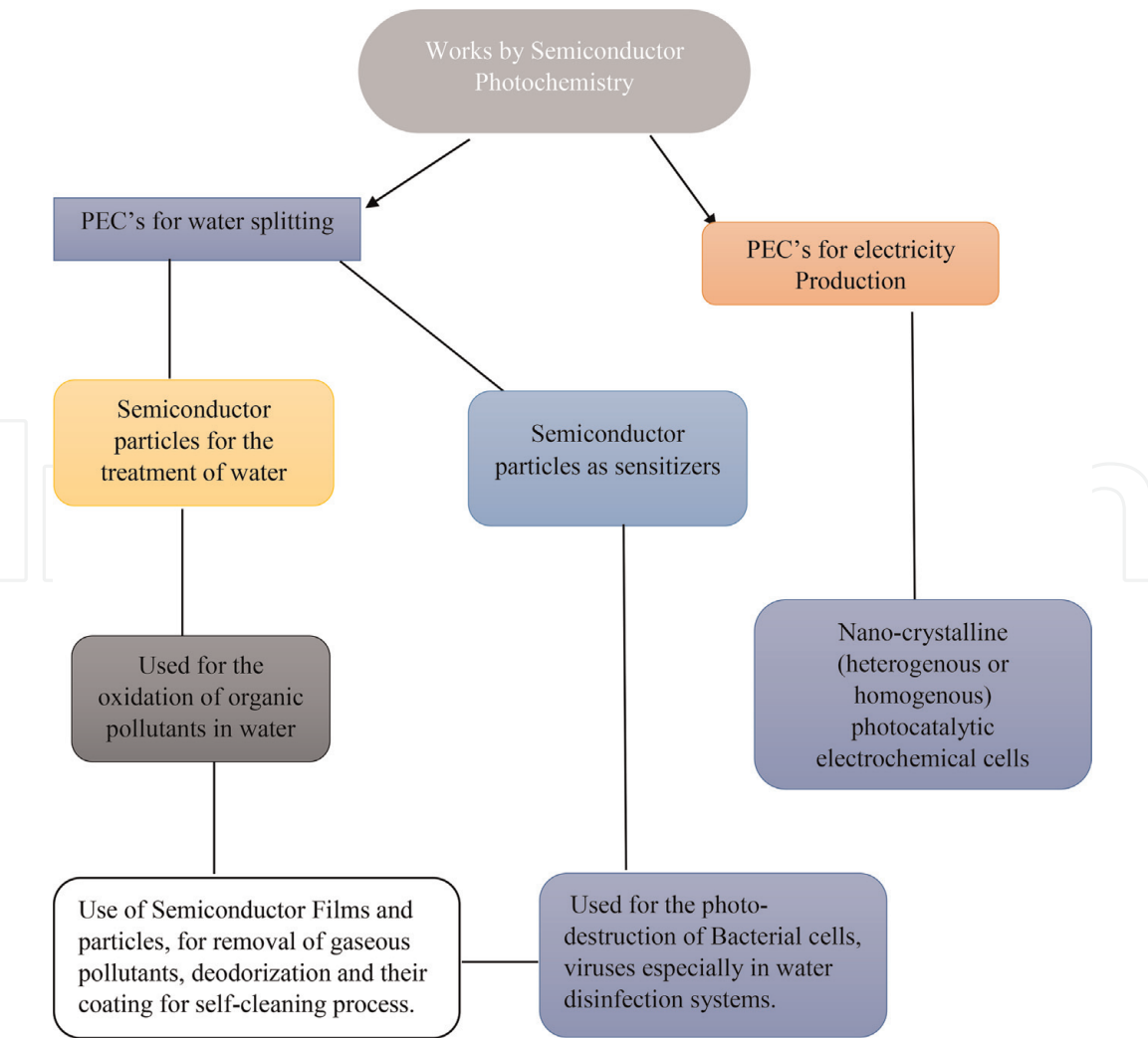The chemistry behind the process is explained as [6]:

$$e^- \, CB + h^+ \, VB \rightarrow energy \tag{1}$$

$$H_2O + h^+ \, VB \rightarrow \bullet OH + H^+ \tag{2}$$

$$O_2 + e^- \, CB \rightarrow O_2^{\bullet -} \tag{3}$$

$$\bullet OH + pollutant \rightarrow\rightarrow\rightarrow H_2O + CO_2 \tag{4}$$

$$O_2^{\bullet -} + H^+ \rightarrow \bullet OOH \tag{5}$$

$$\bullet OOH + \bullet OOH \rightarrow H_2O_2 + O_2 \tag{6}$$

$$O_2^{\bullet -} + pollutant \rightarrow\rightarrow\rightarrow CO_2 + H_2O \tag{7}$$

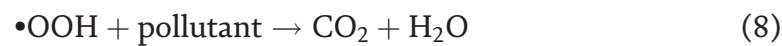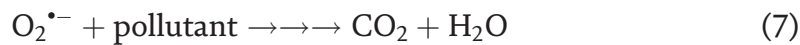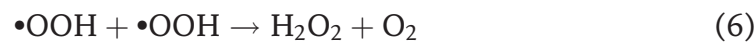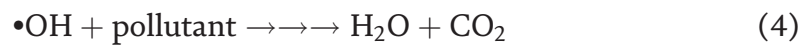$$\bullet OOH + pollutant \rightarrow CO_2 + H_2O \tag{8}$$

Figure 1.
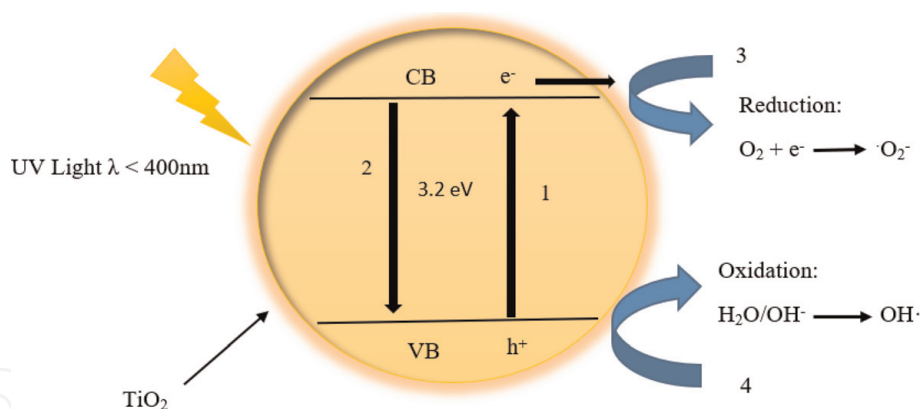*Fields using semiconductors as photocatalysts from early ages to date [3].*

Figure 2.
Primary mechanism of photocatalysis of pristine semiconductor sphere illustrating different steps: (1) Formation of e^-/h^+ as a result of photoexcitation; (2) e^- recombination in absence of no electron acceptor; (3) photo induced electron transportation and reduction of oxygen; (4) oxidation due to hole in VB, while 3.2 eV is E_g between VB and CB.

1.3 Recombination

In **Figure 2**, process "2" is "recombination." When it occurs, the excited electron return to valence band and recombines with hole (by dispersing the absorbed energy as heat) in the absence of electron acceptor in the conduction band. Recombination of photoexcited electron is the major drawback of semiconductors as it lessens the efficiency of overall process. The chances of recombination can be reduced by modifications in the crystalline structure either by doping with metals, non-metals, ions or by the formation of heterostructures [12].

1.4 Basics of heterojunctions

In the internal structure of semiconductors (SCs), there are some band alignments which act as basis for the formation of heterojunctions/heterostructures; prepared for the enhanced activity of SCs' under sunlight. "Heterojunction is the junction in single crystal, formed by the combination of two dissimilar SCs." These heterostructures are formed on the basis of band gap, electron affinity and bands position thus leading to the formation of new energy levels. By the formation of HSs/HJs, the movement of charge carriers in a reaction can be controlled. There are three types of heterostructures depending on the energy band alignments. (i) Type I band alignment; the "Straddling" band Pattern. (ii) Type II band alignment; the "Staggered" band Pattern; (iii) Type III band alignment; the "Broken gap" Pattern. Agrawal [13] **Type I**, the most common band alignment in which the SC with smaller band gap relies under the SC with larger band gap; means band gaps are (not entirely but) overlapped. The charge carriers stay confined in the heterojunction due to the presence of potential barrier. **Type II**, the position of Valence and Conduction band of first SC is higher than that of second SC, the direction of steps in both SCs is same. The potential difference between two SCs causes the band bending at junction site due to this the electron and hole move in opposite directions, thus leading to good separation of charge carriers in heterojunction structure. When the band gaps stops to overlap then the case is known as "zero gap or broken gap" this is **Type III** band alignment, which is formed by the combination of semimetal having non-overlapping bandgap with a semiconductor [14, 15]. The illustration of band gap alignment is given **Figure 3**.
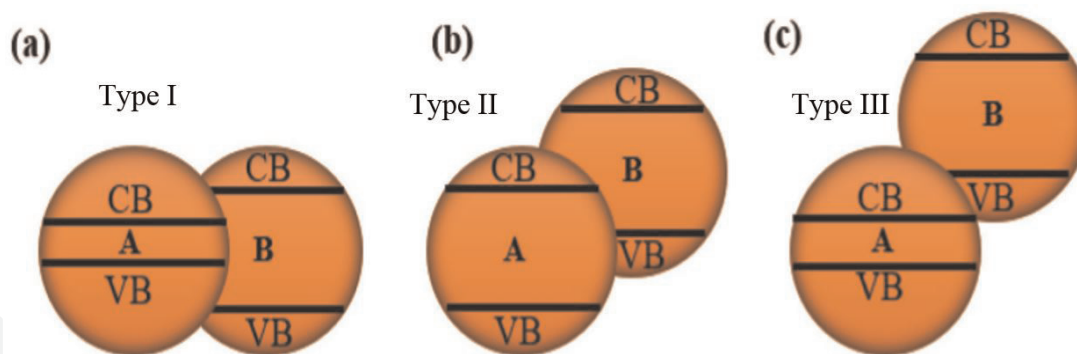
Figure 3.
Schematic illustration of different types of semiconductors heterojunctions [16].

The formation of Type II heterojunctions are good candidates in the field of photocatalysis as it has capability to enhance the charge separation to improve the photoreactions, photocatalytic degradation and water splitting [17].

1.5 General mechanism of water splitting by semiconductors for wastewater treatment

Globally, 1 billion people do not have access to safe drinking water and approximately 2.6 billion people are suffering from safe sanitation, this is particularly an issue in Asia, Africa, South and central America [18], so there is no ambiguity in saying that water management has become an emerging issue for the twenty-first century. Number of anthropogenic activities like industrial activities, discharge of effluents in the water bodies, oil spills and leaching of compounds to groundwater, etc. are interfering the quality of water, thus making it unfit for drinking and domestic purposes and also threatening the natural water resources. It has been estimated that the water quality will be a worst in upcoming decades. In this regard, there is a need for advancement in the fields of water and wastewater treatment because the conventional treatment plants are not capable to remove some persistent pollutants from water [19].

In this perspective the concept of photocatalytic water splitting has been emerged in last decade which are a favorable method for attaining green and renewable energy. For effective water splitting the CB of a SC should be more negative than the redox potential of H^+/H_2 (0 V vs. NHE) and the top of the valence band should be more positive than the redox potential of O_2/H_2O (1.23 V vs. NHE). In splitting process water breaks in oxygen and hydrogen by the photoexcitation of electron leaving a hole behind. Semiconductor absorbs the energy equal to or greater than its band gap, the photogenerated electrons and holes starts the redox reactions. Three key stages of water splitting mechanism are; (i) energy absorbance and generation of e^-/h^+ as result of photoexcitation; (ii) the charges remain separated at the opposite sides of SC crystal as a result of minimal recombination; (iii) charge carriers trigger the oxidation and reduction at valance and conduction band or vice versa. By production of reactive species as result of reduction of oxygen and oxidation of water or hydroxyl ion, like H^+, $OH^\bullet$ and $O_2^{\bullet-}$ the wide variety of organic pollutants in water are mineralized in to CO_2 and H_2O [20]. The water splitting mechanism is given in **Figure 4**.

1.6 Roles of reactive species in pollutant degradation

General reactive or oxidizing species formed during the photocatalytic degradation of pollutants are H^+, OH, HO_2, H_2O_2 and $O_2^{\bullet-}$. These photo-oxidants are formed by the steps as described in Eqs. (2)–(7).

Hole and hydroxyl radical: A hole generates when an electron moves to CB as a result of photo excitation, and hydroxyl radical generates when the hole oxidizes the hydroxyl ion or the water molecule. There is a debate on the reactiveness of hole and a hydroxyl radical, as they both are important for photocatalytic degradation, because it is still uncertain whether the hole or hydroxyl radical is core oxidant, or is there any dependence on the type of substrate. Minero et al. [21] has investigated that $OH^{\bullet}$ has higher oxidizing power as compared to other oxidizing agents as it has the oxidation potential of +2.80 eV slightly less than that of Fluorine +2.87 eV. There are many studies which support the reactivity of $OH^{\bullet}$ as an oxidant [22]. Turchi and Ollis [23] have proposed the four ways by which the $OH^{\bullet}$ oxidizes the pollutant, **Figure 5**.

Draper et al. [8] has investigated the direct oxidation by the hole, it can be said that the oxidation process in the valence band is started by the hole, by the oxidation of H_2O molecule and hydroxyl ion. It would be rational to say that both the hole and $OH^{\bullet}$ deal with different classes of compounds; like the production of hydroxylated rings from the oxidation of aromatic compounds and the degradation of paracetamol (acetaminophen) on the TiO_2 is caused by $OH^{\bullet}$ [24].

Superoxide radical: This specie has been reported to play an important for the degradation/oxidation of many pollutants under both, the visible and ultra violet
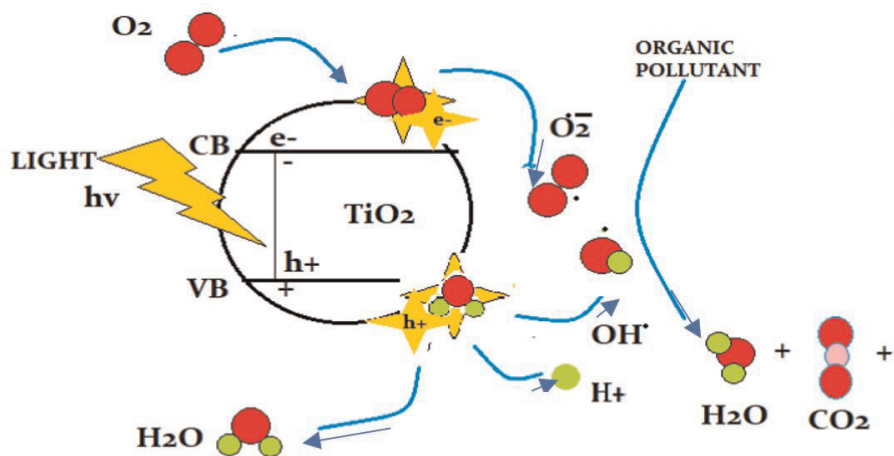

Figure 4.
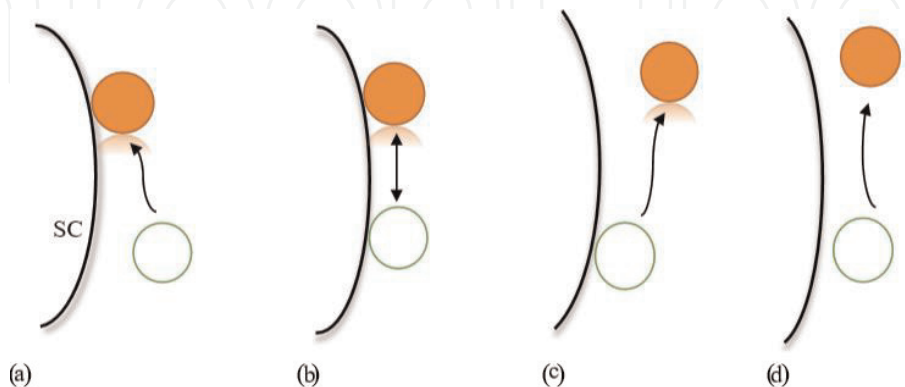*Water splitting mechanism illustration and mineralization of organic pollutant.*

Figure 5.
Scheme of oxidant and pollutant molecule interaction in the presence of a semiconductor. (a) $OH^{\bullet}$ is close to the pollutant molecule, when the latter is adsorbed. (b) Oxidation reaction, when $OH^{\bullet}$ and substrate both are adsorbed. (c) Pollutant is in the vicinity of $OH^{\bullet}$, when latter is adsorbed on SC surface. (d) Pollutant degradation by oxidation, when both are in solution; where ● is the target molecule/substrate and ○ is the hydroxyl radical.

light irradiations. In addition to direct participation in oxidation the formation of superoxides confirms the decreased recombination rate, as it is formed by the reduction of oxygen molecule. Therefore, superoxide formation is a vital process which controls the reaction rate by accepting the excited electron ([25]).

Hydrogen peroxide: Hydrogen peroxide is formed in the solution by the combination of two hydroperoxyl radicals (HOO·) or by the two electron reduction of O_2 in the conduction band as shown in Eqs. (6), (7) and (10). It can affect the photocatalytic reaction by acting as electron acceptor directly from organic or inorganic pollutant or by its dissociation into $OH^\bullet$ due to "homolytic scission" [8]. Reactivity depends on rate of its production and the substrate concentration on the semiconductor. H_2O_2 mostly in the TiO_2 solutions cannot be readily detected due to its high unstable nature. H_2O_2 is dissipated as it is produced into $OH^\bullet$ by reduction [21].

$$O_2 + 2e^-{}_{cb} + H^+ \rightarrow H_2O_2 \qquad (9)$$

$$2H_2O + 2h_{vb}{}^+ \rightarrow H_2O_2 + 2H^+ \qquad (10)$$
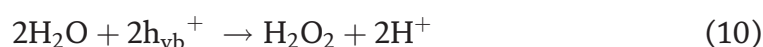
Photoproduced reactive species on the photocatalysts undergo oxidation that have been extensively studied during the last decades for environmental remediation including water disinfection, wastewater treatment, air decontamination, self-cleaning glass/surfaces degradation of organic compounds, etc. The reason to attraction towards this process lies in the end products of any type of pollutant which are CO_2 and H_2O. Actually, the mineralisation of compounds having high carbon hydrogen content, occurs via the formation of many intermediates which also undergo oxidation. In short, the significance of photocatalytic process and photo-oxidation cannot be underestimated because of its emerging demand for the decomposition of refractory organics or recalcitrant compounds.

2. Development of visible light active photocatalysts

Among the several advanced oxidation processes, semiconductor assisted photoreactions are gaining importance in recent years due to their higher mineralization potential of organic pollutants in environment. The main limitation for the pure SC photocatalysts is their large band gap which means there is a need for shorter wavelength of light and high energy photons ($\lambda < 380$ nm) to excite the electron from VB to CB. For this purpose, the photons falling in ultra violet region are required. Under the UV irradiation, the electrons in the VB of SCs are excited and e^-/h^+ pair is formed. The problem is, the UV light makes only 4–5% of the solar spectrum while about 40–45% of the solar light falls in visible spectra. The need of UV light limits the photocatalytic activity due to its less availability [12, 20].

In recent years, Yongquan Quab [26] has pointed some critical requirements for a stable SC catalyst to yield the solar energy which are; firstly, the SC must have an appropriate band gap to produce robust electrons ($E_g > 1.3$ eV commonly >2 eV but <3 eV) and sufficient band gap to allow effective absorption of light under visible region. Secondly, there should be less chances for recombination, i.e., should have an efficient charge separation system; lastly there should be a process to protect the semiconductors from the direct electrochemical reactions to confirm the photoelectrochemical strength of the system.

A single pure semiconductor photocatalyst is unable to fulfill the all above mentioned requirements. Therefore, in order to enhance the photocatalytic activity

of the SC, there is a need to enhance their visible light activity, which can either be done by enhancing the surface modifications, i.e., by increasing the surface area and porosity, or by chemicals modifications like doping of metals, non-metals, ions, non-metal co-doping, dye sensitization or by the formation of junctions unitary, binary and tertiary, i.e., semiconductor/semiconductor, semiconductor/metal, semiconductor/metal oxides or the semiconductors/nano-composites [20].

2.1 Doping/grafting of semiconductor photocatalysts

Among all semiconductors TiO_2 is considered as pristine, first-generation oldest one with many physical and structural properties. In addition to TiO_2 other *d*-orbital metal oxides like WO_3, ZnO, Fe_2O_3 are regarded as *n*-type semiconductors while the semiconductors other than metal oxides are CdS, ZnS, CdSe, ZnSe, CdTe, MoS, Sb_2S_3 among them some have smaller band gaps like CdS and some have higher band gap like ZnS. TiO_2 is found in the three crystalline forms named as anatase, rutile and brookite, being the anatase and rutile are more active with band gaps or 3.2 and 3.0 eV. TiO_2 has been extensively used and widely investigated due to its high photo activity, biodegradability, less-toxicity, low cost and high structural and chemical stability against photocorrosion process [6, 12].

In order to understand, doping can be defined as "when impurities are added to semiconconductors, the band structure is modified; this process is known as doping." During the doping process, the doped atoms can present the interstitial, substitution or defect factor in structure of SC. When a semiconductor is doped with an acceptor atom, it is converted into *p*-type SC, because the acceptor atom is reduced by accepting electrons from VB and increases the production of holes and vice versa. Once SC is doped with any specie, it is supposed to increase the absorption of light in the visible spectrum and the doping material will not disturb the structural or chemical integrity of the SC [22]. The doping positions of dopants are given in **Figure 6**.

2.2 Non-metal-doped semiconductors

For this type of doping to SCs the non-metals like N, C, S and F have been used. The production of visible light active photocatalysts starts with the doping of N to TiO_2 or ZnO lattice, due to its small size, low ionization energy, and high stability. Livraghi et al. [28] proposed that contrary to the concept that nitrogen species are reason for formation of VLA photocatalyst the nitrogen precursor during the doping process induces the oxygen vacancies which renders the SCs able to absorb visible light and to increase phocatalytic activity. In 1986, Sato discovered the addition of NH_4OH in the titania sol followed by the calcination of obtained product, the resulting products was visible light active [29]. After that Asahi et al. [30] first time explored the VL activity of N-doped TiO_2 by the sputter method of TiO_2
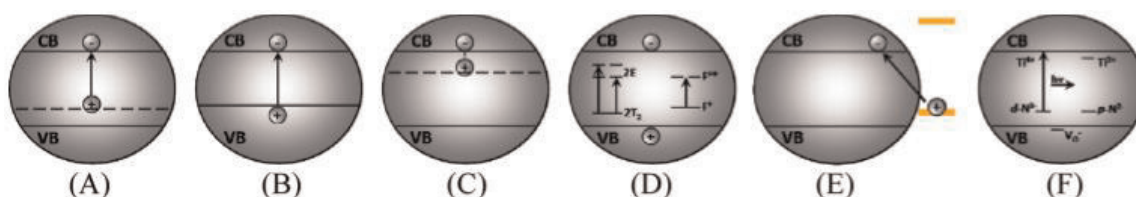

(A)   (B)   (C)   (D)   (E)   (F)

Figure 6.
Six schemes illustrating the different sites for dopants; (A) the localized states above VB; (B) lessened E_g due to non-metal doping; (C) localized states below CB; (D) formation of colored centers between E_g; (E) surface modification by addition of N-containing compounds; (F) interstitial N species and oxygen vacancies [27].

under N-Ar atmosphere. They also proposed that nitrogen doping creates a delocalized mixing/hybridization of O 2p and N 2p orbitals causing the rise in valence band position. Later on, for the efficient doping of N to TiO_2 either in bulk or at surface both types the dry or wet methods have been adopted. Techniques, like sputtering [31, 32] and ion implementation are based on the direct treatment of TiO_2 with nitrogen ions [32, 33].

The most used method of N doping in TiO_2 is sol-gel method, in this method the titanium precursors are combined with the nitrogen containing surfactants, for example, the N-doped TiO_2 have been prepared by using dodecylammonium chloride (DDCA) as surfactant acting as nitrogen source which provided it damaging capability for microcystins-LR under visible irradiation [34] **Figure 7**. Degradation of MC-LR and mineralization of 78% of carbon has also been reported by using Bi-doped TiO_2 under visible light irradiation having OH$^•$ as a reactive oxidation specie [35].

Several processes have been proposed to prepare the nanobelts by doping the 1D titania nanostructure with nitrogen following hydrothermal method having the anatase TiO_2 particles and NaOH as precursors and heating treatment with NH_3 ([25]). Production of N-doped TiO_2 nanotubes by the anodization of Ti in HF/H_2SO_4 electrolyte have been reported [36].

In addition to the N-doped TiO_2, ZnO can also be doped which is one of the most studied SC other than TiO_2 due to its applications in disinfection process and diversity of shapes but it has low stability. ZnO has also three crystalline forms, named as Zinc blend, Rocksalt and Wurtzite, having third one as most stable and active. The example of N-doped ZnO is preparation of zinc nanobundles by thermal treatment of (already prepared) ZnOHF nanobundles with NH_3 at different temperatures, as the temperature was increased the ZnOHF nanobundles were converted to N-ZnO nanobundles (**Figure 8**). These N-ZnO nanobundles gave dramatic increase absorption of light in visible region at $\lambda > 420$ nm [37].

Formation of the N-doped ZnO mesoporous nanospheres is an example of use of solvothermal treatment of Zn $(NO_3)_2.6H_2O$ which is the source of both Zn and nitrogen, in the presence of oleic acid, oleylamine, and octadecene. Mixture was heated at 260°C for 20 min and cooled at room temperature for 2 h followed by centrifugation, washing of precipitate and calcination at 400°C for 2 h led to the production of mesoporous nanospheres having size between 100–300 nm. This structure had the higher photoactivity as compared to pristine ZnO ([38]).
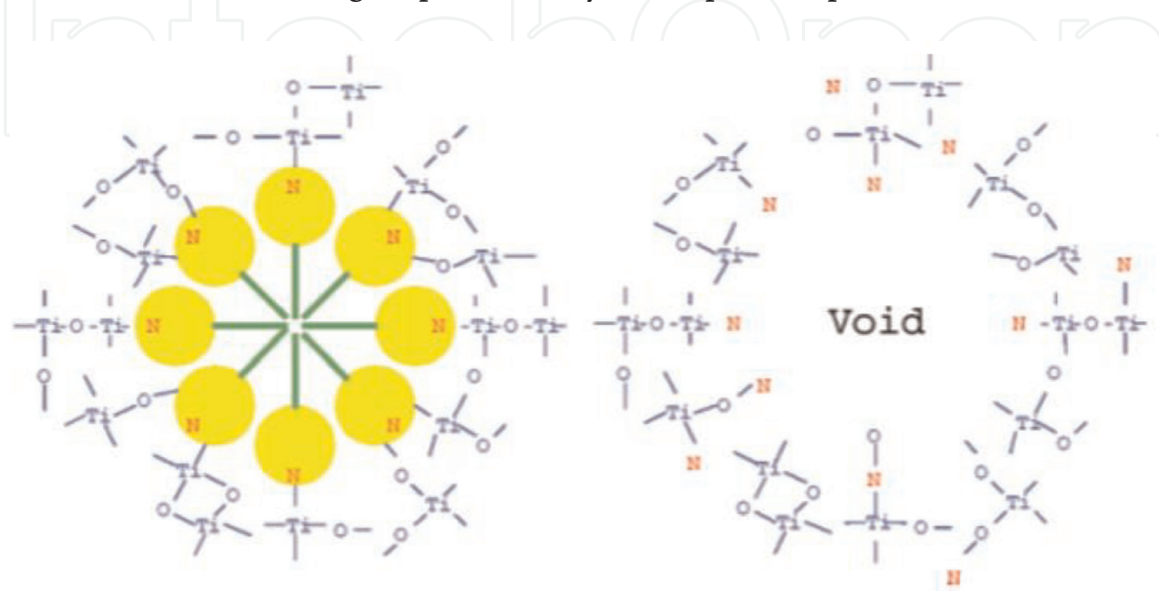

Figure 7.
N-doped TiO₂ using the titanium precursor and nitrogen containing surfactant as N source and pore template.

The nitrogen doped silver deposited ZnO thin films have been successfully prepared on a glass substrate by Kumar et al. via Radio frequency (RF) magnetron sputtering for the degradation of 2-CP under the visible light irradiation λ 390–700 nm and resulted in production of mineralized products as in **Figures 9** and **10** [39].

Nitrogen doped ZnO films were prepared by chemical vapour deposition (CVD) process using metallic zinc, NO_2 and NH_3 as precursors. The nitrogen concentration was varied while the temperature was kept constant at 350°C. The gradual addition of dopant to ZnO films led to the formation of stable nitrogen vacancies clusters and n-type defects, the stability of vacancies is the beauty of this process because the vacancies formed by addition of other impurities are easily removable [40]. Other techniques for the production of N-ZnO films on glass substrate, like high vacuum plasma-assisted chemical vapour deposition (HVP-CVD) [41] and pulsed-filtered cathodic vacuum arc deposition (PFCVAD) [42] have been reported. In both techniques, N_2 or N_2O was used as doping agents and as the dopant quantity was
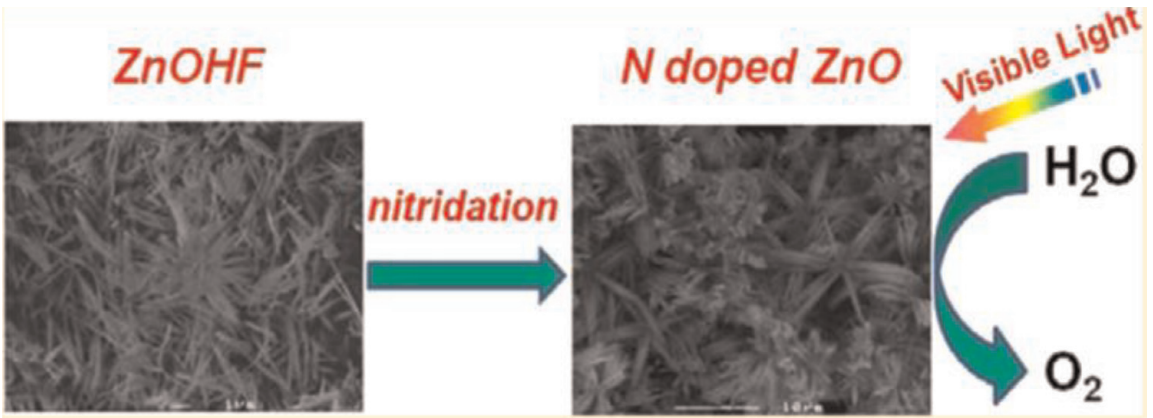

Figure 8.
Nitridation of ZnOHF nanobundles resulting in the formation of N-doped ZnO with similar morphology, showing high absorption to visible region.
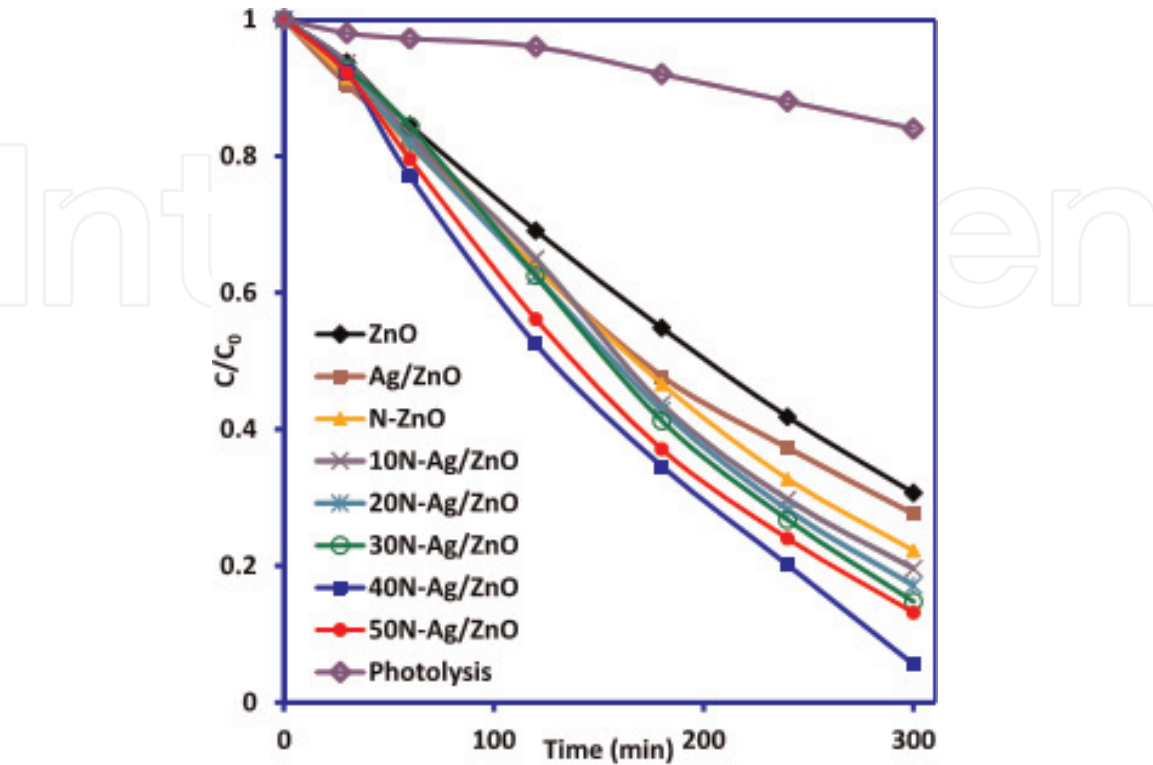

Figure 9.
Photocatalytic degradation of 2-CP on ZnO-based thin films under visible light irradiation [39].
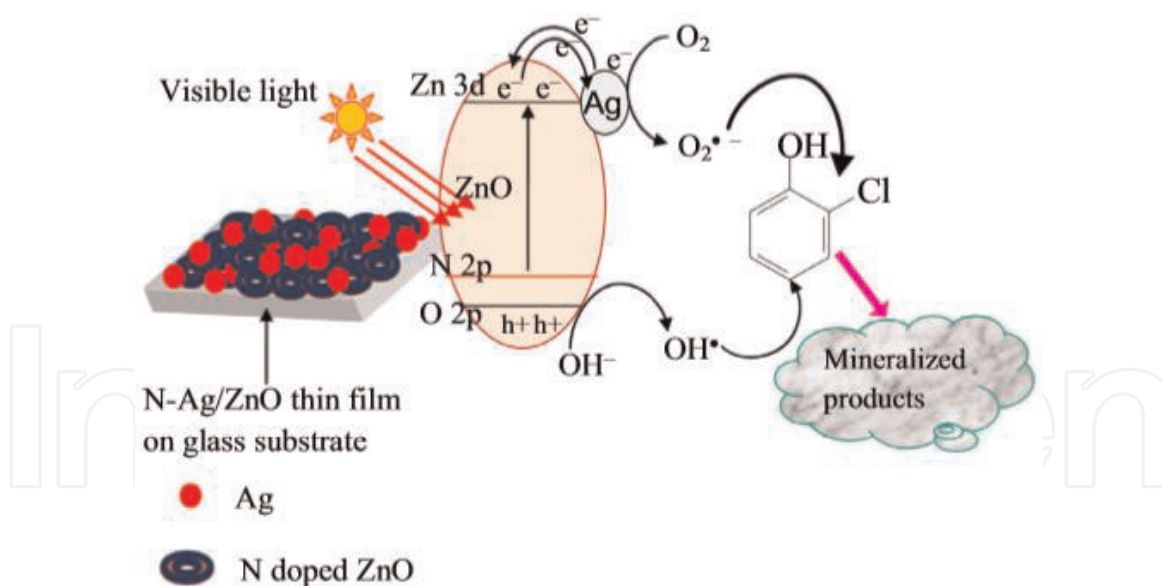
Figure 10.
Illustration of formation of e^-/h^+ pair and degradation of 2-CP by the N-Ag/ZnO thin films [39].

increased the semiconductor changed from *n*-type to *p*-type while the stability of *p*-type was dependent upon the synthesis process. Surprisingly the films synthesized by the PFCVAD process maintained their *p*-type doping for 12 months.

In literature, in addition to the doping of TiO_2 with nitrogen, there are studies which have reported the carbon doped TiO_2 as visible light photocatalyst. In contrast to the nitrogen doped TiO_2 which is commonly present in substitutional form, the carbon is doped to TiO_2 in different ways depending on the doping process, the three possible ways for carbon addition to lattice are (i) replacement of lattice oxygen with carbon; (ii) replacement of Ti atom with carbon atom; (iii) addition of carbon at interstitial position. Due to relatively smaller size of C atom, third one can occur without creating too much strain in structure [43]. The green synthesis for the C-doped TiO_2 has been described by using Ti $(SO_4)_2$ and sucrose as the precursors for Ti and carbon. This hydrothermal method is adoptable due to its low cost, nontoxic and easiness to perform, the C-TiO_2 was prepared by hydrothermal method and post-thermal treatment was applied at different temperatures and this was found to be effective to promote the visible light activity of C-TiO_2 for the degradation of toluene [44]. C-doped TiO_2 material have been prepared by the oxidation of titanium carbide (TiC) coated multiwalled carbon nanotubes (MWCNTs). The MWCNTs were used as a reaction template and carbon source, and titanium powder as the titanium source. XPS results indicated that chemical structure of Ti in TiO_2 coated-MWCNTs was different from that of pristine anatase due to the formation of Ti-O-C strong bond and interaction between TiO_2-MWCNT (**Figure 11**). The photocatalytic activity of this material was tested for the degradation of methylene blue under visible light [45].

Carbon doped TiO_2 has been reported to improve its VL response and photocatalytic activity and has been shown to be more effective than nitrogen doping. C-doped TiO_2 nanomaterials were prepared by the oxidative annealing of titanium (IV) carbide, used as a precursor. XPS analysis revealed that the carbon in the sample was present as carbonate species. The nanopowders were used for the degradation of methylene blue in the aqueous solution and for anti-bactericidal activity of *E. coli* k-12 and 80% inactivation in 30 min was observed [46].

Sulfur can also be used as a promising dopant to enhance the visible light activity despite of its difficulty to doping due to its large ionic radius. Sulfur-doped TiO_2 was prepared by using thiourea and titanium (IV) isopropoxide as precursors
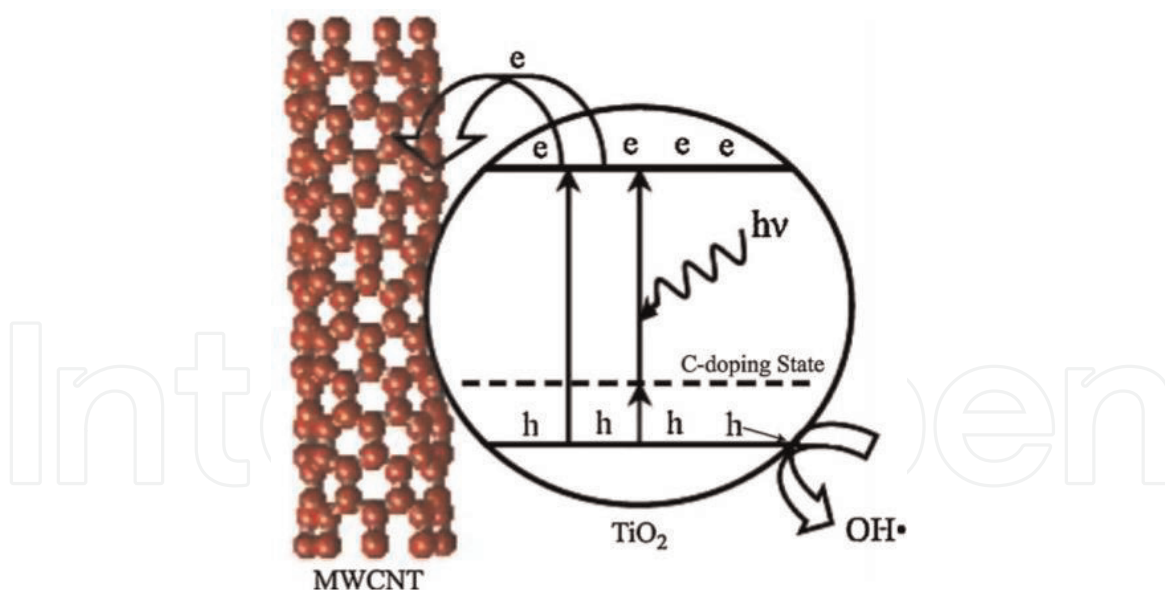
Figure 11.
Proposed mechanism of enhanced physical light activity of MWCNTs-TiO₂ material [45].

followed by mixing and vigorous stirring in ethanol resulted in the production of white powder annealed at 450°C for 4 h, the resulting material was S-doped TiO$_2$. These powders gave degradation of quinoline at λ = 495 nm [47]. S-doped material can be produced by the oxidation heating of TiS$_2$ powder followed by the annealing at 300°C, the XRD and XPS patterns gave the results which confirmed that the S atoms doped into the substitutional site of TiO$_2$ (e.g., the substitution of S for O) are effective for the band gap narrowing. Moreover, band calculations showed that the band gap narrowing due to the S doping originates from mixing the S 3p states with VB, leading to an increase in the VB width [48].

Incorporation of S to ZnO is little difficult due to its low solubility in ZnO and separation of ZnS particles at high temperatures. To overcome this problem, homogenously mixed precursors should be treated at low temperature. Formation of sulfur-doped ZnO films have been reported by pulse laser deposition [49], reactive sputtering ([50]) and chemical spray pyrolysis [51]. S-ZnO films are more appropriate for the uses in electronics, sensors and photoelectrochemical cells. But for the photocatalytic processes, S-ZnO powders give better results than films. Patil et al. [52] has proposed a method to make S-ZnO by a novel two steps process. First was the formation of bis-thiourea zinc oxalate (BTZO) powders by a mecha-nochemical method followed by its thermal decomposition/annealing at different temperatures to produce S-ZnO. At lower temperatures the resulting product was ZnS but as the temperature rose to 600°C the product was S-ZnO. The prepared powder was used to degrade the resorcinol under visible light and complete photocatalytic degradation (PCD) of 150 ppm resorcinol was observed in 7 h of light exposure at pH 7 [52]. ZnO has also been reported to be doped with iodine by following a solvothermal method using zinc salts and iodic acids in polyol medium as precursors with heating at 160°C. XRD and EDX analysis proved the presence of I in ZnO lattice. I doping increased the visible light absorbance, i.e., λ > 510 nm. In addition to the change in absorption spectra, it was proposed that doped I could act as the electron trapping sites thus reducing the chances for recombination [53].

To enhance the absorption in visible spectrum, P doping to TiO$_2$ has been reported using titanium isopropoxide and phosphide and H$_3$PO$_4$ as precursors. The content of P-TiO$_2$ had different properties prepared from two different precursors (Phosphide and H$_3$PO$_4$). A clear red shift in the absorption was observed due to the substitutional position of P^{3-} for oxygen in lattice. The presence of P^{3-} was

confirmed by XPS analysis, the ion-doped product gave 4-CP and acetaldehyde degradation under pure visible light at λ 410–440 nm [54].

Graphitic carbon nitride (g-C$_3$N$_4$) is a polymeric semiconductor, in order to increase its visible light activity and to reduce band gap it is doping with phosphorous has been reported. Ligang et al. prepared P-doped g-C$_3$N$_4$ by one pot green synthesis approach using dicyandiamide and phosphorous containing ionic liquid as precursors. The prepared particles were characterized and analysed and were used for the degradation of organic dyes like Rhodamine B and Methyle Orange under visible light. The photoactivity of particles was dependent on the post annealing temperature, doped particles gave higher photocatalytic activity as compared to pure g-C$_3$N$_4$, and degraded 95% of pollutants for the irradiation time of 180 min [55]. Chai et al. has also reported the degradation of dye by using P-doped gCN under visible light, synthesized by co-pyrolsis method, analysis like XRD, SEM, FESEM, XPS and FTIR were performed to check crystalline, morphological, structural and optical properties of catalyst. Prepared catalyst gave greater photocatalytic activity by substituting P atoms with C resulted in enhanced light harvesting phenomenon as it degraded 95% of dye in 30 min, additionally radical scavenging test unveiled that holes and superoxide radicals were dominant reactive species [56]. Sulfur-doped gCN porous rods were prepared in one pot by a simple pyrolysis method of melamine-trithiocyanuric acid at different temperatures, analysis confirmed the formation of porous rods with high surface area than that of pure gCN, surface area increased with increasing temperature, as prepared catalyst gave higher photocatalytic activity and increased absorption of light in visible region and gave 92% of rhB degradation within 50 min [57]. g-C$_3$N$_4$ has also been reported to be doped with boron [58] and carbon atoms [59], to enhance the photocatalytic activity under visible light.

Some other non-metals like fluorine, bromine, and oxygen have also been reported to dope SCs to enhance the photocatalytic property. Doping of different type of dopant into the lattice structure of some other semiconductors like Ta$_2$O$_5$, Nb$_2$O$_5$, BiVO$_4$, InVO$_4$, Bi$_2$WO$_6$, La$_2$Ti$_2$O$_7$, H$_2$Ti$_4$O$_9$, NaTaO$_3$, Nb$_2$O$_5$,V$_2$O$_5$, Sb$_2$O$_3$, Bi$_2$O$_3$, Fe$_2$O$_3$, NiO, ZrO$_2$, CeO$_2$, Ga$_2$O$_3$, CuO, Cu$_2$O, HNb$_3$O$_8$, WO$_3$, ZnO, K$_2$La$_2$Ti$_3$O$_{10}$, K$_2$Ti$_4$O$_9$, BiMoO$_6$ and TiO$_2$ have been reported. Some doped SCs with their water treating abilities is given in **Table 1**. Among the above mentioned semiconductors some have the large band gaps and show excitation under the UV irradiation only, like ZrO$_2$ has the band gap of 5 eV and Ga$_2$O$_3$ have band gap of 4.8 eV needs the excitation energy of 248–265 nm, while some SCs like WO$_3$ and venedates have small band gaps but they are doped in order to enhance the quantum efficiency of the process. However, dependant on their synthetic approaches and crystalline structures some metal oxides have shown the degradation activity of organic and inorganic compounds under visible light [95].

2.3 Grafting of semiconductors by co-doping

2.3.1 Non-metal co-doping

Photocatalysts are not only doped with single **non-metal**, they can also be doped with more than one or two non-metals resulting to co-doping. A lot of work has been reported on this phenomenon in order to enhance the photocatalytic behaviour of SC. For example, N-C co-doped TiO$_2$ has been reported, being P25 as titanium dioxide source, ammonia as a nitrogen source and different types of alcohols as carbon precursors by using one step hydrothermal method. The mixture was placed at 100°C for 4 h. After thermal treatment, powder was cooled and dried for 24 h at 105°C, the obtained product was N-C doped TiO$_2$. The physicochemical

Pristine photocatalyst	Non-metal dopant	Doping process	Target pollutant for visible light induced degradation	References
TiO_2	Nitrogen	Colloidal solution hydrolysis	Methylene blue	[60]
		DC sputtering and oxidation	Rhodamine B	[61]
		Hydrothermal treatment	2-propanol	[62]
		Sol-gel, hydrothermal and pyrolysis	Microcystin-LR	[63]
		Thermal decomposition, one-step synthesis	MO degradation	[64]
		Microemulsion-hydrothermal method	2,4-dichlorophenol	[65]
	N-P	Sol-gel method	4-Chlorophenol	[66]
	Boron (F-B-S tri-doped)	Solvation/evaporation/sol-gel synthesis	Acid napthol red (ANR)	[67]
	Boron		Trichlorophenol	[68]
	C-S	Solvation/evaporation	Toluene, 2-methlypyridine and MO, *E. coli* sterilization	[69–71]
	F-N	Hydrothermal/sol-gel/ Impregnation	MC-LR 4-CP MB	[72–74]
	C-N-S	Ti_2CN calcination/sol-gel	Reactive brilliant red X-3B, Tetracycline	[75, 76]
	S-C	Mechanochemistry	2-Propanol	[77]
$SrTiO_3$	N	Solvothermal/Sol-gel	MO, MB, RhB	[78]
$NaTaO_3$	I	Hydrothermal	MB	[79]
	N	Hydrothermal	Formaldehyde	[80]
ZrW_2O_8	S	Hydrothermal/ Calcination	O_2 Evolution	[81]
	I	Hydrothermal	RhB	[82, 83]
Bi_2WO_6	F	Hydrothermal HF	MB	[84]
ZnO	N	Decomposition reaction of Zn nitrate	MO	[85]
HNb_3O_8-SiO_2	N	SSR urea	RhB	[86]
WO_3	N	Thermal decomposition in NH_3	MeOH Oxidation, MO oxidation	[87, 88]
	F	Hydrothermal	rhB degradation Phenol	[89, 90]
$BiVO_4$	S	Aqueous thiourea	MB	[91]
$LaCoO_3$	C	Sol-gel process	CO_2 reduction	[92]
$In_2Ga_2ZnO_7$	N	SSR	H_2 Production	[93]
Ce_3O_4	F	PE-CVD	H_2 production	[94]

Table 1.
Visible light active non-metal doped photocatalysts.

properties and photocatalytic activity of catalyst was tested by using phenol as a model contaminant, phenol decomposition by different prepared materials confirmed that activity of catalyst was increased with the chain length of the alcohol precursor, and photoactivity of material was also evaluated [96]. A unique structured photocatalyst, C-S doped TiO_2 (TCS) was prepared by the hydrolysis of tetrabutyl titanate in a mixed aqueous solution of thiourea and urea followed by the stirring of solution at 12–24 h and water in mixture was dried at 80°C. Obtained precipitate was calcined at different temperatures, the obtained product was TCS. XPS analysis was performed which demonstrated Ti^{4+} ions were replaced by S^{4+} and carbonate ions. As prepared catalyst was used for the photodegradation of 4-chlororphenol under visible light (λ = 470 nm) [97]. Another example of C-S doped TiO_2 which is nanoporous highly reactive catalyst as TiO_2(C-TiO_2) and TiO_2 (S-TiO_2) was prepared at room temperature without heat treatment by using sol-gel method. Under visible light irradiation doped material showed high degradation of dye about 99% in 70 min. The catalyst also showed the antibacterial activity about 95% of *E. coli* was killed within 180 min even after 10 cycles for use of S-TiO_2 [98].

In addition to above mentioned non-metals, some halogens have also been reported for doping of TiO_2 [99, 100]. An example for halogens doping is preparation of Cl-B co-doped nanocrystalline titanium dioxide by a hydrothermal method using $TiCl_4$ as a titanium source and mixed hydrobromic acid (HBr) with ethanol as a bromine source, the doping of Cl^- and Br^- indicated narrowing of band gap and enhanced the photocatalytic activity for the overall water splitting process under visible light [101].

Microcystins (MCs) are the effective toxins which are produced and released by algae in the fresh and brackish waters upon cell rapture. Among dozens of congeners MC-LR is becoming a cause for disturbance to water quality and environment due to its concentration in water and high solubility and stability in water. Among many practices, N-F co-doped TiO_2 has been reported to degrade it by the attack of $OH^\bullet$ on the toxic ADDA (3-Amino-9-methoxy-2,6,8-trimethyl-10-phenyldeca-4,6-dienoic acid) chain under the visible light, normally the destruction of ADDA chain eliminates the associated toxicity but this breakage requires UV light <280 nm, but in case of N-F co-doped TiO_2 the production of free radicals due to photoexcitation, reductions and oxidations have reported to attack the ADDA and Mdha (Methyldehydroalanine group) chains and have resulted in the degradation of toxin and production of non-toxic intermediates and products [102].

Among titanates, co-doped K_2TiO_4, $SrTiO_3$, $La_2Ti_2O_7$, $K_2Ti_4O_9$ have been reported. The Co-doping of $SrTiO_3$ with carbon and sulfur has been reported. Co-doped product was produced by the calcination of mixture of thiourea and $SrTiO_3$ powders in lidded crucible at different temperatures. The addition of C and Si were confirmed by FTIR, XRD, XPS analysis, the obtained powder had the enhanced absorption shift from 400 to 700 nm. Cationic sulfur and tetravalent carbon doping increased the oxidative degradation of 2-propanol under visible light at λ 440 nm [77].

Nisar et al. [103] investigated the increased efficiency of $BiTaO_4$ by non-metal mono and co-doping in order to enhance its visible light activity. This SC has the band gap of 2.75 eV but it has ability to absorb only 19% of the visible light. Nitrogen doping to lattice created an electron acceptor state just above the VB in order to increase VBM. The lattice was co-doped with carbon and sulfur and after doping it was compared with the bulk. It was analysed that C-S doping led to the notable band gap reduction about 39% which was very close to the required band gap for a good photocatalytic material. The doped material had good overall water splitting ability [103]. Recently, co-doping of CeO_2 with Carbon and nitrogen has been reported to enhance its visible light photocatalytic activity. Analysis and

calculations revealed the addition of non-metals in the lattice. C-N co-doping shifts the fermi level at the bottom of conduction band by creating impurities in the lattice followed by the increased absorption of light under visible region. The surprising fact about this catalyst was its absorption intensity between 400 and 600 nm was very high as compared to other co-doped and N-doped CeO_2 and C-doped CeO_2 [104].

2.3.2 Non-metal-metal co-doping

To enhance the photocatalytic activity of semiconductors, co-doping with metal and non-metals has also been reported. In case of TiO_2, Bagwasi et al. has reported the synthesis, characterization and application of Bi-B-TiO_2 nanoparticles. The co-doped nanoparticles were prepared by sol-gel method. Results indicated the bismuth and boron were doped in TiO_2 lattice, as Bi substituted Ti as Bi^{3+} which reduced the rate of recombination and B was present as interstitial and substitutional B which enhanced the visible light absorption. Bi-B co-doped samples showed better activities for degradation of acid orange 7 (AO7) and 2,4-dichlorophenol under visible light (λ = 700 nm) irradiation [105].

TiO_2 is also co-doped with boron and nickel in the form of its oxide. As mentioned in **Figure 12**. The addition of boron at substitutional or interstitial position increases the response to visible spectra while the loading of Ni_2O_3 further enhanced its photocatalytic activity. TCP, 2,4-DCP and sodium benzoate were chosen as target pollutants. TCP was not only efficiently degraded under the visible light but also its was mineralized, moreover the degradation of other two pollutants was also same as of TCP [68].

Doping of $NaNbO_3$ powders with Cr-N and Mo-N has been studied by using hybrid density functional theory. Co-doping with two pairs of metal/non-metal was tested separately to check the enhanced visible light activity of doped $NaNbO_3$. Metal atoms (Mo or Cr) replaced the Nb from the lattice while the O was replaced by nearest Nitrogen atom. Analysis and calculations revealed that monodoping of different dopants and co doping of Cr-N are inappropriate for photocatalytic decomposition of water under visible light because the defects formed due to dopants are above the fermi level so they cannot act as charge trapping sites thus resulting to increased rate of recombination. While, the co-doping of Mo-N proved to be an appropriate dopant as it reduced the band gap by creating different energy levels. Whereas the band gap reduction is dependent on the concentration of dopant material. Mo-N doped $NaNbO_3$ have overall enhanced water splitting ability and a promising photocatalyst for pollutant degradation ([107]).

2.4 Metal doping

Doping in the semiconductors mostly become a reason to point defects which introduces the levels or states near, above or below the valence and conduction bands which are identified and calculated by different analysis. When the metal is incorporated in a lattice, it is doped in the form of metal ion which produces a band or energy level in the forbidden energy area thus rendering the photocatalyst able to absorb visible light irradiation. Additionally, doped metal in the form of metal ion can change the equilibrium concentration of charge carriers by acting as an electron acceptor. Thus, increasing the overall quantum efficiency of the photocatalytic process [108]. The doping of semiconductors with metals/metallic ions has also been investigated in recent decades using many procedures including sol-gel, hydrothermal, solvothermal processes, etc. (as discussed earlier). Photocatalysts can be doped with transition metals like Fe, Cr, Mn, W, Ru, Rh, low cost, non-noble
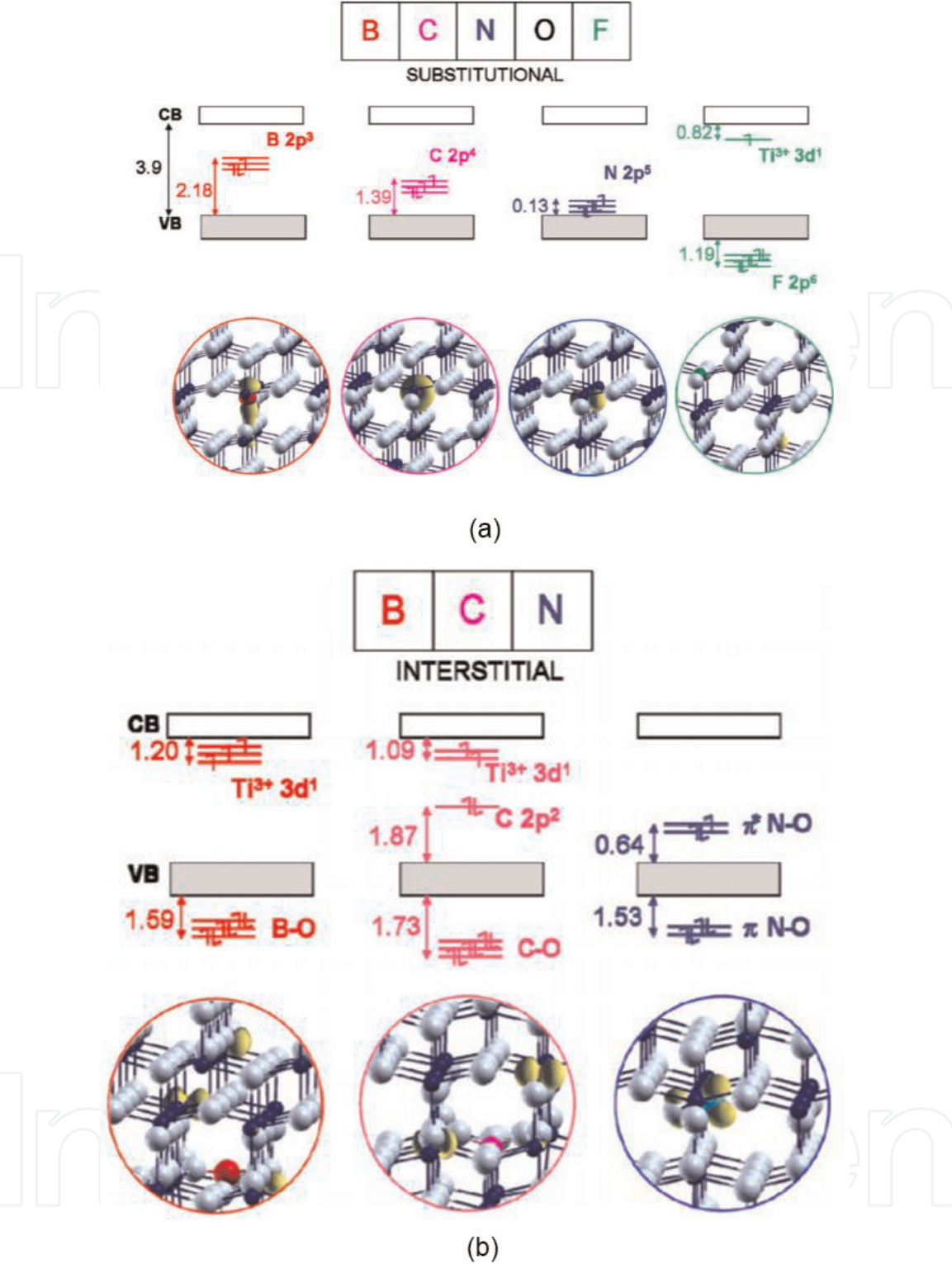
Figure 12.
Schematic illustration of positions of non-metals as dopants in the TiO$_2$ lattice. The effect of electronic structure of replacing O with B, C, N and F at substitutional and interstitial positions is considered; (a) doping of B, C and N atoms at substitutional positions results in magnetic impurities whose energy levels fall in the mid of energy gap. B sits high in the bandgap and N produces a state just above the VB while F being very electronegative occupies the state below O$_2$P of VB resulting the formation of TiO^{3+} ions; (b) at interstitial position, B behaves as a donor with the formation of B^{3+} and Ti^{3+}, carbon donates only two electrons and forma C^{2+}, nitrogen forms bond with O in lattice and does not donate electrons to host atom [106].

transition and earth abundant metals like Co, Cu, Ni and the noble metals like Pt, Au and Ag.

Preparation of **iron** doped TiO$_2$ thin films for the photocatalytic degradation of *Rhodamine B* has been reported by using reactive magnetron sputtering method having microscope slide as substrate and 99.99% pure TiO$_2$ as target and thin film

was prepared by fixing pressure and flow rate. During the preparation of TiO_2 thin films, 99.9% iron pieces was placed on TiO_2 target to produce the doped plate the color of titanium dioxide film changed from light white to dark yellowish indicating the increasing concentration of iron. Analysis depicted as the concentration of Fe was increased, the wavelength of Fe-doped TiO_2 shifted to red due to excitation of Fe^{3+} electron to the conduction band. As prepared doped film was tested for the photocatalytic activity in comparison with undoped thin film and the degradation of rhB was observed under visible light on the doped thin film. The photocatalytic degradation rates of rhB was decreased surprisingly on the highly Fe-doped TiO_2 plates ([109]). **Vanadium** doped TiO_2 was prepared by sol-gel method with the objective to increase visible light response of TiO_2 having V^{4+} substituted at Ti^{4+} place in the lattice using vanadyl acetylacetonate, acetic acid and titanium butoxide as precursors followed by hydrolysis and calcination at 400°C. Analysis revealed that vanadium was highly dispersed inside the lattice and presented the red-shift, as prepared catalyst was used to degrade crystal violet (CV) and methylene blue (MB) under visible light irradiation which was higher than those of undoped powders [110].

Co-doping of N-doped TiO_2 with metals like **Sn** and **Zn** for enhanced activity under visible has been investigated and it is emerging as a promising approach to increase the photocatalytic ability of semiconductors because of synergistic effects in visible light absorption. Zn and Sn was compared for photocatalytic activity by doping with N (N + Zn and N + Sn), having tetracycline as a target pollutant. Different analysis (XRPD, HRTEM, XPS, EDX, and BET) for different calculations revealed that Sn and Zn modification directed to morphological, structural and surface changes, Sn was substituted at Ti site while Zn changed the lattice morphology. It was also determined that catalysts shown different performances in terms of light absorption, as Sn modified sample gave slight red shift by formation of intra-gap states and shown the absorption of light in range of 400–600 nm while Zn modification reduced the band gap by showing detrimental effect to crystallinity and creating surface defects [111].

Radio frequency (RF) sputtering technique was used to deposit **Ag** and ZnO nanoparticle on a substrate at different temperatures on a fixed pressure. Ag and ZnO having high purity of 99.999% targets were used as depositing materials and three different thin films were prepared depending on the substrate temperatures as shown in **Figure 13**. Characterization and analysis revealed the equal distribution of Ag nanoparticles within ZnO matrix, the band gap of the prepared nanoparticles was ranging between 2.7 and 3.1 eV while the pure ZnO has band gap of 3.37 eV. Photocatalytic degradation of 2-CP was tested by using prepared thin films by varying experimental parameters, results determined the enhanced photocatalytic activity of Ag/ZnO as compared to pure ZnO, reason for enhanced photocatalytic activity was the presence of Ag at the surface of film which acted as scavenger for an excited electron. The film prepared at substrate having highest temperature presented stability even after 4 cycles with only 8.7% efficiency loss [112]. Yayapao et al. prepared the undoped and Nd-doped ZnO nanoneedles using ultrasonic assisted solution method by varying the percentages of doped metal. Nd-ZnO nanoneedles gave the best results for the concentration of 1% Nd which was 50 nm in diameter and 3–4 μm long, gave performance about 2.5 times more as compared to the undoped ZnO. Analysis determined the presence of doped Nd^{3+} ions in lattice, which during photocatalysis acted as an electron scavenger and inhibited the process of recombination and promoted the photocatalytic activity by production of $O_2^{\bullet-}$ [113].

Undoped and **Ho**-doped ZnO 3D microstructures were prepared using a sonochemical method having zinc nitrate hexahydrate ($Zn(NO_3)_2 \cdot 6H_2O$), holmium
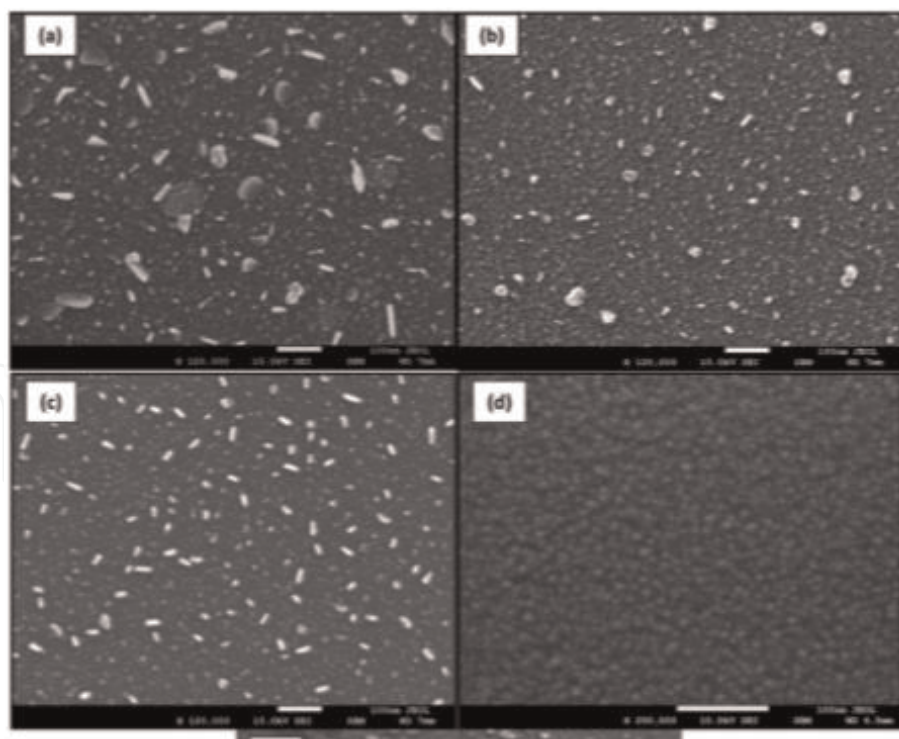
Figure 13.
SEM images of Ag/ZnO thin film co-sputtered at different temperatures (a) Room temperature, (b) 50 C, (c) 100 C and (d) Pure ZnO [112].

nitrate hexahydrate ($Ho(NO_3)_3 \cdot 6H_2O$) as precursors. The dopant concentration was varied from 0 to 3% after the sonication of 5 h the precipitate was washed and characterized. The flower like structure (**Figure 14**) gave the improved photocatalytic activity for the degradation of methylene blue (due to the production of non-selective oxidants) at λ 664 nm. The formation of Ho^{3+} ions at the dopant concentration of 3%, which acted as electron scavenger [114]. Similar positive results were reported by doping of La^{3+} and Sm^{3+} into ZnO lattice for the degradation of 4-nitrophenol in wastewater [115].

For **Copper** doped $BiVO_4$, the monoclinic crystal lattice ($mBiVO_4$) shown the efficient charge carrying capacity due to its smaller effective mass as compared to Ag and Au, which is promising for higher mobility of electrons and holes. In this system the substitution of Cu 3d states at the Bi sites reduces the band gap and also act as an electron acceptor produced by photoexcitation. This doped catalyst has shown the red shift which meant it enhanced the solar light absorbance and utilization, the system has overall great water splitting capacity [116].

Besides TiO_2 and ZnO, **WO₃** is also a promising semiconductor found to degrade the pollutants in water due to its photocatalytic activity with the band gap of 2.8 eV. Despite of short band gap, it can absorb only small portion of visible light. The photocatalytic activity of WO_3 was found to be amplified in the occurrence of dopant. WO_3 was doped with different metal ions using different precursors, each precursor was mixed vigorously with WO_3 to ensure the homogenous mixing followed by the drying and calcination for 4 h at 550°C, the final product was prepared after cooling and grounding of powder. Analysis confirmed the presence of different ions like Mg^{2+}, Al^{3+}, In^{3+}, Fe^{3+}, and Zr^{4+} on the interstitial positions in the WO_3 lattice. Doped SC gave significance change in the photocatalytic property in comparison to pristine WO_3 [117]. Palladium doped WO_3 was used to remove Geosmin (GSM) from the wastewater. Nanocatalyst was prepared by mechanical mixing in a ceramic mortar having Pd and WO_3 powder as a precursor, analysis revealed the size of Pd nanoparticles of about 10 nm which was dispersed evenly on

the surface of WO_3, the photocatalytic degradation was done by spiking of GSM and catalyst in a solution with water (**Figure 15**). Oxidative species analysis depicted that $OH^\bullet$ was dominant oxidative specie. Degradation rate in initial 5 min was 75% indicating higher degradation rate. While in next 20 min the degradation rate was more than 99%, as the amount was catalyst increased gradually. The degradation rate decreased mainly due to the accumulation/agglomeration of catalyst and turbid environment caused hindrance to light penetration. The stability of Pd-WO$_3$ nanocatalyst was tested which retained 94% stability even after the fourth cycle which suggested its reusability for the GSM degradation [118].
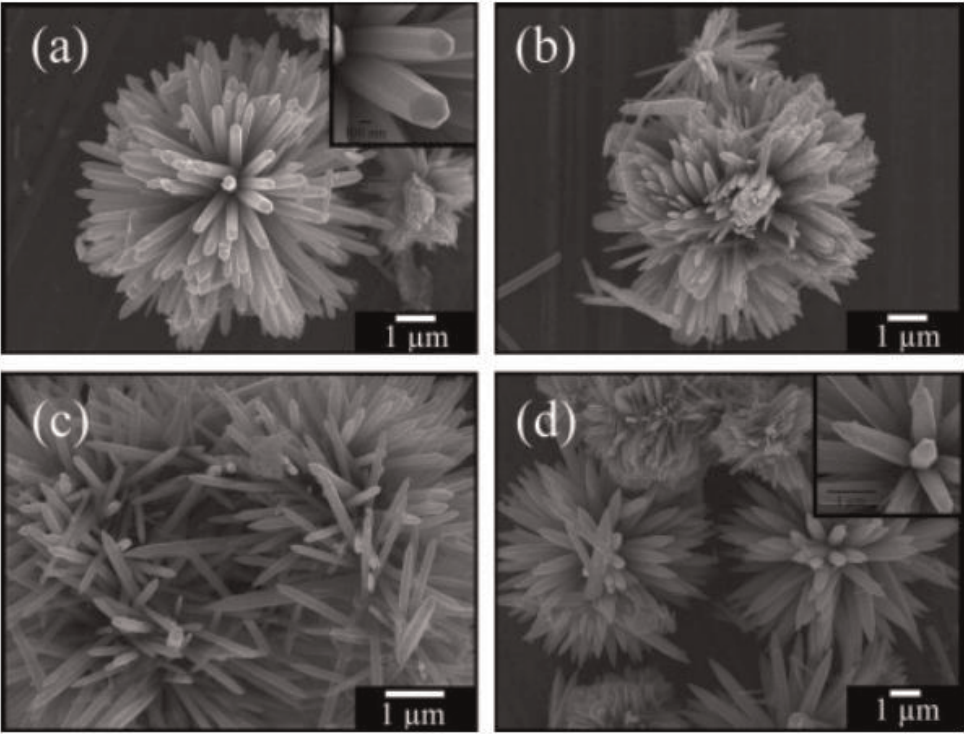

Figure 14.
SEM image of holmium doped ZnO microstructures with (a) 0%, (b) 1%, (c) 2% and (d) 3% of HO having100–400 nm diameter and length of several micrometers [114].
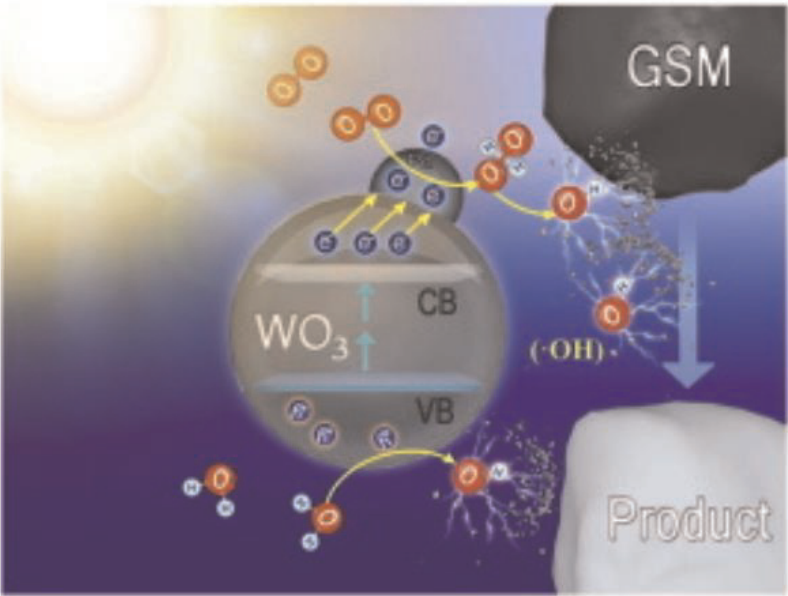

Figure 15.
Photocatalytic degradation of GSM under VL using novel catalyst [118].

Electronic, geometric and optical properties of **chromium** doped $SrTiO_3$ has been studied by Wei et al. by using DFT with GGA scheme. Results revealed that in Cr-doped $SrTiO_3$ structure the VBs did not suffer from any change while the bottom of CB shown a little rise. Cr substituted in lattice at the site of Sr. as Cr^{3+} while band structure and DOS analysis shown that there were also some Cr 3d gap states appeared near the bottom of CB. While Cr substituted at the site of Ti^{4+} was doped as Cr^{6+}. So the results indicated that doped chromium partially take up Sr. and partially Ti, Cr dopants at Cr-Sr site has higher photocatalytic activity as compared to the photoactivity at Cr-Ti dopants sites. Similarly the $SrTiO_3$ doped with less concentrate on of dopant shown less photocatalytic activity and less absorption of visible light and vice versa [119].
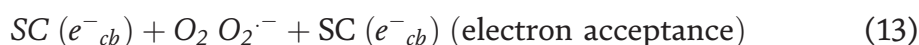
Dysprosium doped WO_3 nanopowders were prepared using $Na_2WO_4 \cdot 2H_2O$ and CTAB as precursors followed by a hydrothermal treatment at 80°C for 1 week. The resulting precipitate was centrifuged and calcined to obtain Dy-doped material. Analysis revealed that metal was doped as Dy^{3+} which acted as an electron donor to the adsorbed O_2 to make superoxide radical and Dy^{4+}, dopant ion also reduced recombination rate by accepting the exciting electron and formed Dy^{3+}, nanopowders showed high photocatalytic activity for the degradation of rohdamine B (rhB) which was used as target pollutant [120]. **Gallium**, a post transition metal has been shown to dope semiconductors. Li et al. have reported the increased charge separation and photocatalytic activity by Ga-doped SnO_2 in different molar ratios varying from 1 to 4%, using $SnCl_4$, $Ga(NO_3)_3$ and HNO_3 as precursors followed by drying and baking at 573 K for 2 h. The resulting product was Ga-doped SnO_2, analysis confirmed the presence of Ga as Ga^{3+} and shifted the absorption spectra towards blue region. To understand the charge separation, production of reactive species and photocatalytic efficiency methyl orange (MO) was used as a target pollutant, mainly due to the formation of $OH^\bullet$ MO was photocatalytically decolorized [121, 122].

Hu et al. reported the band gap-tunable K-doped g-C_3N_4 which had enhanced mineralization capacity, using dicyandiamide monomer and potassium hydrate as precursors followed by mixing, heating and annealing. SEM, TEM, FTIR, XRD and XPS analysis were used for the characterization and catalyst was used for the degradation of organic rhB under visible light and showed 6.5 times greater photocatalytic activity as compared to pristine gCN as it gave 70% decomposition during the irradiation time of 120 min [123]. Tungsten doped porous g-C_3N_4 was synthesized by hydrothermal method using urea, dicyandiamide and $Na_2WO_4.2H_2O$ as precursors and catalysts with varying molar ratios of precursors were prepared and the catalyst W5/PGCN (P stands for porous) gave the highest photocatalytic activity due to separation of charges and shown 99.6% degradation of MO under visible light (λ = 400–420 nm) for the irradiation time of 60 min and 100% in 70 min [124]. Beside W, other transition metals like Yttrium ([125]), Iron [126], Eu, Zr [17], etc. doped gCN for the increased photocatalytic activity has also been reported in literature.

3. Dye sensitized VLA semiconductors

Dye photosensitizations have been reported by different scientists being a most operative mode to increase the response of semiconductors for visible light. Sensitization has been used for different approaches, from development of solar cells to degradation of pollutants in water. Many dyes like erythrosine B, eosin, rose bengal, rhodamine B, cresyl violet, thionine, chlorophyllin, anthracene-9-carboxylic acid, porphyrins, phthalocyanines and carbocyanines have been reported for their work

as sensitizers, in addition to these organic dyes some inorganic dyes and coordination metal complexes are also reported. Inorganic sensitizers are basically the semiconductors with smaller band gap which are highly stable to photodegradation or photocorrosion. Their smaller band gap gives the light absorption at the wider wavelength region and examples are Mn, Fe, Ni, V, and Cr [127]. The principle of sensitization for photodegradation of pollutants is "an electron in a sensitizer molecule under visible light (as dyes have conjugate system that absorbs visible light) is excited (from HOMO to LUMO) to its conduction band from where it jumps quickly to the conduction band of attached semiconductor oxide and dye itself changed into its cationic radical and SC's CB act as an electron mediator where it is accepted by oxygen, thus starting the oxidations reactions by forming superoxide and OOH$^\bullet$, which are then converted to OH$^\bullet$ for the degradation of pollutants"[12]. A main limitation/drawback of sensitization with an organic dye is its steady decomposition because of photocatalytic degradation due to its natural capacity to undergo redox reactions by donating its electrons, to dodge this limitation the addition of sacrificial electron donor is possible like the incorporation of EDTA and TEOA (triethanolamine) will improve the stability of dye. In a dye sensitized process the dye can be used as both a sensitizer or a substrate to be degraded in order to decolorize water [128]. The general mechanism for dye sensitized process for example rhB is given as:

$$rhB\,(ads) + hv\,(554\,nm)\,rhB* \,(\text{excitation of dye electron}) \tag{11}$$

$$rhB* + SC\,rhB^{\cdot+} + SC\,(e^-_{\,cb})\,(\text{electron 3 transfer to SC}) \tag{12}$$

$$SC\,(e^-_{\,cb}) + O_2\,O_2^{\cdot-} + SC\,(e^-_{\,cb})\,(\text{electron acceptance}) \tag{13}$$

$$rhB^{\cdot+} + O_2^{\cdot-}\,CO_2 + H_2O\,(\text{mineralization process}) \tag{14}$$

Many organic dyes have been tested for their excellent sensitizing ability to semiconductors like TiO_2. Degradation of phenylurea herbicide monuron has been reported by using riboflavin-assisted photosensitization, an enhanced photodegradation effect was observed as compared to direct photolysis [129], degradation of micosporine like amino acids (small secondary metabolites produced by organisms that live in environments with high volumes of sunlight, usually marine environments by some type of algae) was observed by using rose bengal and riboflavin sensitizers [130]. Degradation of dye named reactive red 198 has been reported under visible light irradiation by using dye sensitized TiO_2 activated by ultrasound, degradation rates were analysed by varying experimental parameters like initial concentration, pH and catalyst loading, the singlet oxygen and superoxide radical were found as dominant oxidative species which also degraded the produced intermediates like phenols. The results determined that a conventional dye can be used as a photosensitizer of TiO_2 functioning under visible light [131]. A study investigated the application of TiO_2 sensitized by tris(4,4'-dicarboxy-2,2'-bipyridyl) ruthenium(II) complex for CCl_4 deprivation under visible light irradiation. The transferred electrons to the CB of TiO_2 from the excited complex molecule decomposed CCl_4 at $\lambda > 420$ nm, experiment in the absence of TiO_2 revealed that there was no direct transfer between excited sensitizer complex molecule and pollutant, results also determined that sensitizing complex undergo redox reaction and photodegradation decreased in the absence of sacrificial electron donor which restore the Ru^{II} complex which undergo continuous oxidations by electron transfer, to avoid this problem different types of alcohols can be used but 2-propanol was used for Ru^{II}L3/TiO_2/CCl_4, in this process CCl_4 was decomposed in CCl_3 and Cl$^-$ [132].

4. Heterostructures/heterojunctions/nano-composites

Construction of heterojunctions or nanocomposites is a method to increase the charge separation and to increase the absorption towards visible light region in the solar spectrum. As discussed above, the increased charge separation will reduce recombination resulting in increased production of reactive oxidizing species leading to enhanced degradation of contaminants in water and wastewater treatment. The crystal lattice structure at the point of interface or junction plays an important role in tailoring the photocatalytic properties or quantum efficiency of the photocatalyst. A difference in the lattice spacing of two SC crystals cause the lattice mismatch at junction point which is the reason for defects formation which act as excited electron sink and lessens the electron hole fusion [133]. Careful selection of semiconductor material is required with respect to band edge positions. The band edge positions of widely used semiconductors are given in **Figure 16**. The traits for ideal nano-heterostructures which have to be used for photocatalytic processes are; (i) it should have large surface area and contain enough active sites; (ii) it should have high light absorption capacity to make efficient use of solar spectrum; (iii) there should be an effective separation of charge carriers in order to produce active radicals for pollutant degradation; while a co-catalyst in heterostructure should have ability to enhance the reaction rate, provide active sites and should act as electron scavengers [134]. Due to their increasing demand for the degradation of pollutants controllable fabrication of heterostructures/nano-composites is possible, the different techniques which are being used over decades are chemical vapor deposition, chemical deposition, electrodeposition, etc. By using these techniques different types of heterostructures (capped and coupled) such as nano-composites, nano-rods, nano-sheets, nano-wires and core-shells (capped) structures have been reported. In comparison to single/alone SC the heterojunctions like CdS/TiO_2, CdS/ZnO, $ZnSe/ZnO$, ZnS/ZnO, SnO_2/CdS, Bi_2S_3/TiO_2 and some ternary composites like $Fe_3O_4/SiO_2/TiO_2$, $ZnO/TiO_2/CuO$, etc. have been reported.

The heterojunction which are made by the combination of two or more nanocystalline semiconductors are very fruitful for photocatalysis regarding pollutant degradation and water splitting and being very famous as the Z-scheme process. Two main benefits of linking two or more semiconductors are (i) coupling of semiconductor having larger band gap with the semiconductor having smaller one, amplifies the photo response acting as a sensitizer; (ii) recombination is avoided by the transfer of excited electron in the low lying CB of SC bearing larger band gap [135]. So, it is crucial to find a suitable sensitizer for a semiconductor having larger band gap to get enhanced photocatalytic activity under visible light.
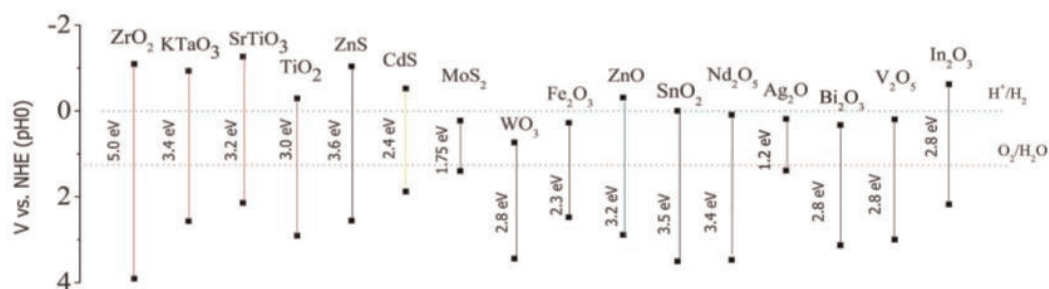

Figure 16.
Band gaps of different semiconductors with respect to NHE [17].

4.1 Some TiO$_2$-based heterostructures/nanocomposites

CdS is an attractive semiconductor with a smaller band gap of 2.4 eV, which means it can be activated under visible irradiation. The drawback to this and some other semiconductors having smaller band gaps is their unstability against photocorrosion. To avoid this problem, this type of semiconductors are coupled with those which have larger band gap like ZnO, ZrO$_2$, TiO$_2$, etc. and play a vital role in improving charge separation. As mentioned above there are many strategies to prepare the heterostructures and one is micro-emulsion method. CdS nanoparticles were coupled with TiO$_2$ via micro-emulsion method under ultrasonic irradiation for the formation of core-shell type of nanostructure with uniformed coating of TiO$_2$ nanoparticles on CdS, the depth of TiO$_2$ shell was in range from 1.4 to 2.3 nm which could be controlled by varying the preparation temperature and precursors concentration. The nanostructure gave the red-shift in spectra which is typical trait of core-shell heterojunction [136]. Another TiO$_2$/CdS core-shell nano-rod heterostructure was obtained by chemical bath deposition method, TiO$_2$ core was prepared firstly by the hydrothermal method and was converted to substrate for the deposition of CdS nanoparticles by dipping it an aqueous bath having 10 ml 0.02 M CdCl$_2$.2.5H$_2$O, 10 ml 0.2 M CH$_4$N$_2$S, 10 ml of 1.5 M NH$_4$NO$_3$ and 10 ml 0.5 M KOH to adsorb CdS nanoparticles on TiO$_2$ rod at 85°C. The resulting structure gave the highest charge separation (**Figure 17**) efficiency at incident wavelength of 500 nm [137].

A thin film heterostructure of copper zinc tin sulfide (Cu$_2$ZnSnS$_4$)-TiO$_2$ was prepared by combining an *n*-type (TiO$_2$) and *p*-type (CZTS) heterostructure. To confirm the formation of visible light active photocatalyst it is suggested that the highly stable semiconductor with higher band gap like TiO$_2$ should be present at most upper/outer layer in the heterostructure which will protect the
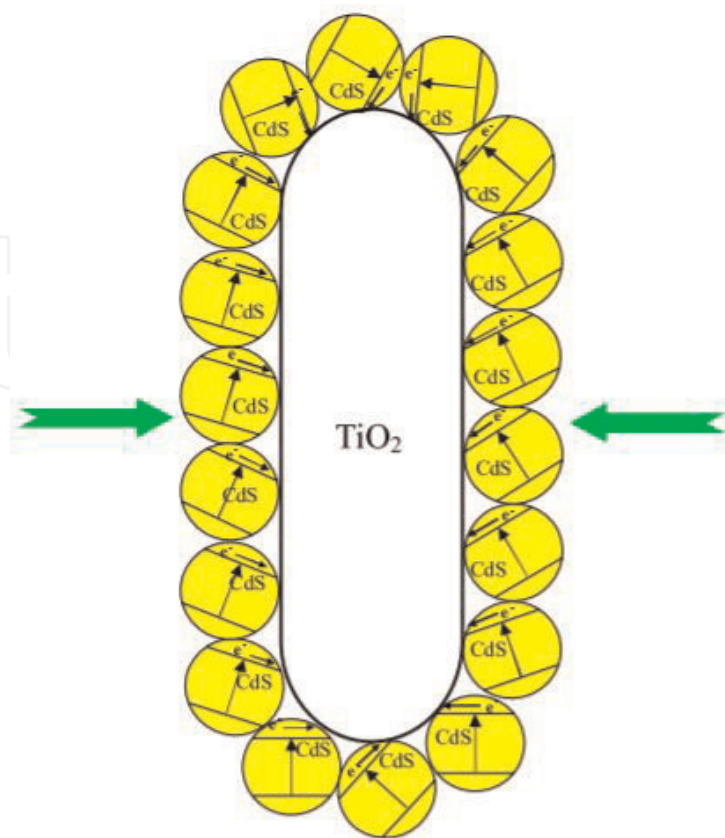

Figure 17.
Scheme illustrating charge injection from excited CdS nanoparticles to TiO$_2$ rod [137].

semiconductors having smaller band gap to come in direct contact with wastewater/water in order to avoid physical or chemical reactions and to absorb penetrated light. In the present study the thickness of outer layers of TiO_2 was varied by changing the concentration of precursor ($TiCl_4$ 0.1 and 0.05 M) and two types of catalysts also tested for photoactivity, uniform crystallinity depended on the thickness of the TiO_2 film. The schematic illustration of photodegradation mechanism is given in **Figure 18**. Analysis like TEM, SEM and EDX discovered the presence of multiple TiO_2 aggregates on the surface of CZTS thin films which have band gap of 1.46 eV. The catalyst prepared from 0.05 M solution exhibited poor Cu and enhanced Zn deposition which led to enhanced charge separation in the composite. Methylene blue dye was degraded under visible light by 0.1 M sample and shown efficiency of 43.50% while 0.05 M sample gave 35.7% removal under wavelength of 400–700 nm. In dark conditions TiO_2-CZTS of 0.05 M gave efficiency of 29.81% after 8 h [138].

Recently, the preparation of magnetic core-shell-shell heterostructure nanocomposite of $Fe_3O_4/SiO_2/TiO_2$ has been reported for the degradation of 2-CP in unreal wastewater under UV irradiation. Catalyst was prepared by three steps-facile synthesis process. Analysis was performed for surface morphology, chemical properties and for crystal structure. The size of NPs of magnetic core was 24.0 nm and that of magnetic shell-shell was 70.2 nm. Experiments were performed by varying the experimental parameters like pH, catalyst loading and pollutant concentration; results determined that effective degradation was pH dependant. Catalyst was regenerated after use by placing magnet under reaction container and retained its efficiency about 60% even after 3 cycles of use [139].

Another example of heterojunction is coupling of Ag_3PO_4 with TiO_2 to degrade the organic pollutants under visible light irradiation using silver nitrate, sodium phosphate and TiO_2 Degussa (P25) as precursors followed by in-situ precipitation method, by coupling the semiconductors the band gap reduced to 2.3–2.5 eV and shown a notable shift from UV region to visible spectra. Analysis confirmed the size of particles and uniform crystallinity 2-CP was selected as the target pollutant because this parent compounds and derivatives are being an emerging pollutant and
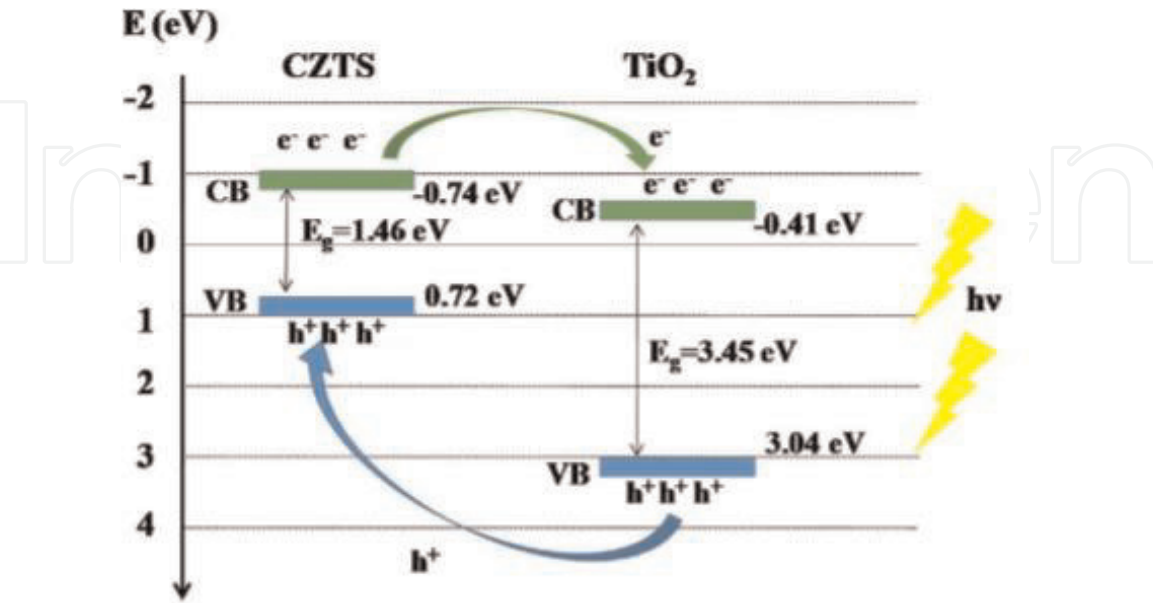
Figure 18.
Schematic illustration of charge separation in thin-film heterostructure; visible light passes through the upper layer of TiO₂ and penetrated in lower CZTS thin film electrons gets excited and transferred to the CB of TiO₂ creating and leaving the hole behind; electron in the VB of TiO₂ gets excited after exposure to UV light and hole produced diffuses to the VB of CZTS thus completing the circuit, while the holes at the VBs act as oxidants and electrons in CBs act as reductants to produce oxidizing species [138].

already in the POPs. Experiments were performed by changing the parameters like pH, catalyst loading and pollutant concentration. At low pH of 3 greater adsorption of pollutant was observed and maximum degradation was reported. The structure maintained its stability to 100% (**Figure 19**) even after 3 cycles of use with fresh 2-CP [112].

Pan et al. has reported a novel structure of TiO$_2$-ZnO nanocomposite spheres decorated with ZnO, this structure was prepared in order to increase the photocatalytic activity by improving charge separation in heterostructure. The composite was prepared by one-pot solvothermal method using tributyl titanate and zinc acetate as precursors and heating the mixed solution at 150°C for 24 h followed by calcination in air, as-prepared product was characterized. Surprisingly, by increasing to amount of Zn precursor the clusters of ZnO were produced on the surface of spheres (**Figure 20**). Analysis determined that prepared ZnO and TiO$_2$ had the particle size in spheres was about 4 nm and spheres' surface thickness was about 5 nm. It was also discovered that the clusters which decorated the spheres
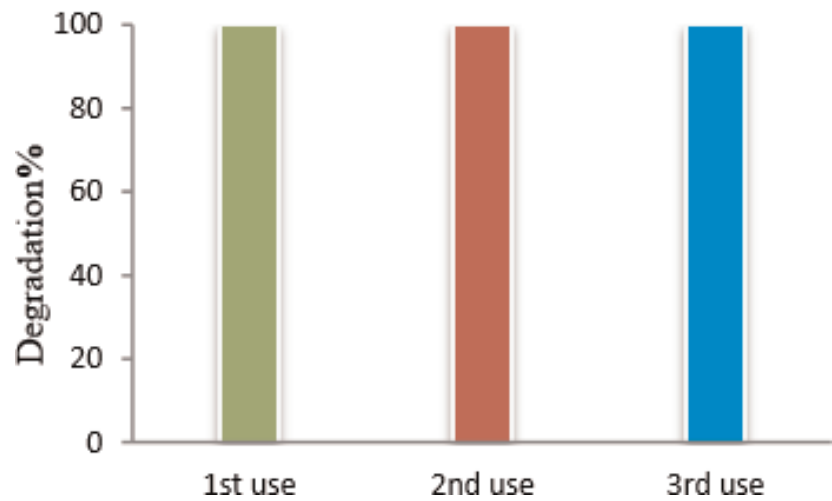

Figure 19.
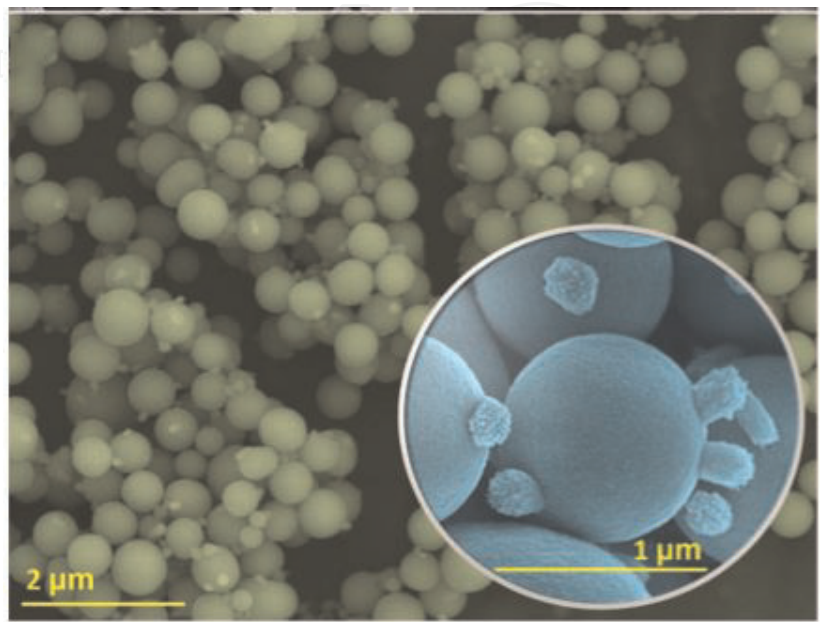*Retained catalytic stability even after 3 cycles of use with fresh 2-CP [112].*

Figure 20.
SEM image of TiO$_2$-ZnO-SC, showing the decorated clusters of ZnO on the TiO$_2$-ZnO nanocomposite [140].

only had Zn and O and did not have Ti atoms. PL spectra for composite indicated the increased charge transfer and separation as compared to pristine ZnO and TiO_2 due to presence of ZnO clusters acting as electron scavengers. To investigate the photocatalytic performance of ZnO-TiO_2-SC rohdamine B (rhB) degradation was tested, $OH^\bullet$ were reported to be the reactive specie, the activity of ZnO-TiO_2-SC for photodegradation was 2.3–2.8 times higher than that of pristine nanoparticles [140].

Stable preparation of core/shell nanocomposite of TiO_2/FeS_2 by solvothermal method has been reported for the photocatalytic production of hydrogen [141]. The benefits for incorporating different metal oxides/sulfides led to the structural and chemical modifications which render them better than that of parent materials. Rashid et al. has reported the formation of stable spherical nanocrystals of anatase-TiO_2/FeS_2 by following wet chemical process, for the degradation of organic pollutants under visible light using $FeSO_4.7H_2O$, $Na_2S_2O_3$ and $TiCl_4$ as precursors. Micrographs and other analysis determined the morphology, chemical properties, crystal structure, oxidation states and band gap positions which was 2.67 eV for the composite and gave the red shift in spectra. The photocatalytic activity of FeS_2 and TiO_2 was tested alone and also for composite but the photoactivity of nanocrystal composite for the degradation of methylene blue, was much higher than that of pristine compounds. Experiments were performed by varying the parameters like pH, catalyst dose and pollutant concentration. Composite was found to be much stable as it shown only 9% loss in photocatalytic activity after 3 cycles of use [142].

Among venedates, bismuth vanadate and indium vanadate have gained much respect mainly due to stability, nontoxicity and photocatalytic activity under visible light ($\lambda > 420$ nm) in coupled or single conditions. For coupled semiconductor heterostructure of $TiO_2/InVO_4$, $InVO_4$ was prepared using organic precursor method and was incorporated with TiO_2 by grinding, the catalyst shown higher photocatalytic degradation of 2-CP under visible light as compared to TiO_2 alone. Among different conditions the best condition for degradation were found at 5pH in 1 g/L of catalyst and 50 mg/L of pollutant with irradiation time of 180 min [143, 144]. Li et al. has reported the unique structure of TiO_2 incorporated on the polymethyl methacrylate (PMMA) nanofibers for the degradation of pollutants under the UV irradiation. The TiO_2 nanoparticles were supported on fibers by the hydrothermal treatment at 135°C for 8 h using titanium n-butoxide and PMMA nanofibers as precursors. Analysis indicated that about 42% of tetragonal anatase TiO_2 particles were adsorbed on the surface of fibers (**Figure 21**). Methylene orange was used as model pollutant and its complete degradation was observed after 50 min using 0.1 g of catalyst for 10 mg/L of pollutant. This good photocatalytic activity could be attributed to the (i) decoration of TiO_2 nanoparticles on the PMMA fibers which assisted the adsorption of pollutants and helped them to come in contact with photocatalyst; (ii) high quantity of adsorbed TiO_2 provides numerous action sites for the degradation of pollutants. Catalyst revealed the efficiency of about 94.4% even at the end of fifth cycle for the degradation of fresh MO which determined the stability and reusability of catalyst [145].

A novel nanocomposite of $BiOBr/TiO_2$ has been reported and prepared for the first time with facile acid assisted precipitation method by using TTIP, KBr and $((BiNO_3)_3.5H_2O)$ as precursors. Catalysts of different percentages were prepared by using different molar ratios of TiO_2 as a base material and 15% $BiOBr/TiO_2$ behaved as an active catalyst. Analysis and characterization revealed the perfect structural integrity, increased surface area and increased absorption of light because of the formation of nanoscale layered butterfly like clustal structures with each flake having the broad absorption spectrum of about 500–800 nm with <50 nm thickness (**Figure 22**). PL spectral analysis determined the band gap of 2.81 eV and wavelength was observed from 480 to 570 nm for 15% $BiOBr/TiO_2$ and it gave the
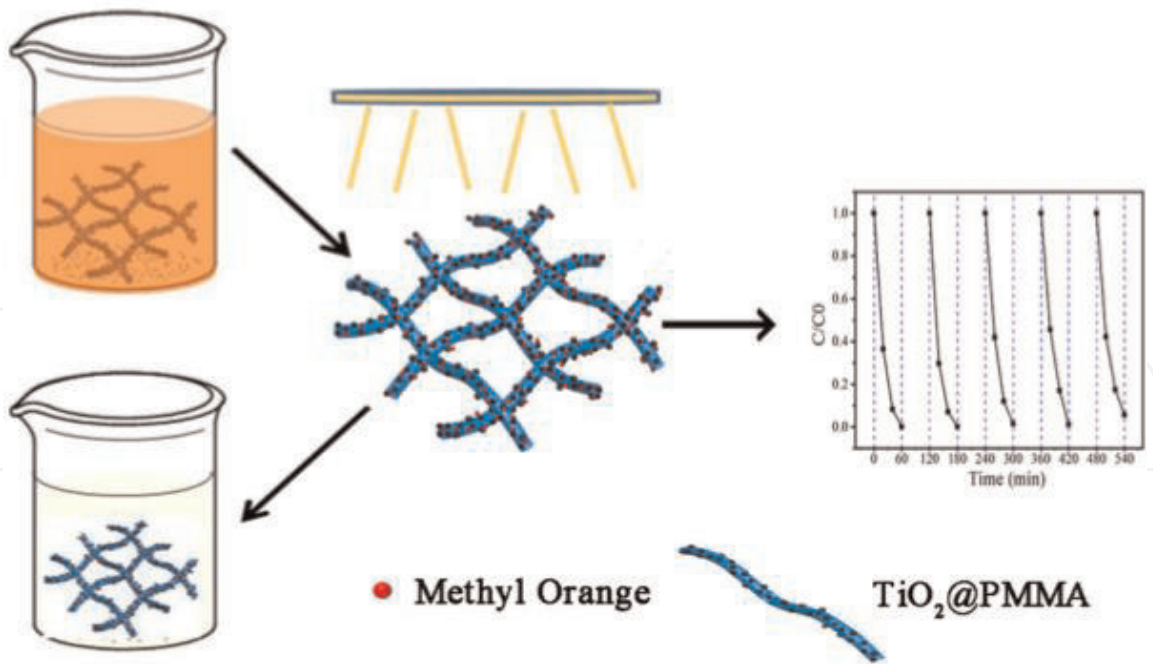
Figure 21.
Schematic illustration of formation of PMMA fibers and their photoactivity [145].

degradation of aqueous ciprofloxacin (target pollutant) under visible light at
$\lambda > 420$ nm about 92.5% and under direct sunlight it gave 100% degradation
utilizing reaction time of 2.5 h. Radical scavenging study indicated that besides
superoxide radicals and holes the OH$^\bullet$ had dominant effect on net photodegradation
process. Results also suggested that the catalyst was 9.4 and 5.2 times active in
degradation than pristine BiOBr and TiO$_2$, reusability experiments determined the
high stability of catalyst as it suffered loss of only 12% even after 5 cycles of fresh
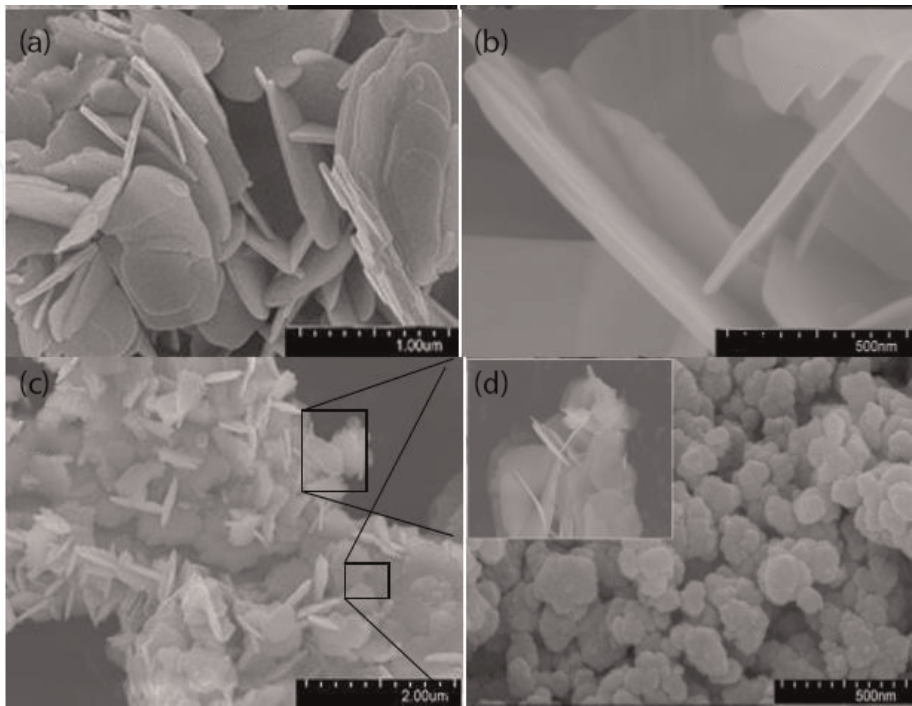CIP degradation [146].

Figure 22.
SEM images of (a, b) pristine BiOBr; and (c, d) 15%BiOBr/TiO$_2$ nanocomposite.

4.2 Heterostructures/nanocomposites of different SCs

In addition to TiO_2 there are numerous semiconductors which can be coupled with other SC and can be incorporated into heterostructures or composites like WO_3, ZnO, $BiVO_4$, ZnSe, C_3N_4, In_2O_3, CuS, MoS, Cu_2O and many more. So another example of inorganic heterostructure is the template free simple synthesis of CdS-ZnO nanocomposites. This self-assembled flower like structure resulted from coupling of two SCs which increased the charge separation and demonstrated greater photocatalytic activity. The average size of flower was 400 nm with the petal size of 100–150 nm and the rod among petals had the size of 10 nm, band gap of composite was analyzed to be 2.19 eV and absorption wavelength of 561 nm was reported. The composite gave the photodegradation of rhB about 90% in 190 min under solar light and 24% in dark. The scheme of process of particles is shown in (**Figure 23**) [147].

Cho et al. prepared three different types of 3D ZnSe/ZnO heterostructures by simple solution-based surface modification reactions. Three different types of heterostructures demonstrated higher photocatalytic activities by exhibiting absorption in visible region (at λ > 486 nm) as compared to pure 3D ZnSe and ZnO structures, the visible light activity of heterostructures varied according to the crystal structures. As shown in (**Figure 24**) the CB of ZnO is in between the CB and VB of ZnSe showing the type II band alignment, before exposure to sunlight the catalysts and orange II (targeted pollutant) were kept at stirring for 30 min in dark to attain an equilibrium for adsorption and desorption, upon exposure to visible light the e^-/h^+ pair was generated in ZnSe crystal, electron transferred to the CB of ZnO to reduce oxygen and holes could oxidize either the water or OH ion or directly oxidize the orange II, ended with the mineralization of organic compound [148].

Zeyan et al. has produced the In_2O_3/ZnO heteronanostructures by the co-precipitation method having average size of 40–60 nm by using the respective precursors. The composite was annealed at different temperatures ranging from 600 to 1000°C, among changed compositions and annealing temperatures the highest photocatalytic activity for the degradation of methylene blue was shown by the composite annealed at 800°C with In/Zn molar ratio of 1:1 and the maximum absorption was about λ = 663 nm. A p-n junction was established at the SCs interface and presence of Zn^{2+} and In^{3+} was reported in lattice, that enhanced the charge separation and production of $OH^\bullet$ and $O_2^{\bullet-}$ attributed as the main reason for enhanced photocatalytic activity semiconductor coupling ([149]). Coupling of
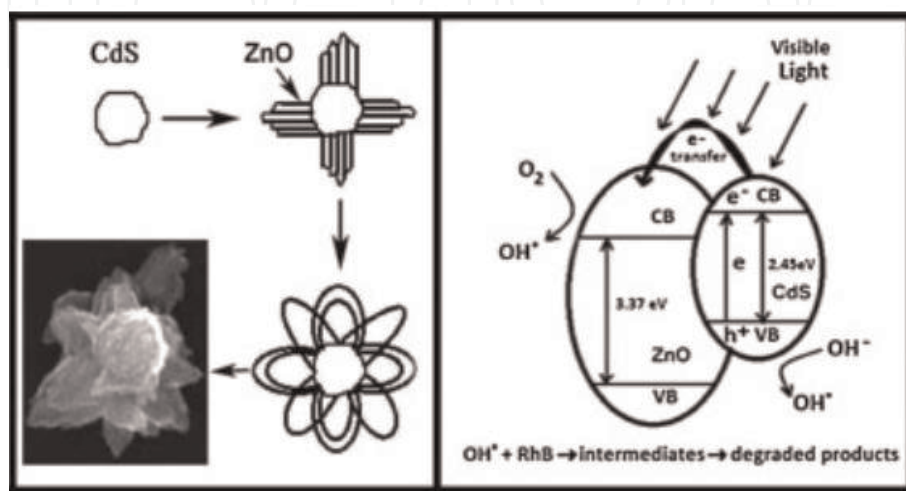

Figure 23.
Structure of flower shaped nanocomposite and admirable charge transfer due to heterostructure formation [147].
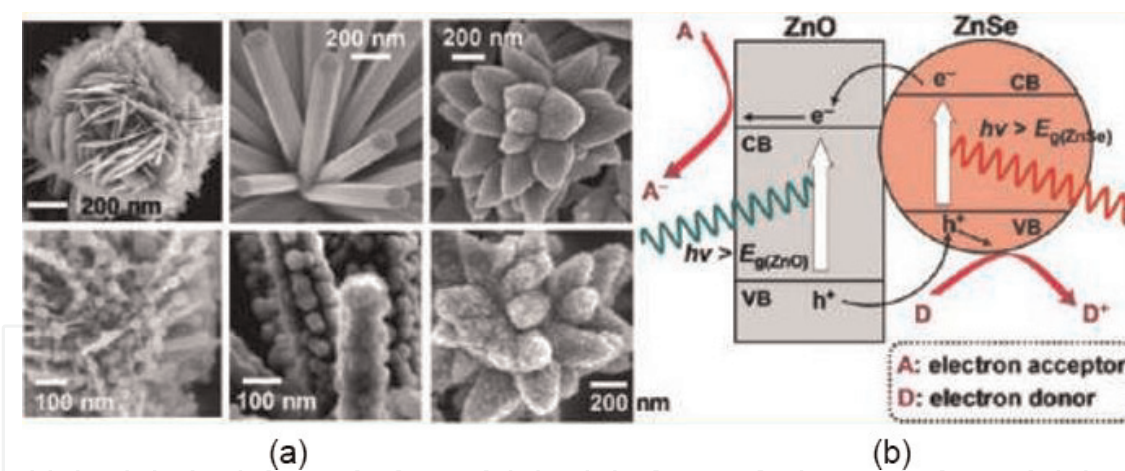
Figure 24.
(a) SEM images of different 3D ZnO/ZnSe heterostructures and; (b) schematic diagram of charge separation by coupling of two SCs [148].

mixed oxide SC with metal oxide has also been reported and have shown some modified properties, example for this type of heterojunction is the nanocomposite of $ZnO-ZnWO_4$ (both are the n-type SCs) prepared by the sol-gel method and was analysed by XRD, BET, SEM and TEM. The nanocomposites were prepared by varying the molar ratio of ZnO and $ZnWO_4$ to study the influence of molarity on photoactivity and $Zn-ZW_{0.25}$ calcined for 2 h at 600°C shown greater photodegradation of 4-nitrophenol (target pollutant). The band gaps for ZnO and $ZnWO_4$ was calculated to be 3.21 and 3.14 eV, when the nanocomposite was exposed to UV light the electron transferred from the CB of ZnO (E_{CB} = −0.36 eV) to CB of $ZnWO_4$ (E_{CB} = −0.14 eV) due to difference in the position of CBs (from cathodic to anodic condition) and same behaviour was proposed for hole to transfer from VB of $ZnWO_4$ (E_{VB} = 3.00 eV) to VB of ZnO (E_{VB} = 2.84 eV), thus enhancing the charge separation and completion of circuit due to formation of heterostructures which resulted from the mixing of two SCs with dissimilar energy levels of VB and CB [150]. In addition to the above mentioned heterostructures other structures like nanorods, nano sheets, nanowires, CdSe/ZnO, CdsSe/ZnO [17], TiO_2/ZnO [151], CuS/ZnO [152] has also been found to enhance visible light activity either for pollutant degradation, overall water splitting or hydrogen production.

BiOCl/BiVO$_4$, another novel p-n heterostructure of coupled semiconductors with type II band alignment was prepared by hydrothermal method for the decomposition of methyl orange under visible light irradiation having ability for active separation of charges (**Figure 25**), the powders were prepared by using NH_4VO_3, $Bi(NO_3)_3 \cdot 5H_2O$, NaOH and HCl as precursors for $BiVO_4$ and BiOCl, followed by the stirring, heating and washing. Catalysts having different molar concentrations were prepared by varying the amount of HCl in the mixture and the catalyst having the molar ratio of 0.75BiOCl/BiVO$_4$ was seemed to be more active. Analysis and characterizations determined th-presence of Bi as Bi^{3+} and vanadium as V^{5+} and O as $O_2^{\bullet-}$ and Cl as Cl^-. For the tests of photocatalytic activity, Degussa P25 was used as control group, and results determined the increased degradation of MO in BiOCl/BiVO$_4$ system and it was about 1.89 times greater than that of TiO_2 and 3.54 times from $BiVO_4$. Free radical scavengers illuminated that the holes in the valence band of *p*-type part of heterojunction played an important role in the direct oxidation of MO, $OH^{\bullet}$ were the dominant species and DO acted as electron acceptor from the CB. The stability of catalyst was tested and after the use of 5 cycles, it did not show any significant loss, which indicated the effectiveness and stability against photocorrosion [153]. Zhijie et al. has reported the fabrication of a novel
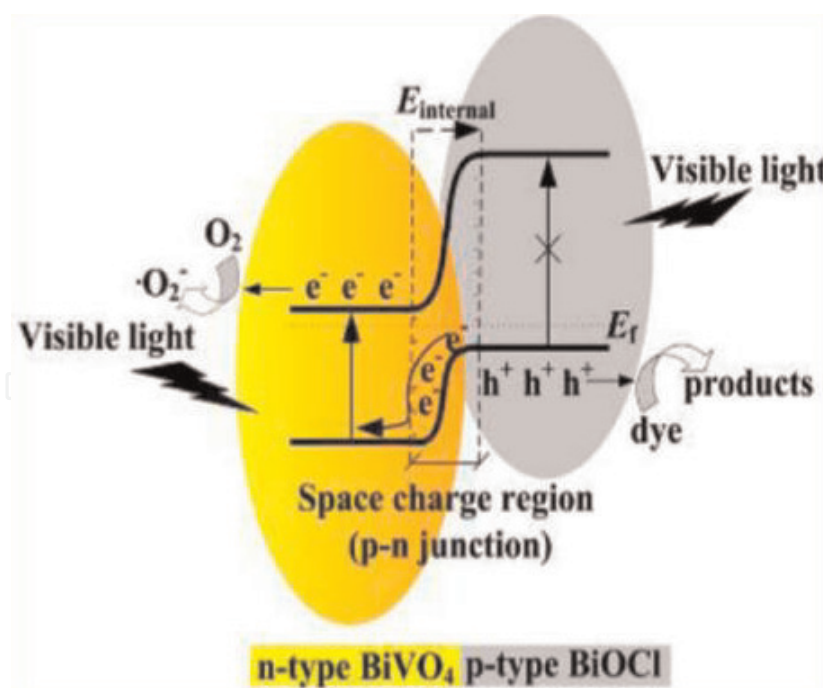
Figure 25.
Schematic illustration of effective charge separation between n- and p-type SC upon exposure to UV and Vis light [153].

nanocomposite of Bi_2S_3/Bi_2WO_6 by hydrothermal method to reduce the limitation of low photocatalytic ability of Bi_2WO_6 resulted from the potential relaxation of electron into hole. In this structure Bi_2S_3 acted as a sensitizer having the band gap of 1.3 eV and the system possessed the photoabsorption of 800 nm which meant it covered almost whole range of visible region. The equipped photocatalyst exhibited much enhanced photocatalytic activity for the degradation of phenol (a colorless pollutant) under visible light which was about 6.2 times greater than that of original Bi_2WO_6. Thanks to efficient charge separation for the enhanced photocatalytic activity resulted from the formation of heterojunction at the semiconductor interface [82, 83]. The heterostructure formed by mixing of graphene with $BiFeO_3$ was prepared by one-pot hydrothermal method. The band gap of composite could be fabricated from 1.78 to 2.24 eV by changing the concentration of OH groups during the synthesis. Raman and XPS analysis revealed that the formation of Fe-O-C bonds enhanced the stability of composite. The increased photodegradation of Congo Red (CR) dye was observed in 2 h which increased from 40 to 71% due to the breakage of azo bonds and naphthalene rings at different wavelengths which can be due to the increased adsorption of CR on the graphene due to the infinite numbers of conjugated π-bond ([122]).

WO$_3$ is a known semiconductor due to its polycrystalline forms and smaller band gap of about 2.4–2.8 eV depending on crystal structure; which means its electrons can be excited by visible light irradiation, the main limitations of this SC which keep it far from becoming a useful semiconductor are; higher rate of recombination and its unstability against photocorrosion [154]. WO$_3$ is incorporated in heterojunctions in order to increase the absorption in visible light region. Shamaila et al. has reported the formation of WO$_3$/BiOCl heterojunction or the degradation of organic pollutants under visible light using $BiCl_3$, Ammonium tungstate and ethanol as precursors, 2D nanoflakes of BiOCl of the size of 75–200 nm were fabricated (**Figure 26**) by following a new low temperature route and nanocomposite was prepared to enhance the visible light response, BiOCl performed the role of a main photocatalyst while WO$_3$ worked as a sensitizer. For the prepared composite the absorption range increased from 360 to 500 nm as the quantity of WO$_3$ increased
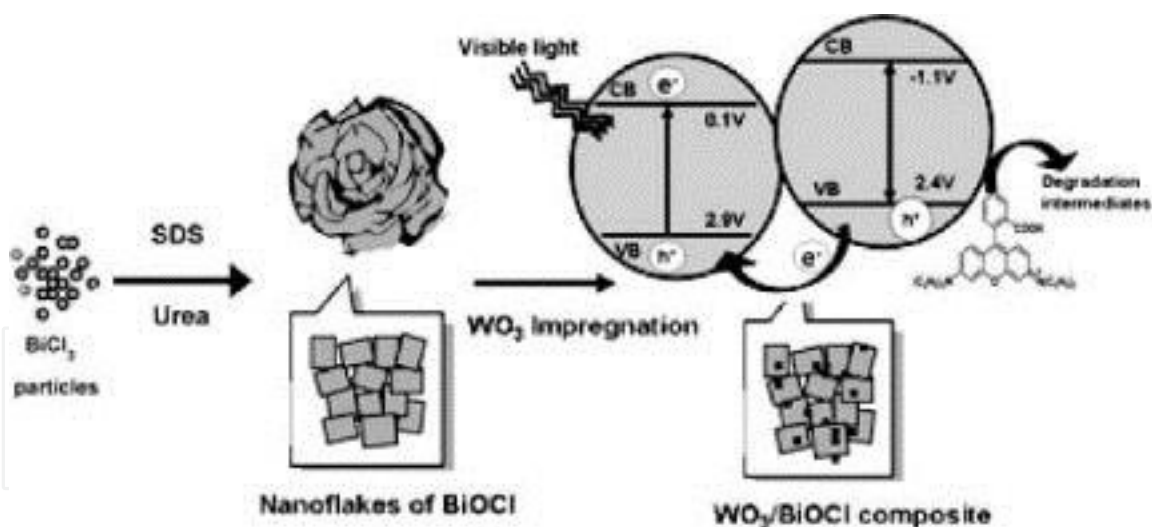
Figure 26.
Composite synthesis route and proposed mechanism for photodegradation of rhB [155].

while synthesis, the catalyst gave 100% deterioration of Rhodamine B was under visible light during the irradiation time of 180 min, which was greater than the activity of WO_3, BiOCl and Degussa P25 [155].

Another heterojunction photocatalyst with high photocatalytic activity is $WO_3/SrNb_2O_6$, was prepared by the milling-annealing method which was found to be better than the direct mixing method as this method could build a firm chemically bonded interface between two semiconductors. Results determined that the composite had higher photocatalytic activity as compared to pure WO_3 and $SrNb_2O_6$. As we know that anything which can scavenge the excited electron can be a reason for increased photocatalytic process so, the effective charge separation among semiconductors and formation of holes and radicals led to the direct or indirect degradation of methyl orange [156]. Ag_3PO_4/WO_3 nanocomposites were prepared by a deposition-precipitation method using $Na_2WO_4 \cdot 2H_2O$, NH_4Cl, $AgNO_3$ and Na_2HPO_4 as precursors and prepared powders were characterized by SEM, XRD and UV-Vis. Catalysts were prepared of variable molar ratios of $Ag_3PO_4:WO_3$ and the catalyst having ratio of 6:4 ($AW_{6/4}$) shown the greater photocatalytic activity for the degradation of rhB and MO at the wavelength $\lambda > 420$ nm, mainly due to the excellent separation of charge carriers. Reusability tests indicated that composite had higher recyclability as compared to Ag_3PO_4 alone as $AW_{6/4}$ gave 97% removal of rhB and MO in 6 and 35 min (after being exposed to visible light) even after the fifth run (had same efficiency for first run) while Ag_3PO_4 gave only 25% degradation at the fifth run due to the absence of sacrificial donor. Stability analysis revealed that catalyst $AW_{6/4}$ was stable against photocorrosion as it retained the XRD pattern even after 5 cycles for degrading fresh rhB, only a small amount of metallic Silver was observed on Ag_3PO_4 after use, SEM analysis also supported stability result [157].

A hybrid photocatalyst $W_{18}O_{49}/TiO_2$ having an urchin like structure (**Figure 27**) was prepared by an alcohol thermal method, which had high surface area of 178 $m^2 g^{-1}$ and shown absorption in the wide range of 200–800 nm and tested for the photodisintegration of MO and phenol under UV-visible irradiation. The hybrid photocatalyst attained synergetic increase in photoactivity and photostability of $W_{18}O_{49}$, well-related band structure enhanced the charge separation and transfer which led to the production of free radicals as well as prevented the $W_{18}O_{49}$ from self-oxidation due to holes as they moved towards TiO_2. Free radical scavenging tests indicated that $O_2^{\bullet-}$ was reactive oxidizing specie for the degradation of MO and phenol. Reusability tests revealed the stability of catalyst as it maintained its
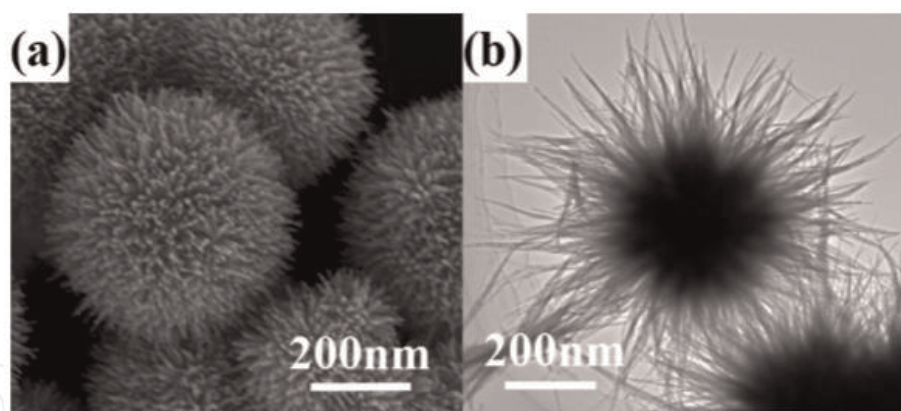
Figure 27.
(a) SEM image of $W_{18}O_{49}$ (b) TEM image of $W_{18}O_{49}$ [158].

XRD spectra even after the fifth cycle which meant catalyst did not suffer any noticeable loss, hybrid composite also maintained its original blue color at the end of fifth run [158].

From metal tungstate an example of a p-n heterojunction is the fabrication of a novel Z-scheme $WO_3/CdWO_4$ photocatalyst by the fusion of sheet like WO_3 (n-type) and rod like nanostructure of $CdWO_4$ (p-type), for this purpose the catalyst were prepared separately by using respective precursors and fusion was done by using hydrothermal and chemisorption methods. As-prepared catalysts were used for the degradation of organic dyes like Methly orange, Rhodamine B and methylene blue, upon exposure of light the transfer of electrons and holes occurs from the $CdWO_4$ to WO_3 and vice versa which led to circuit completion and efficient increase in charge separation, PL spectra gave the smaller curve peak proving the less relaxation of electron towards VB and the absorption intensity of $\lambda > 476$ nm. Stability tests were performed to check the structural reliability of catalyst, it did not show any significant loss even after 3 cycles of reuse for the degradation of fresh dyes. Results also indicated the degradation of dye was about 7 and 2.3 times greater than $CdWO_4$ and WO_3 alone which was credited to enhanced surface area and effective separation of charge carriers [159].

In addition to the binary composites, some tertiary (complex) composites have been reported, where the multi-photon excitation took place in the photoactive materials and charge transfer and separation was increased due to increased surface area and different transition states. $KTaO_3$-CdS-MoS_2 is an example of tertiary composite which was prepared by hydrothermal method by rigorously following the temperature and pressure conditions, the obtained powders were of different structures like nanoleaf, cubic and hexagonal spheres exhibiting activity under both visible and UV light and were used for the degradation of toluene and phenol. The catalysts shown 42% degradation under visible light and 80% degradation of pollutants under UV light. Prepared catalyst exhibited good stability (about 50%) even after 4 cycles for the degradation of fresh toluene [160]. In case of some ternary composites like ZnO-$AgBr$-Ag_2CrO_4 (n-n junctions), two SCs worked as donors of photoexcited electrons and oxidation of pollutants occurred by the formation of superoxide radicals at the CB. By the charge separation the phocatalytic activity of composite was 16 and 7 times higher than those of ZnO and $ZnO/AgBr$ for the degradation of rhB [161]. Rhodamine B also suffered degradation by the photocatalytic activity of In_2O_3-$AgBr$-$BiWO_6$ (**Figure 28**), prepared by microwave assisted irradiation method, optical, morphological and structural properties were analysed by XRD, SEM, TEM, XPS, HRTEM which indicated the flower-like pattern of assembled nanoparticles. The increased photoactivity under UV, visible and solar
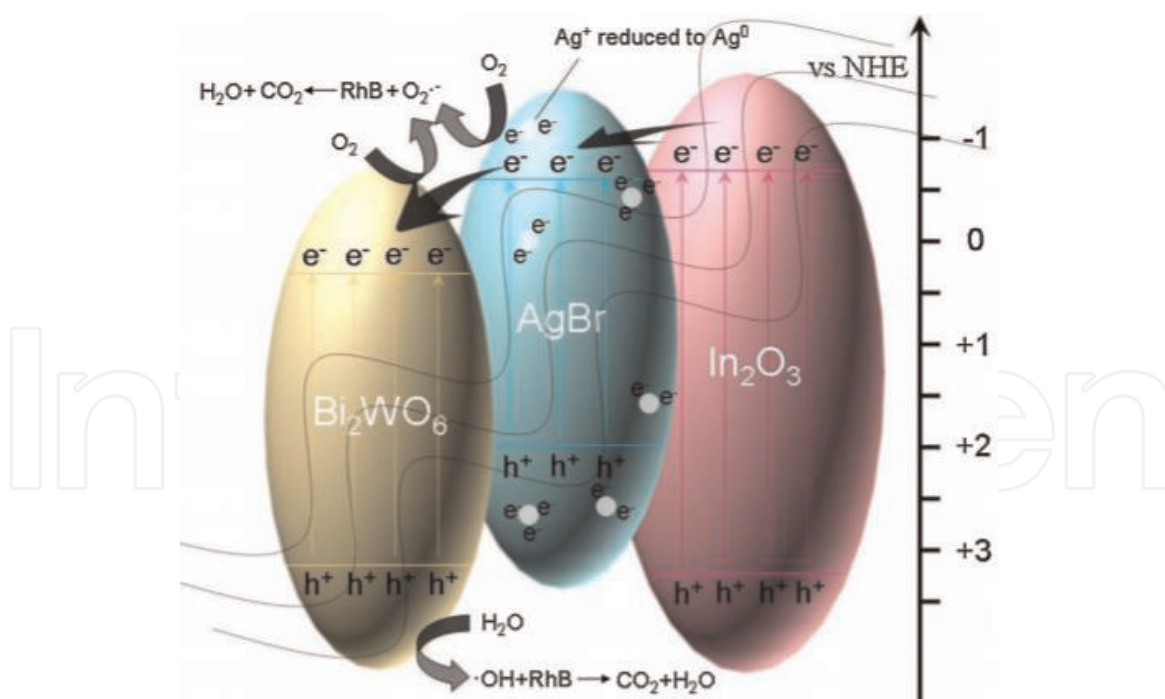
Figure 28.
Proposed mechanism for the degradation of rhB on ternary composite [162].

light was attributed to increased surface area and charge separation due to differences in the redox potentials of SCs bands. Reactive species scavenging testes determined that OH• and superoxide radicals were dominant reactive species [162].

Besides all of the above discussed heterostructures, nanocomposites, coupled semiconductors, either oxides or sulfides, there are numerous other heterojunctions like $WO_3/NiWO_4$ [163], Ag_3PO_4/Bi_2MoO_6 [164], $Ag_3PO_4/AgBr$ [165], CdS/Bi_2MoO_6 [166], CdS/Ta_2O_5 [167], $BiOBr/ZnFe_2O_4$ [168], $Cu_2O/SrTiO_3$ ([169]), $ZnS/CuS/CdS$ [170], $SnO_2/ZnO/ZnWO_4$ [171] and many more have been reported to increase the ability of pure SCs to harvest the sun light either in the field of water or wastewater treatment for the overall splitting of water, degradation of Organic, inorganic pollutants, phenols, MCs, POPs and other emerging contaminants.

5. A glance at g-C₃N₄-based heterostructures/nanocomposites

It has been more than a decade that people are being aware from environmental protection and conservation, the era of industrialization besides increasing the gross productivity also posed serious effects on the health of water bodies by discharging unchecked amounts of effluents and other chemicals, in order to improve the water quality the focuses are being paid to treat water and wastewater, the idea of semiconductor photocatalysis has been emerged which uses solar energy in its full potential, for this purpose many SCs either in single or in heterostructures have been discussed in Section 6.

In addition to first generation photocatalysts, an emerging polymeric photocatalyst is Graphitic Carbon Nitride (g-C₃N₄) which is an earth copious visible light active catalyst, having unique 2D structure with high stability and flexible structure (which can be tailored) and low band gap of 2.7 eV. Pure gCN have high rate of recombination, smaller surface area and low ability to exploit visible light thus reducing the quantum efficiency of photosystem, the VL activity of gCN has been reported to increase by making heterostructures with other SCs by taking the advantage of its layered structure which assisted in hybridization with other

constituents like CdS, TiO_2, $ZnWO_4$, ZnO, etc. either for the degradation of pollutants or for the evolution of O_2 or H_2 gas [172]. Some examples of gCN HSs/HJs/Composites are discussed below.

Novel $g\text{-}C_3N_4/TiO_2$ composites were prepared by the facile sonication method using melamine and titanium tetrachloride as precursors followed by stirring, sonication and drying at room temperature. Different catalysts were prepared by varying the concentrations of precursors and $g\text{-}C_3N_4/TiO_2$-1.5 was found to be more active among other catalysts, as it shown higher photocatalytic degradation of MB under UV and visible light. Results demonstrated that catalyst shown 6.92 and 2.65 time greater activity than pure gCN and TiO_2 under UV light, while 9.27 (gCN) and 7.03 (TiO_2) folds greater photoactivity under visible light, which can be attributed the increased visible light absorption and efficient charge transfer in composite at interfaces of SCs. In the hybrid catalyst gCN could be triggered under visible light and the photoexcited electrons of gCN transferred to the CB of TiO_2 due to interfacial connections and differences of redox potentials [173]. Tunable band gap of some semiconductors is an effective way to harness solar light and among those gCN is a known SC. Two SCs having smaller band gaps (gCN and Bi_2MoO_6) were coupled to prepare a Z-scheme nanocomposite, number of catalysts were prepared by varying the concentrations of precursors and 25% $g\text{-}C_3N_4/Bi_2MoO_6$ was seemed to be most active, structure, morphology, light absorption spectra and charge carriers separation efficiency was analyzed and photocatalytic activities were evaluated for the degradation of MB. Both SCs in composite were excited at the $\lambda = 410$ nm, due to the negative redox potentials of gCN (as compared to Bi_2MoO_6), excited electrons of gCN transferred to CB of Bi_2MoO_6 and holes of later should had been migrated to the VB of gCN, but by this route the holes at the VB of gCN could not react with water of OH ion near its surface and same for Bi_2MoO_6, so it was observed that the excited electrons transferred to their respective CB, the relectrons from the CB of Bi_2MoO_6 were transferred to the VB of gCN (spatial separation) which inhibited the local recombination (**Figure 29**) thus completing the Z-scheme route, the CB of Bi_2MoO_6 and VB of gCN could not react with molecules in their vicinity and the catalyst shown 4.8 and 8.2 folds greater photoactivity than pristine SCs [174].

Feng et al. reported the fabrication of S-doped $g\text{-}C_3N_4/Au/CdS$ composite as Z-scheme photocatalyst where CdS was deposited on g-CNS system in which Au nanoparticles were sandwiched between g-CNS and CdS (two visible light responsive SCs) by the chemical bath deposition and worked as charge transporter (**Figure 30**), whole system increased the degradation of rhB, MO, MB and increased
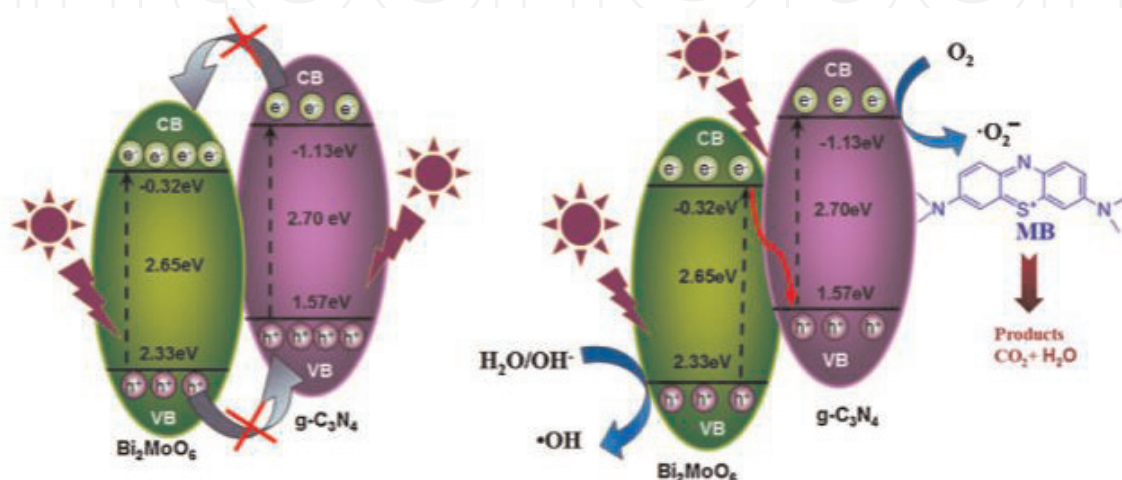

Figure 29.
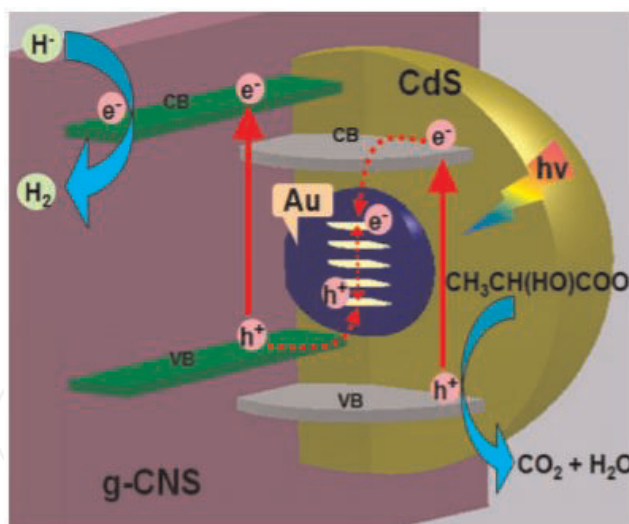*Proposed mechanism of charge transfer in Z-scheme photocatalyst [174].*

Figure 30.
Proposed mechanism of Z-scheme charge separation and transportation in g-CNS/Au/CdS [175].

reduction of water to hydrogen was observed under visible light (λ = 560 nm). The Z-scheme photocatalyst was characterized by SEM, HRTEM, PL spectra, Vis-diffuse spectra. These elementary, crystal and microcrystal analysis demonstrated the uniformity of novel composition, results revealed that the catalyst exhibited great photocatalytic activity as compared to g-CNS, g-CNS/Au, g-CNS/CdS, and pure CdS [175]. Novel organic-inorganic composite of $g-C_3N_4$-CdS has been prepared which gave the degradation of organic pollutants under visible light. Results indicated the higher photocatalytic activity of about 20.5 and 3.1 times for degradation of MO as compared to gCN and CdS alone and 41.6 and 2.7 times higher for the degradation of 4-aminobenzoic acid [176].

GCN has also been reported to be composed with 2D graphene which is being focused due to its unique properties like amazing thermal, mechanical, surficial and electric properties. Tong et al. has prepared 3D porous gCN/graphene oxide aerogel structure by using gCN sheets and graphene oxide as precursors by following hydrothermal treatment method this composition resulted to enhanced visible light absorption, decreased charge relaxation and increased adsorption capacity. Analysis and characterizations were performed to check intrinsic properties. As-prepared catalyst was used for the CO_2 evolution and MO degradation which was about 92% in 4 h under visible light [177]. Han et al. has reported different $g-C_3N_4$/graphene nanocomposites which were proved to be effective for the degradation of dyes under visible light, different hybrids of gCN/graphene were prepared by using different methodologies and synthesis processes like solvothermal treatment, hydrothermal treatment, electrochemical reactions, etc. and their photoactivity was investigated for the hydrogen, oxygen, CO_2 evolution and degradation of different organic compounds [178].

Among ternary composites the novel magnetically recoverable composite of $g-C_3N_4/Fe_3O_4/NiWO_4$ was prepared by refluxing calcination method, different hybrids were prepared by varying the precursor's concentration among which $gCN/Fe_3O_4/NiWO_4$ (30%) was found to be more active, catalysts were characterized for their morphology, texture, electronic, thermal and magnetic properties. Hybrid catalyst shown their high photocatalytic activity under visible light for the degradation of rhB, MO, MB, fuchsine and phenolic compounds. Results confirmed that formation of HJs between $gCN/M/NiWO_4$ increased the surface area and charge separation (**Figure 31**), thus increasing the quantum efficiency of system, photocatalytic activity of $gCN/M/NiWO_4$ (30%) was 12, 30, 52 and 6 folds greater for rhB, MB, MO, fuchsine and phenol as compared to gCN, Fe_2O_3 and $NiWO_4$
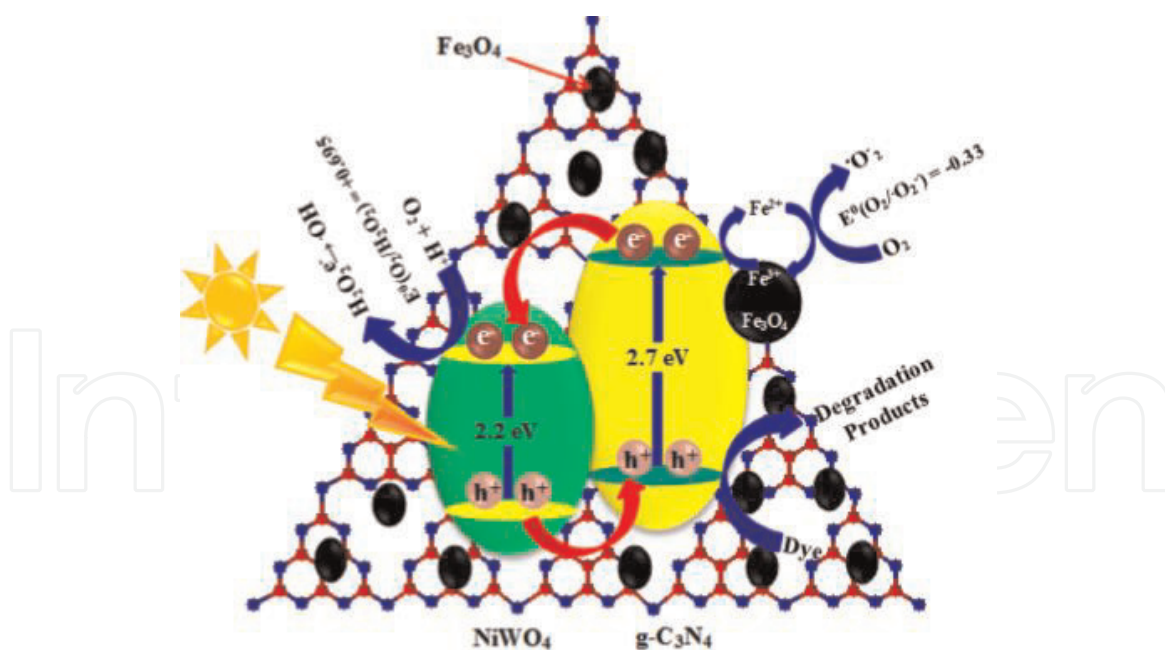
Figure 31.
Proposed mechanism of charge transfer in gCN/M/NiWO$_4$ nanocomposites [179].

alone. Additionally the prepared composites exhibited high degree of stability even after the 4 cycles of reusability as it degraded about 87% of rhB at fourth cycle, unluckily, nanohybrid suffered from reduced surface area after the last run which was attributed to the blockage of degradation reaction intermediates at surface sites [179]. Zhang et al. has used one-step solvothermal method for the preparation of spinel ZnFe$_2$O$_4$ nanoparticles and its decoration on g-C$_3$N$_4$ sheets for formation of water soluble magnetic-functionalized g-C$_3$N$_4$/ZnFe$_2$O$_4$. The magnetic properties of composite were controlled by the size of composite and decorated quantity of ZnFe$_2$O$_4$. Results indicated that catalyst exhibited efficient photocatalytic activity for degradation of MO under visible light and it was mainly due to the synergist effect of both SCs like smaller particle size and high solubility in water, interestingly the catalyst could be separated from aqueous solution by magnet. CN-ZnFe showed 98% of degradation of MO in 180 min which was 6.4 and 5.6 times higher than g-C$_3$N$_4$ and ZnFe$_2$O$_4$ alone. Free radical scavenging test revealed the decrease in efficiency indicated the vital role of OH$^{\bullet}$ and superoxide radical in the pollutant degradation. The increased photocatalytic activity was credited to sufficient charge separation ([180]). Synthesis of novel magnetic CdS/ZnFe$_2$O$_4$ nanocomposites has been reported (by two-step hydrothermal method) in order to enhance photocatalytic activity and photostability of SCs under visible region [181].

Heterojunctions of g-C$_3$N$_4$ with carbonaceous particles has been reported to make recyclable, stable and more efficient photocatalyst for the water treatment purposes. Chai et al. synthesized the g-C$_3$N$_4$ modified with fullerene for the removal of dyes from water under visible light. Fullerenes (C$_{60}$) are known to have 30 molecular orbits with 60 π electrons with closed shell structure which helped in separation and transport of charge carriers, especially the photoexcited electrons. Because of the larger surface area and unique morphology, the electrons excited from g-C$_3$N$_4$ shifted on C$_{60}$ thus got separated from hole and lessened the electron relaxation towards hole, the electron hole pair separation resulted in the opening of benzene ring during the process of organic molecule degradation [182, 183]. Bai et al. prepared g-C$_3$N$_4$/fullerene composite using thermal polymerization of dicyandiamide in the availability of C$_{60}$ at 550°C. Addition of C$_{60}$ in the gCN,

shifted the VB of gCN at lower energy level thus its oxidation potential under visible light was increased. **Figure 32** demonstrate the increased photocatalytic activity due to effective electron hole pair separation, when the catalyst was exposed to visible light electrons got excited from VB (formed by N2p orbitals) to CB (formed by 2Cp orbitals) of g-C_3N_4 leaving the holes behind in the VB, the excited electrons jumped to C_{60} from CB of gCN thus retaining the separation. Results demonstrated the enhanced degradation of MB and phenol at $\lambda > 420$ nm, degradation was about 2.9 and 3.2 time greater than that of bulk gCN, due to the efficient production of $OH^\bullet$ from holes, which acted as oxidation species and played a vital role in opening of benzene rings ([184]).

In addition to above discussed g-C_3N_4-based nanocomposites, there is a lot of literature based on the synthesis, uses and types of heterostructures based on the multifunctional approaches, as g-C_3N_4-based nanostructures (either with oxides or sulfides, either binary or tertiary) have become the main member of semiconductor photocatalysis family for the degradation of pollutants in environment specially in water. Besides g-C_3N_4/Fe_2O_3, g-C_3N_4/CeO_2 g-C_3N_4/MoO_3, g-C_3N_4/Fe_3O_4, g-C_3N_4/$Ni(OH)_2$, g-C_3N_4/Ag_2O, g-C_3N_4/MoS_2, g-C_3N_4/NiS, g-C_3N_4/TaON, g-C_3N_4/ZnO, g-C_3N_4/g-C_3N_4, g-C_3N_4/In_2O_3, g-C_3N_4/WO_3, SiO_2/g-C_3N_4 and some ternary composites like, gCN/Fe_3O_4/$CuWO_4$, BiOCl/Bi_2MoO_6/g-C_3N_4, Ag_2CrO_4/g-C_3N_4/GO, g-C_3N_4/TiO_2/CNT, G-C_3N_4/CeO_2/ZnO there are innumerable gCN composites, some composites with their photocatalytic activity and efficiency under visible light are mentioned in **Table 2**.
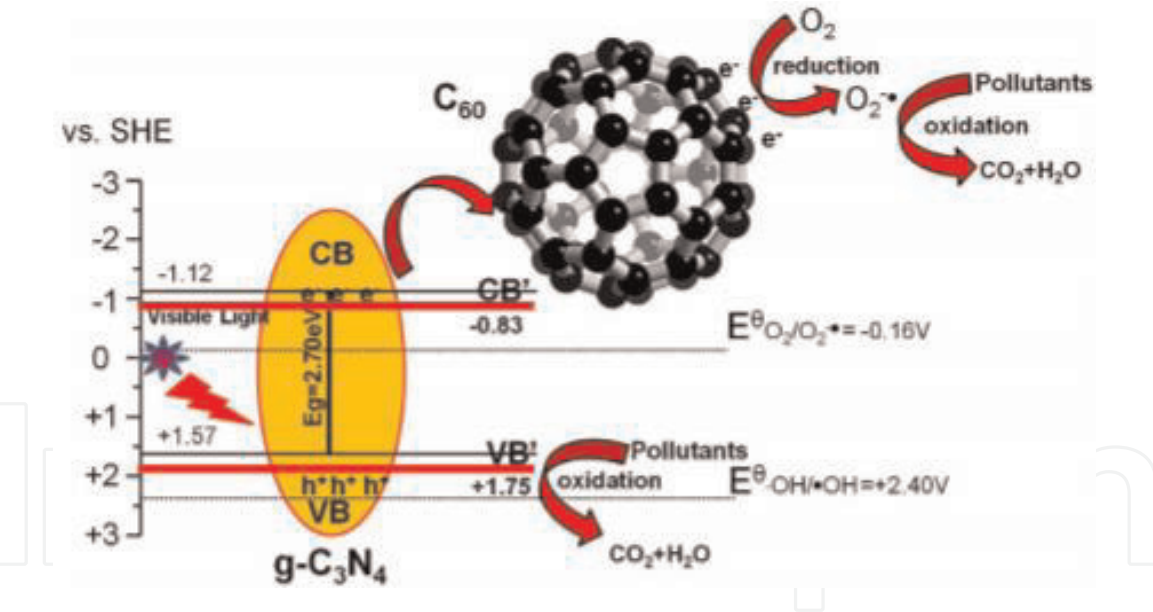
Figure 32.
Schematic illustration of charge separation and decomposition mechanism of organic pollutants by production of free radicals ([184]).

Composite	Precursor/synthesis method	Targeted pollutant	Degradation efficiency/reason under visible light	References
TiO_2/g-C_3N_4	P-25 and dicyandiamide	Methylene blue	90% degradation in 300 min, 3.5 greater efficiency than SC alone.	[185]
WO_3/ g-C_3N_4	Dicyandiamide and $(NH_4)_5H_5[H_2(WO_4)_6]\cdot H_2O$	MB and 4-CP	Degraded 97% of MB and 43% of 4-CP	[186]
$CdWO_4$/ g-C_3N_4	Melamine/mixed calcination synthesis	rhB	Degradation of rhB due to $O_2^{\bullet-}$ radical formation, 1.6 and 54.6	[187]

Composite	Precursor/synthesis method	Targeted pollutant	Degradation efficiency/reason under visible light	References
			times greater efficiency than gCN and CWO.	
In_2S_3/ g-C_3N_4	Urea/hydrothermal synthesis	rhB	HJ formation widened the light absorption spectra, increased EHP separation and $O_2^{\bullet-}$ were reactive OS.	[188]
V_2O_5/ g-C_3N_4	Melamine/one-pot synthesis	rhB	Deterioration of rhB due to $O_2^{\bullet-}$ and $OH^{\bullet}$, charge separation increased quantum efficiency under visible light.	[189]
ZnO/ g-C_3N_4	Melamine and zinc acetate/simple calcination method	MO and p-nitrophenol	Degraded 97% of MO in 80 min, which was three and six times greater than gCN and ZnO alone.	[190]
$ZnWO_4$/g-C_3N_4	Melamine/facile chemisorption	MB	Higher electron hole pair separation, OH and $O_2^{\bullet-}$ were reactive species	[191]
BiOI/ BiOBr/g-C_3N_4	Dicyandiamide	MB	Effective charge separation, production of $OH^{\bullet}$, $O_2^{\bullet-}$ and h^+	[192]
ZnO/ZnS/g-C_3N_4	Melamine/two-step facile synthesis	H_2 Production	Hydrogen production 1205 µmol/g-C_3N_4:16 µmol/g	[193]
YVO_4/g-C_3N_4/Ag	Hydrothermal/urea deposition method	MO	3 times higher activity as compared to gCN alone	[194]
C_3N_4/CNT/NiS	Sol-gel method/direct precipitation of cyanamide	H_2 Production	148 times higher activity than pure gCN/CNT	[195]
Ag_3PO_4/ GO/g-C_3N_4	Dicyandiamide/ precipitation	RhB degradation	94.8% degradation in 50 min.	[196]
g-C_3N_4/AgBr/RGO	Urea/hydrothermal treatment	Tetracycline and 2,4-DP	78.4% degradation in 90 min and 68.2% within 6 h.	[197]
g-C_3N_4/TiO_2/ZnO	Hydrothermal treatment	p-toluene sulfonic acid	90% degradation by composite, while only 40% by gCN	[198]
g-C_3N_4/ CeO_2/ZnO	Urea/pyrolysis and exfoliation method	MB	11 times greater degradation than bare gCN	[199]
Ag/g-C_3N_4/ $NaTaO_3$	Melamine/photo deposition process	Dyes and tetracycline	Improved dye degradation and 95.47% removal of tetracycline.	[200]

Table 2.
g-C_3N_4-based heterostructures/nanocomposite.

6. Conclusions

Majority organic, inorganic and other numerous pollutants which are either in the records of EPAs or not, are the refractory compounds and tend to become the part of fresh or potable water thus making it unfit for use. Besides employing membrane systems, VLA semiconductor photocatalysis has gained fame due to their cost effectiveness and eco-friendly nature and becoming a promising phenomenon for the treatment of water on global scale. The rapid development in field of nanotechnology has opened the doors for various advanced photocatalytic systems which includes the formation of complex structures by doping, co-doping,

heterostructures, 0D to 3D structures and nanocomposites as heterogeneous photocatalysts, has been developed in recent decades and has helped the environment and water to get rid of stubborn pollutant species, such as bacteria like *E. coli*, *B. subtilis*, giardia cysts, harmful cyanobacteria and their toxins like microcystins LR, RR, YR, LA (types of Microcystins), etc. which are harmful for different life forms. However, the application of visible light active semiconductors in the long run will be a reason of development of sustainable environment, due to development of advanced oxidation processes which are triggered by sunlight, will become a renewable energy source for example the evolution of hydrogen, oxygen and carbon dioxide gas. Therefore, an effective assessment of SCs nanomaterials is still required to test true photoactivity and to enhance the commercialization for future regards.

Author details

Fatima Imtiaz[1], Jamshaid Rashid[1,2]* and Ming Xu[2]

1 Department of Environmental Science, Faculty of Biological Sciences, Quaid-i-Azam University, Islamabad, Pakistan

2 Key Laboratory of Geospatial Technology for the Middle and Lower Yellow River Regions, College of Environment and Planning, Henan University, Jinming Avenue, Kaifeng, China

*Address all correspondence to: jamshaidrashid@gmail.com; jrashid@qau.edu.pk

IntechOpen

References

[1] Serpone N. Advanced oxidation processes. In: Kirk-Othmer Encyclopedia of Chemical Technology. Vol. 1. Toronto, Canada: John Wiley and Sons, Inc.; 2000. pp. 1-17

[2] Fujishima A, Zhang X, Tryk DA. TiO_2 photocatalysis and related surface phenomena. Surface Science Reports. 2008;**63**:515-582. DOI: 10.1016/j.surfrep.2008.10.001

[3] Mills A, Le Hunte S. An overview of semiconductor photocatalysis. Journal of Photochemistry and Photobiology A: Chemistry. 2000;**108**:1-35

[4] Ohtani B. Photocatalysis A to Z— What we know and what we do not know in a scientific sense. Journal of Photochemistry and Photobiology, C: Photochemistry Reviews. 2011;**11**: 157-178. DOI: 10.1016/j.jphotochemrev.2011.02.001

[5] Goodeve CF, Kitchener JA. Photosensitisation by titanium dioxide. Transactions of the Faraday Society. 1938;**34**:570-579. DOI: 10.1039/TF9383400570

[6] Nuno M, Ball RJ, Bowen CR. Photocatalytic properties of commercially available TiO_2 powders for pollution control. In: Semiconductor Photocatalysis—Materials, Mechanisms and Applications. United Kingdom: IntechOpen; 2016. pp. 613-633. DOI: 10.5772/62894

[7] Serpone N, Emeline AV. Semiconductor photocatalysis—Past, present, and future outlook. Journal of Physical Chemistry Letters. 2012;**3**: 673-677. DOI: 10.1021/jz300071j

[8] Hoffmann MR, Martin ST, Choi W, Bahnemann DW. Environmental applications of semiconductor photocatalysis. Chemical Reviews. 1995; **95**:69-96. DOI: 10.1021/cr00033a004

[9] Kisch H. Semiconductor photocatalysis—Mechanistic and synthetic aspects. Angewandte Chemie, International Edition. 2013;**52**:812-847. DOI: 10.1002/anie.201201200

[10] Herrmann J. Titania-based true heterogeneous photocatalysis. Environmental Science and Pollution Research. 2012;**19**:3655-3665. DOI: 10.1007/s11356-011-0697-8

[11] Herrmann J. Heterogeneous photocatalysis: Fundamentals and applications to the removal of various types of aqueous pollutants. Catalysis Today. 1999;**53**:115-129

[12] Pelaez M, Nolan NT, Pillai SC, Seery MK, Falaras P, Kontos AG, et al. A review on the visible light active titanium dioxide photocatalysts for environmental applications. Applied Catalysis B: Environmental. 2012;**125**: 331-349. DOI: 10.1016/j.apcatb.2012.05.036

[13] Agrawal A. Chapter 4 type I and type II band alignments in ZnO/MgZnO bilayer films. Applied Physics Letters. 2014;**105**:081603

[14] Kroemer H. Band Diagrams in Real Space: I2009. pp. 1-13

[15] Wang Y, Wang Q. Visible light driven type II heterostructures and their enhanced photocatalysis properties: A review nanoscale. Nanoscale. 2015;**5**:8326-8339. DOI: 10.1039/c3nr01577g

[16] Opoku F, Govender KK, van Sittert CGCE, Govender PP. Recent progress in the development of semiconductor-based photocatalyst materials for applications in photocatalytic water splitting and degradation of pollutants. Advanced Sustainable Systems. 2017;**1**: 1700006. DOI: 10.1002/adsu.201700006

[17] Wang Y, Wang Y, Li Y, Shi H, Xu Y, Qin H, et al. Simple synthesis of Zr-doped graphitic carbon nitride towards enhanced photocatalytic performance under simulated solar light irradiation. Catalysis Communications. 2015;**72**:24-28. DOI: 10.1016/j.catcom.2015.08.022

[18] Ibhadon AO, Fitzpatrick P. Heterogeneous photocatalysis: Recent advances and applications. 2013;**3**: 189-218. DOI: 10.3390/catal3010189

[19] Fragalà ME, Di Mauro A, Cristaldi DA, Cantarella M, Impellizzeri G, Privitera V. ZnO nanorods grown on ultrathin ZnO seed layers: Application in water treatment. Journal of Photochemistry and Photobiology A: Chemistry. 2017;**332**: 497-504. DOI: 10.1016/j.jphotochem.2016.09.032

[20] Martyna M, Diak M, Kozak M, Adriana Zaleska-Medynska EG. Some unitary, binary, and ternary non-TiO_2 photocatalysts. In: Semiconductor Photocatalysis—Materials, Mechanisms and Applications. United Kingdom: IntechOpen; 2016. DOI: 10.5772/62583

[21] Gaya UI. Heterogenous Photocatalysis Using Inorganic Semiconductor Solids. Switzerland: Springer; 2014

[22] Medina-Ramírez AH-RI. Photocatalytic Semiconductors. Switzerland: Springer; 2015. DOI: 10.1007/978-3-319-10999-2

[23] Turchi CS. Photocatalytic degradation of organic water contaminants: Mechanisms involving hydroxyl radical attack. Journal of Catalysis. 1990;**192**:178-192

[24] Ray MB. Photocatalytic oxidation of paracetamol: Dominant reactants, intermediates, and reaction mechanisms. Environmental Science & Technology. 2009;**43**:460-465

[25] Wang J, Tafen DN, Lewis JP, Hong Z, Manivannan A, Zhi M, et al. Origin of photocatalytic activity of nitrogen-doped TiO_2 nanobelts. JACS. 2009;**131**: 12290-12297

[26] Yongquan Quab XD. Progress, challenge and perspective of heterogeneous photocatalysts. The Royal Society of Chemistry. 2012;**42**: 2568-2580. DOI: 10.1039/c2cs35355e

[27] Marschall R, Wang L. Non-metal doping of transition metal oxides for visible-light photocatalysis. Catalysis Today. 2014;**225**:111-135. DOI: 10.1016/j.cattod.2013.10.088

[28] Livraghi S, Paganini MC, Giamello E, Selloni A, Di Valentin C, Pacchioni G. Origin of photoactivity of nitrogen-doped titanium dioxide under visible light. Journal of the American Chemical Society. 2006;**128**:15666-15671. DOI: 10.1021/ja064164c

[29] Sato S, Nakamura R, Abe S. Visible-light sensitization of TiO_2 photocatalysts by wet-method N doping. Applied Catalysis A: General. 2005;**284**:131-137. DOI: 10.1016/j.apcata.2005.01.028

[30] Asahi AR, Morikawa T, Ohwaki T, Aoki K, Taga Y, Lee V, et al. Visible-light photocatalysis in nitrogen-doped titanium oxides. Science. 2001;**293**: 269-271

[31] Abadias G, Paumier F, Eyidi D, Gu P, Girardeau T, Wiley J. Structure and properties of nitrogen-doped titanium dioxide thin films produced by reactive magnetron sputtering. Surface and Interface Analysis. 2010;**42**:970-973. DOI: 10.1002/sia.3220

[32] Martínez-ferrero BE, Sakatani Y, Boissière C, Grosso D, Fuertes A. Nanostructured titanium oxynitride porous thin films as efficient visible-active photocatalysts. Advanced Functional Materials. 2007;**17**:

3348-3354. DOI: 10.1002/adfm. 200700396

[33] Premkumar J. Development of super-hydrophilicity on nitrogen-doped TiO$_2$ thin film surface by photoelectrochemical method under. Chemistry of Materials. 2004;**16**: 3980-3981. DOI: 10.1021/cm049055g

[34] Choi H, Antoniou MG, Pelaez M, De la Cruz AA, Shoemaker JA, Dionysiou DD. Mesoporous nitrogen-doped TiO$_2$ for the photocatalytic destruction of the cyanobacterial toxin microcystin-LR under visible light irradiation. Environmental Science & Technology. 2007;**41**:7530-7535. DOI: 10.1021/es0709122

[35] Yang J, Chen DX, Deng AP, Huang YP, Chen CC. Visible-light-driven photocatalytic degradation of microcystin-LR by Bi-doped TiO$_2$. Research on Chemical Intermediates. 2011;**37**:47-60. DOI: 10.1007/ s11164-010-0224-4

[36] Vitiello RP, Macak JM, Ghicov A, Tsuchiya H, Dick LFP, Schmuki P. N-doping of anodic TiO$_2$ nanotubes using heat treatment in ammonia. Electrochemistry Communications. 2006;**8**:544-548. DOI: 10.1016/j. elecom.2006. 01.023

[37] Zong X, Sun C, Yu H, Chen ZG, Xing Z, Ye D, et al. Activation of photocatalytic water oxidation on N-doped ZnO bundle-like nanoparticles under visible light. The Journal of Physical Chemistry. 2013;**117**:4937-4942. DOI: 10.1021/ jp311729b

[38] Zhang D, Gong J, Han G, Tong Z. A facile method for synthesis of N-doped ZnO mesoporous nanospheres and enhanced photocatalytic activity. Dalton Transactions. 2013;**42**:16556-16561. DOI: 10.1039/c3dt52039k

[39] Kumar R, Abdel-wahab MS, Barakat MA, Rashid J, Salah N, Al-ghamdi AA.

Role of N doping on the structural, optical and photocatalytic properties of the silver deposited ZnO thin films. Journal of the Taiwan Institute of Chemical Engineers. 2016; **69**:131-138. DOI: 10.1016/j.jtice.2016. 09.027

[40] Tuomisto F, Rauch C, Wagner MR, Hoffmann A, Eisermann S, Meyer BK, et al. Nitrogen and vacancy clusters in ZnO. Journal of Materials Research. 2013;**28**:1977-1983. DOI: 10.1557/jmr. 2013.195

[41] Barnes TM, Olson K, Wolden CA. On the formation and stability of type conductivity in nitrogen-doped zinc oxide. Applied Physics Letters. 2005;**86**: 112. DOI: 10.1063/1.1884747

[42] Tuzemen ES, Kara K, Elagoz S, Takci DK, Altuntas I, Esen R. Structural and electrical properties of nitrogen-doped ZnO thin films. Applied Surface Science. 2014;**318**:157-163. DOI: 10.1016/j.apsusc.2014.02.118

[43] Di Valentin C, Pacchioni G, Selloni A. Theory of carbon doping of titanium dioxide. Chemistry of Materials. 2005; **17**:6656-6665. DOI: 10.1021/cm051921h

[44] Dong F, Guo S, Wang H, Li X, Wu Z. Enhancement of the visible light photocatalytic activity of C-doped TiO$_2$ nanomaterials prepared by a green synthetic approach. The Journal of Physical Chemistry. 2011;**115**: 13285-13292. DOI: 10.1021/jp111916q

[45] Cong Y, Li X, Qin Y, Dong Z, Yuan G, Cui Z, et al. Carbon-doped TiO$_2$ coating on multiwalled carbon nanotubes with higher visible light photocatalytic activity. Applied Catalysis B: Environmental. 2011;**107**: 128-134. DOI: 10.1016/j.apcatb.2011. 07.005

[46] Gamage McEvoy J, Cui W, Zhang Z. Degradative and disinfective properties of carbon-doped anatase-rutile TiO$_2$

mixtures under visible light irradiation. Catalysis Today. 2013;**207**:191-199. DOI: 10.1016/j.cattod.2012.04.015

[47] Rockafellow EM, Stewart LK, Jenks WS. Is sulfur-doped TiO_2 an effective visible light photocatalyst for remediation? Applied Catalysis B: Environmental. 2009;**91**:554-562. DOI: 10.1016/j.apcatb.2009.06.027

[48] Umebayashi T, Yamaki T, Itoh H, Asai K. Band gap narrowing of titanium dioxide by sulfur doping. Applied Physics Letters. 2002;**454**:3-6. DOI: 10.1063/1.1493647

[49] Xu H, Zhou Y-N, Lu F, Fu Z-W. Electrochemistry of $ZnO_{1−x}S_x$ thin film with lithium. Journal of the Electrochemical Society. 2011;**158**:A285. DOI: 10.1149/1.3532037

[50] Meyer BK, Polity A, Farangis B, He Y, Hasselkamp D, Krämer T, et al. Structural properties and bandgap bowing of thin films deposited by reactive sputtering. Applied Physics Letters. 2004;**4929**:2002-2005. DOI: 10.1063/1.1825053

[51] Ratheesh R, Thankalekshmi ACR. Structure and optical band gap of $ZnO_{1-x}S_x$ thin films synthesized by chemical spray pyrolysis for application in solar cells. Journal of Applied Physics. 2012;**112**:063708. DOI: 10.1063/1.4754014

[52] Patil AB, Patil KR, Pardeshi SK. Ecofriendly synthesis and solar photocatalytic activity of S-doped ZnO. Journal of Hazardous Materials. 2010;**183**:315-323. DOI: 10.1016/j.jhazmat.2010.07.026

[53] Zheng YZ, Tao X, Hou Q, Wang DT, Zhou WL, Chen JF. Iodine-doped ZnO nanocrystalline aggregates for improved dye-sensitized solar cells. Chemistry of Materials. 2011;**23**:3-5. DOI: 10.1021/cm101525p

[54] Iwase M, Yamada K, Kurisaki T, Prieto-mahaney OO, Ohtani B, Wakita H. Applied catalysis B: Environmental visible-light photocatalysis with phosphorus-doped titanium (IV) oxide particles prepared using a phosphide compound. Applied Catalysis B: Environmental. 2013;**132–133**:39-44. DOI: 10.1016/j.apcatb.2012.11.014

[55] Mu X, Hou T, Zhang L, Jiang Y, Guan J, Chen X. Facile synthesis of phosphorus doped graphitic carbon nitride polymers with enhanced visible-light photocatalytic activity. Materials Research Bulletin. 2013;**48**:3485-3491. DOI: 10.1016/j.materresbull.2013.05.040

[56] Chai B, Yan J, Wang C, Ren Z, Zhu Y. Enhanced visible light photocatalytic degradation of Rhodamine B over phosphorus doped graphitic carbon nitride. Applied Surface Science. 2017;**391**:376-383. DOI: 10.1016/j.apsusc.2016.06.180

[57] Fan Q, Liu J, Yu Y, Zuo S, Li B. A simple fabrication for sulfur doped graphitic carbon nitride porous rods with excellent photocatalytic activity degrading RhB dye. Applied Surface Science. 2017;**391**:360-368. DOI: 10.1016/j.apsusc.2016.04.055

[58] Yan SC, Li ZS, Zou ZG. Photodegradation of rhodamine B and methyl Orange over boron-doped g-C_3N_4 under visible light irradiation. Langmuir. 2010;**26**:3894-3901. DOI: 10.1021/la904023j

[59] Dong G, Zhao K, Zhang L. Carbon self-doping induced high electronic conductivity and photoreactivity of g-C_3N_4. Chemical Communications. 2012;**48**:6178-6180. DOI: 10.1039/c2cc32181e

[60] Gole JL, Stout JD, Burda C, Lou Y, Chen X. Highly efficient formation of visible light tunable $TiO_{2-x}N_x$ photocatalysts and their transformation

at the nanoscale. The Journal of Physical Chemistry. B. 2004;**108**:1230-1240

[61] Jiang W, Ullah N, Divitini G, Ducati C, Kumar RV, Ding Y, et al. Vertically oriented TiO_xN_y nanopillar arrays with embedded Ag nanoparticles for visible-light photocatalysis. Langmuir. 2012;**28**:5427-5431. DOI: 10.1021/la203617u

[62] Rhee CH, Bae SW, Lee JS. Template-free hydrothermal synthesis of high surface area nitrogen-doped Titania photocatalyst active under visible light. Chemistry Letters. 2005;**34**:660-661. DOI: 10.1246/cl.2005.660

[63] Livraghi S, Pelaez M, Biedrzycki J, Corazzari I, Giamello E, Dionysiou DD. Influence of the chemical synthesis on the physicochemical properties of N-TiO_2 nanoparticles. Catalysis Today. 2013;**209**:54-59. DOI: 10.1016/j.cattod.2012.12.020

[64] Fang J, Shi F, Bu J, Ding J, Xu S, Bao J, et al. One-step synthesis of bifunctional TiO_2 catalysts and their photocatalytic activity. Journal of Physical Chemistry C. 2010;**114**: 7940-7948

[65] Cong Y, Zhang J, Chen F, Anpo M. Synthesis and characterization of nitrogen-doped TiO_2 nanophotocatalyst with high visible light activity. Journal of Physical Chemistry C. 2007;**111**: 6976-6982. DOI: 10.1021/jp0685030

[66] Lin L, Zheng RY, Xie JL, Zhu YX, Xie YC. Synthesis and characterization of phosphor and nitrogen co-doped titania. Applied Catalysis B: Environmental. 2007;**76**:196-202. DOI: 10.1016/j.apcatb.2007.05.023

[67] Li F, Yin X. Investigation on F-B-S tri-doped nano-TiO_2 films for the photocatalytic degradation of organic dyes. Journal of Nanoparticle Research.

2011;**13**:4839-4846. DOI: 10.1007/s11051-011-0461-5

[68] Zhao W, Ma W, Chen C, Zhao J, Shuai Z. Efficient degradation of toxic organic pollutants with $Ni_2O_3/TiO_{2-x}B_x$ under visible irradiation. Journal of the American Chemical Society. 2004;**126**: 4782-4783. DOI: 10.1021/ja0396753

[69] Dong F, Zhao W, Wu Z. Characterization and photocatalytic activities of C, N and S co-doped TiO_2 with 1D nanostructure prepared by the nano-confinement effect. Nanotechnology. 2008;**19**:10. DOI: 10.1088/0957-4484/19/36/365607

[70] Ohno T, Tsubota T, Toyofuku M, Inaba R. Photocatalytic activity of a TiO_2 photocatalyst doped with C^{4+} and S^{4+} ions having a rutile phase under visible light. 2004;**98**:255-258

[71] Hamal DB, Haggstrom JA, Marchin GL, Ikenberry MA, Hohn K, Klabunde KJ. A multifunctional biocide/sporocide and photocatalyst based on titanium dioxide (TiO_2) Codoped with silver, carbon, and sulfur. Langmuir. 2010;**26**: 2805-2810. DOI: 10.1021/la902844r

[72] Pelaez M, Falaras P, Likodimos V, Kontos AG, De AA, Kevin O, et al. Synthesis, structural characterization and evaluation of sol-gel-based NF-TiO_2 films with visible light-photoactivation for the removal of microcystin-LR. Applied Catalysis B: Environmental. 2010;**99**:378-387. DOI: 10.1016/j.apcatb.2010.06.017

[73] Huang D, Liao S, Liu J, Dang Z, Petrik L. Preparation of visible-light responsive N–F-codoped TiO_2 photocatalyst by a sol-gel-solvothermal method. Journal of Photochemistry and Photobiology A: Chemistry. 2006;**184**: 282-288. DOI: 10.1016/j.jphotochem.2006.04.041

[74] Lv Y, Fu Z, Yang B, Xu J, Wu M, Zhu C, et al. Preparation N–F-codoped

TiO_2 nanorod array by liquid phase deposition as visible light photocatalyst. Materials Research Bulletin. 2011;**46**: 361-365. DOI: 10.1016/j.materresbull. 2010.12.011

[75] Ao Y, Xu J, Fu D, Yuan C. Synthesis of C, N, S-tridoped mesoporous titania with enhanced visible light-induced photocatalytic activity. Microporous and Mesoporous Materials. 2009;**122**: 1-6. DOI: 10.1016/j.micromeso.2008. 11.010

[76] Wang P, Yap P, Lim T. C-N-S tridoped TiO_2 for photocatalytic degradation of tetracycline under visible-light irradiation. Applied Catalysis A: General. 2011;**399**:252-261. DOI: 10.1016/j.apcata.2011.04.008

[77] Ohno T, Tsubota T, Nakamura Y, Sayama K. Preparation of S, C cation-codoped $SrTiO_3$ and its photocatalytic activity under visible light. Applied Catalysis A: General. 2005;**288**:74-79. DOI: 10.1016/j.apcata.2005.04.035

[78] Zou F, Jiang Z, Qin X, Zhao Y, Jiang L, Zhi J. Template-free synthesis of mesoporous N-doped $SrTiO_3$ perovskite with high visible-light-driven photocatalytic activity. Chemical Communications. 2012;**48**:8514-8516. DOI: 10.1039/c2cc33797e

[79] Han P, Su Y, Meng Y, Wang S, Jia Q, Wang X. Preparation and photocatalytic performance of iodine-doped $NaTaO_3$ nanoparticles. Journal of Nanoscience and Nanotechnology. 2011;**11**: 9600-9606. DOI: 10.1166/jnn.2011.5277

[80] Fu H, Zhang S, Zhang L, Zhu Y. Visible-light-driven $NaTaO_{3-x}N_x$ catalyst prepared by a hydrothermal process. Materials Research Bulletin. 2008;**43**:864-872. DOI: 10.1016/j. materresbull.2007.05.013

[81] Jiang L, Wang Q, Li C, Yuan J, Shangguan W. ZrW_2O_8 photocatalyst and its visible-light sensitization via sulfur anion doping for water splitting. International Journal of Hydrogen Energy. 2010;**35**:7043-7050. DOI: 10.1016/j.ijhydene.2009.12.187

[82] Zhang J, Huang Z, Xu Y, Kang F. Hydrothermal synthesis of iodine-doped Bi_2WO_6 nanoplates with enhanced visible and ultraviolet-induced photocatalytic activities. International Journal of Photoenergy. 2012;**2012**. DOI: 10.1155/2012/915386

[83] Zhang Z, Wang W, Wang L, Sun S. Enhancement of visible-light photocatalysis by coupling with narrow-band-gap semiconductor: A case study on Bi_2S_3/Bi_2WO_6. Applied Materials & Interfaces. 2012;**4**:593-597. DOI: 10.1021/am2017199

[84] Shi R, Huang G, Lin J, Zhu Y. Photocatalytic activity enhancement for Bi_2WO_6 by fluorine substitution. Journal of Physical Chemistry C. 2009;**113**: 19633-19638

[85] Shifu C, Wei Z, Sujuan Z, Wei L. Preparation, characterization and photocatalytic activity of N-containing ZnO powder. Chemical Engineering Journal. 2009;**148**:263-269. DOI: 10.1016/j.cej.2008.08.039

[86] Li X, Pan H, Hu Q, Zhang C. Nitrogen-doped SiO_2–HNb_3O_8 for rhodamine B photodegradation under visible light. Journal of Alloys and Compounds. 2011;**509**:6252-6256. DOI: 10.1016/j.jallcom.2011.03.033

[87] Takeuchi M, Shimizu Y, Yamagawa H, Nakamuro T, Anpo M. Preparation of the visible light responsive N_3-doped WO_3 photocatalyst by a thermal decomposition of ammonium paratungstate. Applied Catalysis B: Environmental. 2011;**110**:1-5. DOI: 10.1016/j.apcatb.2011.08.004

[88] Liu Y, Li Y, Li W, Han S, Liu C. Photoelectrochemical properties and photocatalytic activity of

nitrogen-doped nanoporous WO_3 photoelectrodes under visible light. Applied Surface Science. 2012;**258**: 5038-5045. DOI: 10.1016/j.apsusc. 2012.01.080

[89] Liu S, Yin K, Ren W, Cheng B, Yu J. Tandem photocatalytic oxidation of Rhodamine B over surface fluorinated bismuth vanadate crystals. Journal of Materials Chemistry. 2012;**22**: 17759-17767. DOI: 10.1039/c2jm33337f

[90] Ji K, Jiang H, Liu Y, Deng J, Dai H, Zhang L. Porous F-doped $BiVO_4$: Synthesis and enhanced photocatalytic performance for the degradation of phenol under visible-light illumination. Solid State Sciences. 2013;**17**:2127. DOI: 10.1016/j. solidstatesciences.2012.12.009

[91] Zhao Z, Dai H, Deng J, Liu Y, Au CT. Enhanced visible-light photocatalytic activities of porous olive-shaped sulfur-doped $BiVO_4$-supported cobalt oxides. Solid State Sciences. 2013;**18**:98-104. DOI: 10.1016/j.solidstatesciences.2013.01.009

[92] Jia L, Li J, Fang W, Song H, Li Q, Tang Y. Visible-light-induced photocatalyst based on C-doped $LaCoO_3$ synthesized by novel microorganism chelate method. Catalysis Communications. 2009;**10**:1230-1234. DOI: 10.1016/j.catcom.2009. 01.025

[93] Martha S, Parida KM. Fabrication of nano N-doped $In_2Ga_2ZnO_7$ for photocatalytic hydrogen production under visible light. International Journal of Hydrogen Energy. 2012;**37**: 17936-17946. DOI: 10.1016/j.ijhydene. 2012.09.025

[94] Gasparotto A, Barreca D, Bekermann D, Devi A, Fischer R a, Fornasiero P, et al. F-doped Co_3O_4 photocatalysts for sustainable H_2 generation from water/ethnol. Journal of the American Chemical Society.

2011;**133**:193-625. DOI: 10.1021/ja210078d

[95] Sreethawong T, Ngamsinlapasathian S, Yoshikawa S. Synthesis of crystalline mesoporous-assembled ZrO_2 nanoparticles via a facile surfactant-aided sol-gel process and their photocatalytic dye degradation activity. Chemical Engineering Journal. 2013;**228**:256-262. DOI: 10.1016/j.cej.2013. 04.111

[96] Dolat D, Quici N, Kusiak-nejman E, Morawski AW, Puma GL. Environmental one-step, hydrothermal synthesis of nitrogen, carbon co-doped titanium dioxide (N, C TiO_2) photocatalysts. Effect of alcohol degree and chain length as carbon dopant precursors on photocatalytic activity and cata. Applied Catalysis B: Environmental. 2012;**115–116**:81-89. DOI: 10.1016/j.apcatb.2011.12.007

[97] Sun H, Bai Y, Cheng Y, Jin W, Xu N. Preparation and characterization of visible-light-driven carbon-sulfur-codoped TiO_2 photocatalysts. Industrial and Engineering Chemistry Research. 2006;**45**:4971-4976. DOI: 10.1021/ie060350f

[98] Uk H, Chang S, Hae S, Son B, Jae S, Jin H, et al. Highly visible-light active nanoporous TiO_2 photocatalysts for efficient solar photocatalytic applications. Applied Catalysis B: Environmental. 2013;**129**:106-113. DOI: 10.1016/j.apcatb.2012.09.010

[99] Yang K, Dai Y, Huang B, Whangbo MH. Density functional characterization of the band edges, the band gap states, and the preferred doping sites of halogen-doped TiO_2. Chemistry of Materials. 2008;**20**:6528-6534. DOI: 10.1021/cm801741m

[100] Zhang L, Zhang H, Xu H, Deng F, Zheng Z. Hierarchical chlorine-doped rutile TiO_2 spherical clusters of

nanorods: Large-scale synthesis and high photocatalytic activity. Journal of Solid State Chemistry. 2008;**181**: 2516-2522. DOI: 10.1016/j.jssc. 2008.06.019

[101] Luo H, Takata T, Lee Y, Zhao J, Domen K, Yan Y. Photocatalytic activity enhancing for titanium dioxide by Co-doping with bromine and chlorine. Chemistry of Materials. 2004;**16**: 846-849. DOI: 10.1021/cm035090w

[102] Andersen J, Han C, O'Shea K, Dionysiou DD. Revealing the degradation intermediates and pathways of visible light-induced NF-TiO_2 photocatalysis of microcystin-LR. Applied Catalysis B: Environmental. 2014;**154–155**:259-266. DOI: 0.1016/j. apcatb.2014.02.025

[103] Nisar J, Wang B, Moyses C, Ferreira A. Band gap engineering by anion doping in the photocatalyst $BiTaO_4$: First principle calculations. International Journal of Hydrogen Energy. 2012;**37**:3014-3018. DOI: 10.1016/j.ijhydene.2011.11.068

[104] Yang K, Huang W, Xu L, Luo K, Yang Y, Huang G. Materials science in semiconductor processing insights into enhanced visible-light photocatalytic activity of CeO_2 doped with nonmetal impurity from the first principles. Materials Science in Semiconductor Processing. 2016;**41**:200-208. DOI: 10.1016/j.mssp.2015.08.039

[105] Bagwasi S, Tian B, Zhang J, Nasir M. Synthesis, characterization and application of bismuth and boron Co-doped TiO_2: A visible light active photocatalyst. Chemical Engineering Journal. 2013;**217**:108-118. DOI: 10.1016/j.cej.2012.11.080

[106] Di Valentin C, Pacchioni G. Trends in non-metal doping of anatase TiO_2: B, C, N and F. Catalysis Today. 2013;**206**: 12-18. DOI: 10.1016/j.cattod.2011.11.030

[107] Wang G, Chen H, Wu G, Kuang A. Hybrid density functional study on mono- and Co-doped $NaNbO_3$ for visible-light photocatalysis. ChemPhysChem. 2016;**17**:489-499. DOI: 10.1002/cphc.201501037

[108] Murakami N, Chiyoya T, Tsubota T, Ohno T. Switching redox site of photocatalytic reaction on titanium(IV) oxide particles modified with transition-metal ion controlled by irradiation wavelength. Applied Catalysis A: General. 2008;**348**:148-152. DOI: 10.1016/j.apcata.2008.06.040

[109] Carneiroa JO, Portinha VT, Dupak L, Magalhaes A, Coutinho P. Study of the deposition parameters and Fe-dopant effect in the photocatalytic activity of TiO_2 films prepared by dc reactive magnetron sputtering. Vacuum. 2005;**78**:37-46. DOI: 10.1016/j. vacuum.2004.12.012

[110] Wu JCS, Chen CH. A visible-light response vanadium-doped titania nanocatalyst by sol-gel method. Journal of Photochemistry and Photobiology A: Chemistry. 2004;**163**:509-515. DOI: 10.1016/j.jphotochem.2004.02.007

[111] Rimoldi L, Pargoletti E, Meroni D, Falletta E, Cerrato G, Turco F, et al. Concurrent role of metal (Sn, Zn) and N species in enhancing the photocatalytic activity of TiO_2 under solar light. Catalysis Today. 2018;**313**:4046. DOI: 10.1016/j.cattod.2017.12.017

[112] Rashid J, Barakat MA, Salah N, Habib SS. Ag/ZnO nanoparticles thin films as visible light photocatalysts. The Royal Society of Chemistry. 2014;**4**: 56892-56899. DOI: 10.1039/c4ra12990c

[113] Yayapao O, Thongtem T, Phuruangrat A, Thongtem S. Ultrasonic-assisted synthesis of Nd-doped ZnO for photocatalysis. Materials Letters. 2013; **90**:83-86. DOI: 10.1016/j.matlet.2012. 09.027

[114] Phuruangrat A, Yayapao O, Thongtem T, Thongtem S. Preparation, characterization and photocatalytic properties of Ho doped ZnO nanostructures synthesized by sonochemical method. Superlattices and Microstructures. 2014;**67**:118-126. DOI: 10.1016/j.spmi.2013.12.023

[115] Khatamian M, Khandar AA, Divband B, Haghighi M, Ebrahimiasl S. Heterogeneous photocatalytic degradation of 4-nitrophenol in aqueous suspension by Ln (La^{3+}, Nd^{3+} or Sm^{3+}) doped ZnO nanoparticles. Journal of Molecular Catalysis A: Chemical. 2012;**365**:120-127. DOI: 10.1016/j.molcata.2012.08.018

[116] Ding K, Wen L, Xu L, Wu H, Ye Y, Zhang Y. Predicting the electronic and optical properties of IB metals doped monoclinic BiVO$_4$: First principle calculations. International Journal of Quantum Chemistry. 2015;**116**:388-395. DOI: 10.1002/qua.25051

[117] Tang JW, Wang DF, Zou ZG, Je Y. Modification of photophysical properties of WO$_3$ by doping different metals. Materials Science Forum. 2003;**425**:163-166. DOI: 10.4028/www.scientific.net/MSF.423-425.163

[118] Xue Q, Liu Y, Zhou Q, Utsumi M, Zhang Z, Sugiura N. Photocatalytic degradation of geosmin by Pd nanoparticle modified WO$_3$ catalyst under simulated solar light. Chemical Engineering Journal. 2016;**283**:614-621. DOI: 10.1016/j.cej.2015.08.016

[119] Wei W, Ying D, Hao J, Huang B. Density functional characterization of the of Cr-doped SrTiO$_3$. Journal of Physics D: Applied Physics. 2009;**42**. DOI: 10.1088/0022-3727/42/5/055401

[120] Liu H, Peng T, Ke D, Peng Z, Yan C. Preparation and photocatalytic activity of dysprosium doped tungsten trioxide nanoparticles. Materials Chemistry and Physics. 2007;**104**: 377-383. DOI: 10.1016/j.matchemphys.2007.03.028

[121] Li J, Hu W, Zhong J, Zeng J, Huang S, Xiao Z, et al. Photo-induced charge separation and photocatalytic activity of Ga-doped SnO$_2$. Applied Physics A: Materials Science & Processing. 2014;**116**:2149-2156. DOI: 10.1007/s00339-014-8428-x

[122] Li Z, Shen Y, Guan Y, Hu Y, Lin Y, Nan CW. Bandgap engineering and enhanced interface coupling of graphene-BiFeO$_3$ nanocomposites as efficient photocatalysts under visible light. Journal of Materials Chemistry A. 2014;**2**:1967-1973. DOI: 10.1039/c3ta14269h

[123] Hu S, Li F, Fan Z, Wang F, Zhao Y, Lv Z. Band gap-tunable potassium doped graphitic carbon nitride with enhanced mineralization. Dalton Transactions. 2014;**44**:1084-1092. DOI: 10.1039/c4dt02658f

[124] Rong X, Qiu F, Rong J, Zhu X, Yan J, Yang D. Enhanced visible light photocatalytic activity of W-doped porous. Materials Letters. 2016;**164**: 127-131. DOI: 10.1016/j.matlet.2015.10.131

[125] Wang Y, Li Y, Bai X, Cai Q, Liu C, Zuo Y, et al. Facile synthesis of Y-doped graphitic carbon nitride with enhanced photocatalytic performance. Catalysis Communications. 2016;**84**:179-182. DOI: 10.1016/j.catcom.2016.06.020

[126] Song X, Tao H, Chen L, Sun Y. Synthesis of Fe/g-C$_3$N$_4$ composites with improved visible light photocatalytic activity. Materials Letters. 2014;**116**: 265-267. DOI: 10.1016/j.matlet.2013.11.043

[127] Chatterjee D, Dasgupta S. Visible light induced photocatalytic degradation of organic pollutants. Journal of Photochemistry and Photobiology C: Photochemistry Reviews. 2005;**6**:

186-205. DOI: 10.1016/j.jphotochemrev. 2005.09.001

[128] Abe R, Sayama K, Arakawa H. Dye-sensitized photocatalysts for efficient hydrogen production from aqueous I—Solution under visible light irradiation. Journal of Photochemistry and Photobiology A: Chemistry. 2004;**166**: 115-122. DOI: 10.1016/j.jphotochem. 2004.04.031

[129] Chu W, Chan KH, Jafvert CT, Chan YS. Removal of phenylurea herbicide monuron via riboflavin-mediated photosensitization. Chemosphere. 2007;**69**:177-183. DOI: 10.1016/j.chemosphere.2007.04.055

[130] Whitehead K, Hedges JI. Photodegradation and photosensitization of mycosporine-like amino acids. Journal of Photochemistry and Photobiology B: Biology. 2005;**80**: 115-121. DOI: 10.1016/j.jphotobiol. 2005.03.008

[131] Kaur S, Singh V. Visible light induced sonophotocatalytic degradation of reactive red dye 198 using dye sensitized TiO_2. Ultrasonics Sonochemistry. 2007;**14**:531-537. DOI: 10.1016/j.ultsonch.2006.09.015

[132] Lee C, Hyeon T, Lee H. Visible light-induced degradation of carbon tetrachloride on. Environmental Science & Technology. 2001;**35**:966-970

[133] Shim M, Mcdaniel H, Oh N. Prospects for strained type-II nanorod heterostructures. The Journal of Physical Chemistry Letters. 2011;**2**: 2722-2727

[134] Tian J, Zhenhuan Zhaoa AK, Boughton RI, Liu H. Nanostructured surface heterostructures: A review. Chemical Society Reviews. 2014;**43**: 6920-6937. DOI: 10.1039/x0xx00000x

[135] Beydoun D, Amal R, Low G. Role of nanoparticles in photocatalysis.

Journal of Nanoparticle Research. 1999; **1**:439-458. DOI: 10.1023/A: 1010044830871

[136] Ghows N, Entezari MH. Fast and easy synthesis of core—Shell nanocrystal (CdS/TiO_2) at low temperature by micro-emulsion under ultrasound. Ultrasonics Sonochemistry. 2011;**18**:629-634. DOI: 10.1016/j. ultsonch.2010.08.003

[137] Jia H, Xu H, Hu Y, Tang Y, Zhang L. TiO_2 @ CdS core—Shell nanorods films: Fabrication and dramatically enhanced photoelectrochemical properties. Electrochemistry Communications. 2007;**9**:354-360. DOI: 10.1016/j.elecom.2006.10.010

[138] Covei M, Perniu D, Bogatu C, Duta A. CZTS-TiO_2 thin film heterostructures for advanced photocatalytic wastewater treatment. Catalysis Today. 2019;**321– 322**:172-177. DOI: 10.1016/j.cattod.2017. 12.003

[139] Rashid J, Barakat MA, Ruzmanova Y. $Fe_3O_4/SiO_2/TiO_2$ nanoparticles for photocatalytic degradation of 2-chlorophenol in simulated wastewater. Environmental Science and Pollution Research. 2015;**22**:3149-3157. DOI: 10.1007/s11356-014-3598-9

[140] Pan L, Shen G, Zhang J, Wei X, Wang L, Zou J, et al. TiO_2—ZnO composite sphere decorated with ZnO clusters for E ff ective charge isolation in photocatalysis. Industrial and Engineering Chemistry Research. 2015; **54**:7226-7232. DOI: 10.1021/acs. iecr.5b01471

[141] Lee G, Kang M. Physicochemical properties of core/shell structured pyrite FeS_2/anatase TiO_2 composites and their photocatalytic hydrogen production performances. Current Applied Physics. 2013;**13**:1482-1489. DOI: 10.1016/j.cap.2013.05.002

[142] Rashid J, Saleem S, Awan SU, Iqbal A, Kumar R, Barakat MA, et al.

Stabilized fabrication of anatase-TiO_2/FeS_2 (pyrite) semiconductor composite nanocrystals for enhanced solar light-mediated photocatalytic degradation of methylen blue. RSC Advances. 2018;**8**: 11935-11945. DOI: 10.1039/c8ra02077a

[143] Rashid J, Barakat M. $InVO_4$/TiO_2 composite for visible-light photocatalytic degradation of 2-chlorophenol in wastewater. Environmental Technology. 2014;**35**: 2153-2159. DOI: 10.1080/09593330. 2014.895051

[144] Rashid J, Barakat MA. Ag_3PO_4 Enhanced TiO_2 for Visible Light Photocatalysis of 2-Chlorophenol in Wastewater. Institute of Research Engineers and Doctors, USA; 2014. pp. 3-7

[145] Li Y, Zhao H, Yang M. TiO_2 nanoparticles supported on PMMA nanofibers for photocatalytic degradation of methyl orange. Journal of Colloid and Interface Science. 2017;**508**: 500-507. DOI: 10.1016/j.jcis.2017.08.076

[146] Rashid J, Abbas A, Chang LC, Iqbal A, Ihsan-ul-Haq A, Rehman SUA, et al. Butterfly cluster like lamellar BiOBr/ TiO_2 nanocomposite for enhanced sunlight photocatalytic mineralization of aqueous ciprofloxacin. Science of the Total Environment Elsevier B. 2019;**665**: 668-677. DOI: 10.1016/j.scitotenv. 2019.02.145

[147] Jana TK, Pal A, Chatterjee K. Self assembled flower like CdS–ZnO nanocomposite and its photo catalytic activity. Journal of Alloys and Compounds. 2014;**583**:510-515. DOI: 10.1016/j.jallcom.2013.08.184

[148] Cho S, Jang JW, Kim J, Lee JS, Choi W, Lee KH. Three-dimensional type II ZnO/ZnSe heterostructures and their visible light photocatalytic activities. Langmuir. 2011;**27**:10243-10250. DOI: 10.1021/la201755w

[149] Wang Z, Huang B, Dai Y, Qin X, Zhang X, Wang P, et al. Highly photocatalytic ZnO/In_2O_3 heteronanostructures synthesized by a coprecipitation method. The Journal of Physical Chemistry. 2009;**113**:4612-4617

[150] Hamrouni A, Moussa N, Di Paola A, Parrino F, Houas A, Palmisano L. Characterization and photoactivity of coupled ZnO-$ZnWO_4$ catalysts prepared by a sol-gel method. Applied Catalysis B: Environmental. 2014;**154–155**:379-385. DOI: 10.1016/j.apcatb. 2014.02.042

[151] Hernández S, Hidalgo D, Sacco A, Chiodoni A, Lamberti A, Cauda V, et al. Comparison of photocatalytic and transport properties of TiO_2 and ZnO nanostructures for solar-driven water splitting. Physical Chemistry Chemical Physics. 2015;**17**:7775-7786. DOI: 10.1039/c4cp05857g

[152] Katsumata H, Gomathisankar P, Funasaka K, Kaneco S, Suzuki T, Hachisuka K. Photocatalytic hydrogen production with CuS/ZnO from aqueous Na_2S + Na_2SO_3 solution. International Journal of Hydrogen Energy. 2013;**38**: 8625-8630. DOI: 10.1016/j.ijhydene. 2013.04.131

[153] He Z, Shi Y, Gao C, Wen L, Chen J, Song S. BiOCl/$BiVO_4$ p–n heterojunction with enhanced photocatalytic activity under visible-light irradiation. The Journal of Physical Chemistry. 2014;**118**:389-398. DOI: 10.1021/jp409598s

[154] Tahir MB, Nabi G, Rafique M, Khalid NR. Nanostructured-based WO_3 photocatalysts: Recent development, activity enhancement, perspectives and applications for wastewater treatment. International journal of Environmental Science and Technology. 2017;**14**: 2519-2542. DOI: 10.1007/s13762-017-1394-z

[155] Shamaila S, Khan A, Sajjad L, Chen F, Zhang J. WO_3/BiOCl, a novel heterojunction as visible light

photocatalyst. Journal of Colloid and Interface Science. 2011;**356**:465-472. DOI: 10.1016/j.jcis.2011.01.015

[156] Huang T, Lin X, Xing J, Wang W, Shan Z, Huang F. Photocatalytic activities of hetero-junction semiconductors $WO_3/SrNb_2O_6$. Materials Science & Engineering, B: Solid-State Materials for Advanced Technology. 2007;**141**:49-54. DOI: 10.1016/j.mseb.2007.05.007

[157] Zhang J, Yu K, Yu Y, Lou LL, Yang Z, Yang J, et al. Highly effective and stable Ag_3PO_4/WO_3 photocatalysts for visible light degradation of organic dyes. Journal of Molecular Catalysis A: Chemical. 2014;**391**:12-18. DOI: 10.1016/j.molcata.2014.04.010

[158] Huang Z, Zou J, Pan L, Wang S, Zhang X, Wang L. Synergetic promotion on photoactivity and stability of $W_{18}O_{49}/TiO_2$ hybrid. Applied Catalysis B: Environmental. 2014;**147**: 167-174. DOI: 10.1016/j.apcatb.2013. 08.038

[159] Aslam I, Cao C, Tanveer M, Farooq MH, Khan SW, Tahir M, et al. A novel Z-scheme $WO_3/CdWO_4$ photocatalyst with enhanced visible-light photocatalytic activity for the degradation of organic pollutants. RSC Advances. 2015;**5**:6019-6026. DOI: 10.1039/C4RA15847D

[160] Zaleska A, Winiarski M, Klimczuk T, Bajorowicz B, Cybula A. Surface properties and photocatalytic activity of $KTaO_3$, CdS, MoS_2 semiconductors and their binary and ternary semiconductor composites. Molecules. 2014;**19**: 15339-15360. DOI: 10.3390/molecules190915339

[161] Pirhashemi M, Habibi-yangjeh A. Ternary $ZnO/AgBr/Ag_2CrO_4$ nanocomposites with tandem n–n heterojunctions as novel visible-light-driven photocatalysts with excellent activity. Ceramics International. 2015; **41**:14383-14393. DOI: 10.1016/j.ceramint.2015.07.072

[162] Zhang W, Li Y, Song Q, Zhang J, Chen X, Liu D, et al. Multi-pathway photoelectron migration in globular flower-like $In_2O_3/AgBr/Bi_2WO_6$ synthesized by microwave-assisted method with enhanced photocatalytic activity. Journal of Molecular Catalysis A: Chemical. 2015;**414**:27-36. DOI: 10.1016/j.molcata.2015.12.023

[163] Mohamed MM, Ahmed SA, Khairou KS. Unprecedented high photocatalytic activity of nanocrystalline $WO_3/NiWO_4$ hetero-junction towards dye degradation: Effect of template and synthesis conditions. Applied Catalysis B: Environmental. 2014;**150–151**:63-73. DOI: 10.1016/j.apcatb.2013.12.001

[164] Xu YS, De Zhang W. Monodispersed Ag_3PO_4 nanocrystals loaded on the surface of spherical Bi_2MoO_6 with enhanced photocatalytic performance. Dalton Transactions. 2013;**42**:1094-1101. DOI: 10.1039/c2dt31634j

[165] Cao J, Luo B, Lin H, Xu B, Chen S. Visible light photocatalytic activity enhancement and mechanism of $AgBr/Ag_3PO_4$ hybrids for degradation of methyl orange. Journal of Hazardous Materials. 2012;**217–218**:107-115. DOI: 10.1016/j.jhazmat.2012.03.002

[166] Feng Y, Yan X, Liu C, Hong Y, Zhu L, Zhou M, et al. Applied surface science hydrothermal synthesis of CdS/Bi_2MoO_6 heterojunction photocatalysts with excellent visible-light-driven photocatalytic performance. Applied Surface Science. 2015;**353**:87-94. DOI: 10.1016/j.apsusc.2015.06.061

[167] Ghugal SG, Umare SS, Sasikala R. Photocatalytic mineralization of anionic dyes using bismuth doped $CdS–Ta_2O_5$ composite. RSC Advances. 2015;**5**:

63393-63400. DOI: 10.1039/
C5RA09974A

[168] Kong L, Jiang Z, Xiao T, Lu L, Jones O, Edwards PP. Exceptional visible-light-driven photocatalytic activity over. Chemical Communications. 2011;**47**: 5512-5514. DOI: 10.1039/c1cc10446b

[169] Liu C, Li P, Wu G, Luo B, Lin S, Ren A, et al. Enhanced photoelectrochemical and photocatalytic activity by $Cu_2O/SrTiO_3$ p–n heterojunction via a facile deposition–precipitation technique. RSC Advances. 2015;**5**:33938-33945. DOI: 10.1039/C5RA03086B

[170] Hong E, Kim D, Kim JH. Heterostructured metal sulfide (ZnS-CuS-CdS) photocatalyst for high electron utilization in hydrogen production from solar water splitting. Journal of Industrial and Engineering Chemistry. 2014;**20**:3869-3874. DOI: 10.1016/j.jiec.2013.12.092

[171] Moussa N, Houas A, Parrino F, Di Paola A, Hamrouni A, Palmisano L. Photocatalytic activity of binary and ternary $SnO_2–ZnO–ZnWO_4$ nanocomposites. Journal of Photochemistry and Photobiology A: Chemistry. 2015;**309**:47-54. DOI: 10.1016/j.jphotochem.2015.05.001

[172] Zhao Z, Yanjuan S, Dong F. Graphitic carbon nitride based nanocomposites: A review. Nanoscale. 2015;**7**:15-37. DOI: 10.1039/c4nr03008g

[173] Song G, Chu Z, Jin W, Sun H. Enhanced performance of $g-C_3N_4/TiO_2$ photocatalysts for degradation of organic pollutants under visible light. Chinese Journal of Chemical Engineering. 2015;**23**:1326-1334. DOI: 10.1016/j.cjche.2015.05.003

[174] Lv J, Dai K, Zhang J, Geng L, Liang C, Liu Q, et al. Applied surface science facile synthesis of Z-scheme graphitic-C_3N_4/Bi_2MoO_6 nanocomposite for enhanced visible photocatalytic properties. Applied Surface Science. 2015;**358**:377-384. DOI: 10.1016/j. apsusc.2015.06.183

[175] Dai S, Hua F, Li W, Hou H, Yue J, Feng C. Fabrication of sulfur-doped $g-C_3N_4/Au/CdS$ Z-scheme photocatalyst to improve the photocatalytic performance under visible light. Applied Catalysis B: Environmental. 2015;**168–169**:465-471. DOI: 10.1016/j. apcatb.2015.01.012

[176] Fu J, Chang B, Yanlong Tian FX, Dong X. Novel C_3N_4-CdS composite photocatalysts with organic-inorganic heterojunctions: In suit synthesis, exceptional activity, high stability and photocatalytic mechanism. Journal of Materials Chemistry A. 2013;**1**:3083-3090. DOI: 10.1039/c2ta00672c

[177] Tong Z, Yang D, Shi J, Nan Y, Sun Y, Jiang Z, et al. Three-dimensional porous aerogel constructed by $g-C_3N_4$ and graphene oxide nanosheets with excellent visible-light photocatalytic performance. Applied Materials & Interfaces. 2015;**7**:25693-25701. DOI: 10.1021/acsami.5b09503

[178] Han Q, Chen N, Zhang J, Qu L. Graphene/graphitic carbon nitride hybrids for catalysis. Materials Horizons. 2017:832-850. DOI: 10.1039/c7mh00379j

[179] Mousavi M, Habibi-Yangjeh A. Integration of $NiWO_4$ and Fe_3O_4 with graphitic carbon nitride to fabricate novel magnetically recoverable visible-light-driven photocatalysts. Journal of Materials Science. 2018;**53**:9046-9063. DOI: 10.1007/s10853-018-2213-8

[180] Zhang S, Li J, Zeng M, Zhao G, Xu J, Hu W, et al. In situ synthesis of water-soluble magnetic graphitic carbon nitride photocatalyst and its synergistic catalytic performance. ACS Applied Materials & Interfaces. 2013;**5**:12735-12743

53

[181] Zou L, Wang H, Yuan G, Wang X. Magnetically separable CdS/ZnFe$_2$O$_4$ composites with highly efficient photocatalytic activity and photostability under visible light. ACS Applied Nano Materials. 2018;**1**:831-838. DOI: 10.1021/acsanm.7b00243

[182] Chai B, Liao X, Song F, Zhou H. Fullerene modified C$_3$N$_4$ composites with enhanced photocatalytic activity under visible light irradiation. Dalton Transactions. 2014;**43**:982-989. DOI: 10.1039/c3dt52454j

[183] Fu H, Xu T, Zhu S, Zhu Y. Photocorrosion inhibition and enhancement of photocatalytic activity for ZnO via hybridization with C$_6$O. Environmental Science & Technology. 2008;**42**:8064-8069. DOI: 10.1021/es801484x

[184] Zhu Y, Bai X, Yao W, Wang L, Wang Y. Enhanced oxidation ability of g-C$_3$N$_4$ photocatalyst via C60 modification. Applied Catalysis B: Environmental. 2014b;**152–153**:262-270. DOI: 10.1016/j.apcatb.2014.01.046

[185] Zhu H, Chen D, Yue D. In-situ synthesis of g-C$_3$N$_4$-P$_{25}$TiO$_2$ composite with enhanced visible light photoactivity. Journal of Nanoparticle Research. 2014;**16**:1-10. DOI: 10.1007/s11051-014-2632-7

[186] Huang L, Xu H, Li Y, Li H, Cheng X, Xia J, et al. Visible-light-induced WO$_3$/g-C$_3$N$_4$ composites with enhanced photocatalytic activity. Dalton Transactions. 2013;**4**:8606-8616. DOI: 10.1039/c3dt00115f

[187] Tian N, Huang H, Zhang Y. Mixed-calcination synthesis of CdWO$_4$/g-C$_3$N$_4$ heterojunction with enhanced visible-light-driven photocatalytic activity. Applied Surface Science. 2015;**358**:343-349. DOI: 10.1016/j.apsusc.2015.07.154

[188] Xing C, Wu Z, Jiang D, Chen M. Hydrothermal synthesis of In$_2$S$_3$/g-C$_3$N$_4$ heterojunctions with enhanced photocatalytic activity. Journal of Colloid and Interface Science. 2014;**433**:9-15. DOI: 10.1016/j.jcis.2014.07.015

[189] Liu Q, Fan C, Tang H, Sun X, Yang J, Cheng X. One-pot synthesis of g-C$_3$N$_4$/V$_2$O$_5$ composites for visible light-driven photocatalytic activity. Applied Surface Science. 2015;**358**:188-195. DOI: 10.1016/j.apsusc.2015.09.010

[190] Sun JX, Yuan YP, Qiu LG, Jiang X, Xie AJ, Shen YH, et al. Fabrication of composite photocatalyst g-C$_3$N$_4$-ZnO and enhancement of photocatalytic activity under visible light. Dalton Transactions. 2012;**41**:6756-6763. DOI: 10.1039/c2dt12474b

[191] Wang Y, Wang Z, Muhammad S, He J. Graphite-like C$_3$N$_4$ hybridized ZnWO$_4$ nanorods: Synthesis and its enhanced photocatalysis in visible light. CrystEngComm. 2012;**14**:5065-5070. DOI: 10.1039/c2ce25517k

[192] Yuan D, Huang L, Li Y, Xu Y, Xu H, Huang S, et al. Synthesis and photocatalytic activity of g-C$_3$N$_4$/BiOI/BiOBr ternary composites. RSC Advances. 2016;**6**:41204-41213. DOI: 10.1039/C6RA05565F

[193] Dong Z, Wu Y, Thirugnanam N, Li G. Applied surface science double Z-scheme ZnO/ZnS/g-C$_3$N$_4$ ternary structure for efficient photocatalytic H$_2$ production. Applied Surface Science. 2018;**430**:293-300. DOI: 10.1016/j.apsusc.2017.07.186

[194] Gao Y, Lin J, Zhang Q, Yu H, Ding F, Xu B, et al. Facile synthesis of heterostructured YVO4/g-C$_3$N$_4$/Ag photocatalysts with enhanced visible-light photocatalytic performance. Applied Catalysis B: Environmental. 2018;**224**:586-593. DOI: 10.1016/j.apcatb.2017.11.003

[195] Zhong Y, Yuan J, Wen J, Li X, Xu Y, Liu W, et al. Earth-abundant NiS co-catalyst modified metal-free mpg-C_3N_4/CNT nanocomposites for highly efficient visible-light photocatalytic H_2 evolution. Dalton Transactions. 2015;**44**:18260-18269. DOI: 10.1039/c5dt02693h

[196] Yan J, Song Z, Wang X, Xu Y, Pu W, Xu H, et al. Enhanced photocatalytic activity of ternary Ag_3PO_4/GO/g-C_3N_4 photocatalysts for rhodamine B degradation under visible light radiation. Applied Surface Science. 2019;**466**:70-77. DOI: 10.1016/j.apsusc.2018.09.234

[197] Zhou Y, Li J, Liu C, Huo P, Wang H. Construction of 3D porous g-C_3N_4/AgBr/rGO composite for excellent visible light photocatalytic activity. Applied Surface Science. 2018;**458**:586-596. DOI: 10.1016/j.apsusc.2018.07.121

[198] Jiang D, Yu H, Yu H. Modified g-C_3N_4/TiO_2 nanosheets/ZnO ternary facet coupled heterojunction for photocatalytic degradation of p-toluenesulfonic acid (p-TSA) under visible light. Physica E: Low-dimensional Systems and Nanostructures. 2017;**85**:1-6. DOI: 10.1016/j.physe.2016.08.014

[199] Yuan Y, Huang G, Hu W, Xiong D, Zhou B, Chang S. Construction of g-C_3N_4/CeO_2/ZnO ternary photocatalysts with enhanced photocatalytic performance. Journal of Physics and Chemistry of Solids. 2017;**106**:1-9. DOI: 10.1016/j.jpcs.2017.02.015

[200] Deng Y, Wang J, Liu Y, Wang J, Feng H, Tang L, et al. Enhanced photocatalytic activity of ternary Ag/g-C_3N_4/$NaTaO_3$ photocatalysts under wide spectrum light radiation: The high potential band protection mechanism. Applied Catalysis B: Environmental. 2018;**230**:102-114. DOI: 10.1016/j.apcatb.2018.02.031